Space-Clock Field Theory: A Single Metric Candidate for Dark Sector Unification

Mauro Alfonso Montenegro*
Independent researcher, Austin, Texas, USA
(Dated: September 8, 2026)

Spacetime is conventionally treated as a four-dimensional background within which matter and gravitational phenomena occur. Space-Clock Field Theory (SCFT-A) advances a field-first alternative: the Lorentzian metric is the gravitational field, and physical space is the clock-orthogonal spatial state of that field, rather than an independent background container in which gravity resides. A dynamical scalar clock T selects the physical foliation and distinguishes cosmological clock-field time T from matter proper time t, the invariant time measured along material worldlines. Along homogeneous clock-comoving trajectories, the two physical times satisfy $dT = Q\,dt$, so that $\mathcal{N}_T \equiv dt/dT = Q^{-1}$ and $H_T = H/Q$. Because T carries stress, conjugate momentum, conserved charge, and gravitational backreaction, this distinction changes relational observables and cannot be removed by a coordinate transformation. The theory's central reciprocal statement is: As physical space expands, cosmological time contracts or moves slower; as physical space contracts, cosmological time expands or moves faster. The expanding branch obeys the on-shell response $d\mathcal{N}_T/dH < 0$. An explicit unbraided contracting branch has $\dot{Q} > 0$; this clock-rate statement has a different response sign and is proved only on its stated branch. This gravitational–clock architecture motivates the proposed extended equivalence principle,

$$\text{gravity} \mathrel{\widehat{=}} \text{proper acceleration} \mathrel{\widehat{=}} \text{physical space} \mathrel{\widehat{=}} \text{relativistic aether} \mathrel{\widehat{=}} \text{vacuum},$$

where $\widehat{=}$ denotes identity of physical sector rather than mathematical equality among curvature, acceleration, spatial geometry, causal structure, and vacuum states. SCFT-A realizes these principles using one universally coupled metric and one shift-symmetric scalar clock. The same operator family admits specified approximately matter-like regimes, a late self-accelerating endpoint, and a controlled local stationary MOND/AQUAL operator limit, without a separate cold-dark-matter action, dark-energy fluid, bare cosmological constant, or second matter metric. These are classical branch results, rather than a completed dark-sector unification theorem.

A convex kinetic interpolation and positive spatial derivative operators define a deliberately constructed classical example. An explicit revised coefficient point, $\kappa_m/H_d^2 = 10^{30}$, $\delta = 10^{-140}$ and $\sigma = 10^{-6}$, replaces uncertified numerical extrema by proved sufficient bounds. It preserves all-momentum local scalar positivity and a positive tensor spectrum. A generalized endpoint polynomial proves positive scalar kinetic and restoring coefficients, and an exact decreasing energy controls every endpoint scalar mode despite redshifting momentum. The revised stationary correction ratio is strictly below 10^{-14} at a declared subhorizon scale. Both homogeneous backgrounds and all 42 finite-time ideal-fluid responses are recomputed; the largest sampled unit response is 1.0011357323900973. The companion supplies the gravitational and ideal-fluid cubic functionals. The vacuum gravity–clock Cauchy problem is locally Hadamard well posed on the strongly regular boundaryless torus domain specified below, including lapse–trace reconstruction, existence, uniqueness, continuous dependence, and constraint propagation. The stated results concern this classical local domain and do not make claims about a strong-coupling completion, radiative protection, nonlinear bounded-domain evolution, unspecified visible-matter dynamics, or nonlinear cosmological galaxy matching.

I. INTRODUCTION

The standard cosmological model gives an economical account of the background expansion, the cosmic microwave background, and large-scale structure by supplementing general relativity with cold dark matter and a cosmological constant [1–3]. Its empirical success does not identify the microscopic nature of dark matter, remove the radiative instability of vacuum energy, or explain why the matter and acceleration scales are comparable at the present epoch [4, 5]. These open questions allow a logically distinct possibility: the gravitational effects assigned to two dark substances may arise from additional dynamics within the gravitational sector itself.

The starting point of Space-Clock Field Theory is operational. Cosmological expansion is inferred through relations among clocks, photons, redshifts, rulers, and freely falling matter. A derivative called an expansion rate is therefore

* Corresponding author: mamontenegro@liberty.edu

meaningful only after the physical clock with respect to which it is taken has been specified. This observation does not permit a coordinate lapse to create new physics: a relabeling of time leaves relational observables unchanged. It instead motivates a theory in which the clock is a covariant field with stress, conjugate momentum, and backreaction.

The physical interpretation is field first. The Lorentzian metric $g_{\mu\nu}$ is the gravitational field, and its projection onto the leaves selected by a scalar clock T is the instantaneous spatial geometry. There is no additional background container in which the gravitational field resides. Matter proper time t and clock-field time T are distinct physical functionals of one solution, related on a homogeneous clock-comoving trajectory by

$$\mathrm{d}T = Q\,\mathrm{d}t, \qquad \mathcal{N}_T \equiv \frac{\mathrm{d}t}{\mathrm{d}T} = \frac{1}{Q}, \qquad H_T = \frac{H}{Q}. \tag{1}$$

We define a reciprocal branch by an on-shell response: the matter-clock interval per unit field time decreases as the expansion rate increases,

$$\frac{\mathrm{d}\mathcal{N}_T}{\mathrm{d}H} < 0. \tag{2}$$

The motivating interpretation is that the physical clock rate can decrease as space expands. In the expanding benchmark studied here this means $Q' = \mathrm{d}Q/\mathrm{d}\ln a < 0$. The response in Equation (2) is a separate condition involving H', not a consequence of $H > 0$ alone. At an exact de Sitter point $Q' = H' = 0$, the response is defined only as a limit along a specified neighboring solution. The unbraided contracting construction in Section VII D proves $\dot{Q} > 0$ when $H < 0$. It does not establish a contracting extension through the nonzero braid.

This decomposition motivates the extended equivalence principle

$$\text{gravity} \mathrel{\widehat{=}} \text{proper acceleration} \mathrel{\widehat{=}} \text{physical space} \mathrel{\widehat{=}} \text{relativistic aether} \mathrel{\widehat{=}} \text{vacuum}. \tag{3}$$

The symbol $\widehat{=}$ denotes identity of physical sector, not equality between tensors or observables of different mathematical type. Curvature, an observer's four-acceleration, the induced spatial metric, a causal cone, and a vacuum solution remain distinct objects. The statement is that they are dynamical, kinematic, geometric, causal-inertial, and state descriptions of one gravitational–clock architecture. In particular, identifying physical space with the clock-orthogonal state of the metric does not erase the distinction between removable connection coefficients and invariant tidal curvature.

A coordinate-only clock cannot realize these ideas. If a homogeneous clock has no action, stress, momentum, constraint contribution, or nontrivial coupling, the lapse cancels from the Friedmann equations and no relational observable changes. The theory must therefore cross a precise no-free-clock boundary by making T dynamical.

The single-metric seed operator template is

$$\boxed{S_{\mathrm{seed}} = \frac{M_{\mathrm{Pl}}^2}{2}\int \mathrm{d}^4x\,\sqrt{-g}\,\Big[R + 2\mathcal{K}(Q) + 2\mathcal{B}(Q)\Theta - 2a_0^2\mathcal{J}(Y)\Big] + S_{\mathrm{vis}}[\Psi, g_{\mu\nu}].} \tag{4}$$

Here Q is the norm of the timelike clock gradient, Θ is the expansion of the clock congruence, and Y is its squared acceleration in units of a_0^2. All visible matter, photons, neutrinos, and tensor gravitational waves couple to the same metric. The function $\mathcal{K}(Q)$ supplies the exterior finite-stiffness, approximately pressureless regime; $\mathcal{B}(Q)\Theta$ kinetically braids the clock norm with expansion and permits late self-acceleration; and $\mathcal{J}(Y)$ modifies the stationary lapse constraint to give a MOND/AQUAL-type galactic force law. The completed SCFT-A action below changes the kinetic function in a small neighborhood of $Q = 1$ and adds spatial operators with positive floors. Its spatially flat exterior background agrees with this seed template; its exterior perturbation action differs. The action contains no separate cold-dark-matter action, dark-energy fluid, bare cosmological constant, or second matter metric.

The closest action-level precedents are kinetic gravity braiding and relativistic khronon theories [6–9]. The former supplies scalar–metric kinetic mixing and self-accelerating branches; the latter combines a scalar foliation, generalized-dark-matter behavior, MOND-like galactic dynamics, and universal metric coupling. The present construction adds the reciprocal clock condition, a compact braiding sector that generates acceleration without $\mathcal{J}(0)$ or a bare Λ, and a field-first interpretation in which the same scalar is the physical ordering field. It is also distinct from TeVeS and AeST, which contain an independent vector sector [10, 11]; from mimetic dust, which uses an exact constraint [12, 13]; and from timescape cosmology, where clock differences arise from inhomogeneous averaging rather than a local propagating clock scalar [14, 15].

The completed action is specified in Equation (59). Its compact kinetic interpolation matches the local DBI exterior to all orders, while its spatial completion has uniform positive floors. The all-momentum local-transition theorem in Theorem XIII.1 includes every switch derivative. The exact nonlinear auxiliary operators and their coercive domain appear in Sections VI A and VI L. The nonlinear results are distinguished in Section XIV C: the exact vacuum gravity–clock Cauchy equations are locally Hadamard well posed on an open strongly regular boundaryless torus domain, with tame lapse–trace reconstruction, a loss-free sixth-order energy, existence, uniqueness, continuous dependence, and propagation of the full constraint set. The theorem is local in time and does not assert a nonlinear initial-boundary-value result or an unconditional extension to an unspecified visible-matter evolution system.

Every numerical perturbation result in this paper is calculated from Equation (59), with the spatial completion retained. The homogeneous exterior is unchanged, but its perturbations are not. The completed matter reduction gives the fixed-background ultraviolet factor Equation (445), the canonical evolution Equation (482), and the nonzero metric slip Equation (486). The response calculation on $1 \le a \le 10$ uses a specified finite-time baryon-density input, not a primordial transfer prescription. No two-derivative mode data are used as evidence for the completed action.

The revised coefficient point separates the local spatial scale from H_d^{-1}. Its endpoint spectrum and decreasing scalar energy are proved in Sections XII B and XII C; its stationary hierarchy is checked exactly in Section XX C. The switches, floors, and very small coupling are existence choices supported by inequalities. No microscopic mechanism selects them. The source-free and loaded numerical backgrounds, figures, and response tables below all use the revised point.

A. Conventions

The metric signature is $(-,+,+,+)$ and $c = \hbar = 1$. The coefficient of the Einstein–Hilbert term defines the action-level coupling $G_* \equiv (8\pi M_{\rm Pl}^2)^{-1}$. For the acceleration function adopted below, the locally measured high-acceleration Newton constant is $G_{\rm N} = \gamma_{\rm N} G_*$. Greek indices are spacetime indices and Latin indices are spatial indices on a clock-selected leaf. A dot denotes differentiation with respect to matter proper time t unless another time variable is displayed explicitly. The clock field T has dimensions of time, so Q is dimensionless; $\mathcal{K}$ has dimensions of inverse time squared, $\mathcal{B}$ of inverse time, a_0 of inverse time, and $\mathcal{J}$ is dimensionless.

II. COVARIANT SPACE-CLOCK KINEMATICS

The four-dimensional metric description is retained exactly. The physical proposal is that operational spacetime is reconstructed from a gravitational field, a clock field, matter fields, and their couplings, rather than treated as an additional substance beyond those fields. A differentiable manifold supplies topology, differentiability, tensor bundles, and an integration domain; lengths, durations, and causal relations arise only after the dynamical fields are specified.

A. Clock geometry and physical space

Let $T(x)$ have timelike gradient on a domain $\mathcal{U} \subset \mathcal{M}$,

$$Q \equiv \sqrt{-g^{\mu\nu}\nabla_\mu T \nabla_\nu T} > 0. \tag{5}$$

The future-directed unit normal to the leaves $T =$ constant and the orthogonal projector are

$$u_\mu = -\frac{\nabla_\mu T}{Q}, \qquad h_{\mu\nu} = g_{\mu\nu} + u_\mu u_\nu, \qquad h_\mu{}^\nu u_\nu = 0. \tag{6}$$

The intrinsic spatial geometry is the pullback of $h_{\mu\nu}$ to a leaf Σ_T. The Lorentzian metric recomposes exactly as

$$g_{\mu\nu} = h_{\mu\nu} - u_\mu u_\nu. \tag{7}$$

This is the orthogonal decomposition of one metric, not a second-metric construction. The expansion and acceleration of the clock congruence are

$$\Theta \equiv \nabla_\mu u^\mu, \tag{8}$$

$$\mathcal{A}_\mu \equiv u^\nu \nabla_\nu u_\mu = -h_\mu{}^\nu \nabla_\nu \ln Q, \tag{9}$$

$$Y \equiv \frac{\mathcal{A}_\mu \mathcal{A}^\mu}{a_0^2} \ge 0. \tag{10}$$

On an FLRW solution, $\mathcal{A}_\mu = 0$ and $\Theta = 3H$.

The field-first interpretation can be stated precisely. The metric is the gravitational field; $h_{\mu\nu}$ is its clock-orthogonal spatial state; and T supplies physical temporal ordering, foliation, momentum, calibration, and backreaction.

Operational spacetime is the collection of relational observables generated by $(g_{\mu\nu}, T, \Psi)$ and their couplings. Thus physical space is not a passive container surrounding gravity. It is the geometry carried by the gravitational field on the simultaneity leaves selected by the clock.

If γ lies within one leaf, its spatial length is

$$L[\gamma; T_0] = \int_\gamma \sqrt{h_{\mu\nu}\, \mathrm{d}x^\mu \mathrm{d}x^\nu}. \tag{11}$$

For a timelike worldline Γ followed by matter universally coupled to $g_{\mu\nu}$, the proper time is

$$t[\Gamma] = \int_\Gamma \sqrt{-g_{\mu\nu}\, \mathrm{d}x^\mu \mathrm{d}x^\nu}. \tag{12}$$

The scalar value T is not automatically equal to this proper time. Coordinate time x^0 is a chart label, clock-field time T orders the preferred foliation, and matter proper time t is the invariant worldline functional in Equation (12).

B. Dual time with one physical metric

Along a homogeneous worldline comoving with the clock congruence,

$$\frac{\mathrm{d}T}{\mathrm{d}t} = u^\mu \nabla_\mu T = Q, \qquad \mathrm{d}T = Q\,\mathrm{d}t, \qquad \mathcal{N}_T \equiv \frac{\mathrm{d}t}{\mathrm{d}T} = \frac{1}{Q}. \tag{13}$$

There are therefore two physical derivatives of one scale factor,

$$H \equiv \frac{1}{a}\frac{\mathrm{d}a}{\mathrm{d}t}, \qquad H_T \equiv \frac{1}{a}\frac{\mathrm{d}a}{\mathrm{d}T} = \mathcal{N}_T H = \frac{H}{Q}, \qquad H = QH_T. \tag{14}$$

No second metric is required. The distinction between t and T is physical because T is a field with its own momentum and stress. For any homogeneous scalar observable F,

$$\frac{\mathrm{d}F}{\mathrm{d}T} = \mathcal{N}_T \frac{\mathrm{d}F}{\mathrm{d}t} = \frac{1}{Q}\frac{\mathrm{d}F}{\mathrm{d}t}. \tag{15}$$

Definition II.1 (Reciprocal space-clock branch)**.** A homogeneous solution belongs to the reciprocal space-clock branch on an interval if $Q > 0$, $H > 0$, and

$$\frac{\mathrm{d}\mathcal{N}_T}{\mathrm{d}H} < 0 \tag{16}$$

along the physical cosmological trajectory. Equivalently, Q and H vary in the same direction whenever $\dot{H} \neq 0$.

The reciprocal statement is therefore an on-shell response of one physical clock to the gravitational evolution, not a coordinate convention.

III. EXTENDED EQUIVALENCE PRINCIPLE

The ordinary equivalence principle identifies local freely falling physics with special-relativistic physics at an event. It does not identify curvature with proper acceleration and does not remove tidal effects. The present extension preserves these distinctions while asserting that gravity, acceleration, physical space, relativistic aether, and vacuum need not be independent substrates.

Let

$$\mathfrak{G}_T \equiv \big(g_{\mu\nu}, T; S_{\text{grav+clock}}, S_{\text{coupling}}\big) \tag{17}$$

denote the gravitational–clock sector. We write

$$\text{gravity} \mathrel{\widehat{=}} \text{proper acceleration} \mathrel{\widehat{=}} \text{physical space} \mathrel{\widehat{=}} \text{relativistic aether} \mathrel{\widehat{=}} \text{vacuum}, \tag{18}$$

where $\widehat{=}$ denotes identity of physical sector rather than equality of mathematical type.

Postulate III.1 (Extended equivalence principle)**.** Gravity, proper acceleration, physical space, relativistic aether, and vacuum are respectively the dynamical, local-kinematic, spatial-geometric, causal-inertial, and state descriptions of the single gravitational–clock sector $\mathfrak{G}_T$. This role identity does not license componentwise identification of the Riemann tensor, an observer's four-acceleration, the induced metric, a characteristic cone, or a vacuum solution.

A. Curvature and proper acceleration

For an observer with unit tangent w^μ, proper acceleration is

$$a^\mu[w] = w^\nu \nabla_\nu w^\mu, \qquad a_\mu w^\mu = 0. \tag{19}$$

A freely falling observer has $a^\mu = 0$ even in curved geometry, whereas a Rindler observer has $a^\mu \neq 0$ in flat geometry. At an event one may choose local inertial coordinates satisfying

$$g_{\mu\nu}(p) = \eta_{\mu\nu}, \qquad \Gamma^\mu{}_{\alpha\beta}(p) = 0, \tag{20}$$

but geodesic deviation remains

$$\frac{D^2\xi^\mu}{\mathrm{d}t^2} = -R^\mu{}_{\nu\alpha\beta} w^\nu \xi^\alpha w^\beta. \tag{21}$$

The extended principle therefore relates physical roles without erasing the invariant distinction between kinematics and curvature.

B. Space, aether, and vacuum

On each leaf Σ_T, $h_{\mu\nu}$ determines lengths, areas, volumes, and intrinsic curvature. In this precise sense, physical space is the state of the gravitational field after the clock field specifies simultaneity. Tensor perturbations transverse and traceless with respect to h_{ij} describe spatial strain. Perturbative quantization of a healthy tensor sector would identify its spin-two quanta as gravitons. The classical tensor calculation below neither demonstrates graviton detection nor constructs a quantum completion.

The term *relativistic aether* refers to a causal and inertial field structure, following Einstein's nonmechanical terminology [16]. The dynamical preferred foliation can nevertheless produce preferred-frame gravitational effects; universal matter coupling alone does not exclude them. The preferred direction u^μ is physical because it is constructed from the dynamical clock, while photons and tensors share the low-momentum propagation speed. The completed tensor action is dispersive at finite momentum, as derived in Section XI.

Vacuum denotes a source-free, ground-state, or low-invariant solution of the coupled field equations, with its precise meaning fixed by the action and boundary conditions. It is not the absence of $g_{\mu\nu}$ or T, and it need not be globally flat. This interpretation does not by itself cancel quantum vacuum energy; it specifies which field state carries the classical late-time stress.

IV. COORDINATE-ONLY CLOCK THEOREM

A field-first interpretation does not make a clock physical by assertion. A scalar used only as a label is gauge.

Theorem IV.1 (Coordinate-only clock no-go)**.** *Let gravity be described by the Einstein–Hilbert action, let all matter species be minimally coupled to one metric $g_{\mu\nu}$, and let a proposed homogeneous clock carry no stress, no conjugate momentum, no modification of the gravitational constraint, and no nontrivial matter coupling. Replacing a coordinate time by that clock cannot alter any relational cosmological observable, including the Friedmann and acceleration equations measured by matter proper time.*

Proof. Write

$$\mathrm{d}s^2 = -N^2(T)\mathrm{d}T^2 + a^2(T)\mathrm{d}\boldsymbol{x}^2, \qquad \mathrm{d}t = N\mathrm{d}T, \qquad H = \frac{1}{N}\frac{1}{a}\frac{\mathrm{d}a}{\mathrm{d}T}. \tag{22}$$

For comoving matter, $G_{00} = 3N^2H^2$ and $T_{00} = N^2\rho$, so the common factor cancels:

$$3M_{\mathrm{Pl}}^2 H^2 = \rho. \tag{23}$$

For pressureless matter and radiation, $\rho_m \propto a^{-3}$ and $\rho_r \propto a^{-4}$, while the spatial equation gives

$$\frac{\ddot{a}}{a} = -\frac{\rho_m + 2\rho_r}{6M_{\mathrm{Pl}}^2} \leq 0. \tag{24}$$

Neither equation depends on the coordinate lapse. A monotonic replacement $T \mapsto f(T)$ changes N and the coordinate derivative but leaves t, H, redshift, and all relational observables unchanged. $\square$

Corollary IV.2 (Physicality criterion)**.** *A reciprocal clock relation can affect observables only if the clock carries effective stress or a conserved charge, modifies a gravitational constraint or kinetic operator, or enters a specified nontrivial coupling. A dynamically empty lapse cannot produce missing gravity.*

The action in Equation (4) crosses this boundary in three ways: the $\mathcal{K}$ and $\mathcal{B}$ terms contribute stress and change the lapse constraint, shift symmetry produces a conserved clock charge, and $\mathcal{J}(Y)$ modifies the weak-field constraint. Space-Clock Field Theory is therefore a modified-gravity theory with a physical clock degree of freedom.

The technical contribution studied below is a classical construction with positive scalar quadratic coefficients on specified vacuum backgrounds. The construction is an existence example within an established foliation-based operator class. It is not presented as a demonstrated replacement for the observed dark sector. In particular, the low-charge DBI interval and the cosmological branch ending at Q_d are different solution regimes, and the revised coefficients supply a controlled local stationary ordering at a declared subhorizon scale. No claim of cosmologically matched galactic behavior is made beyond that stated local operator regime. These distinctions delimit the opening motivation; the exact scale test is given in Sec. XX C.

V. SINGLE-METRIC ACTION AND THE FIXED SCFT-A BENCHMARK

The final SCFT-A action is a single-metric, single-clock theory. The exterior seed functions $(\mathcal{K}_{\mathrm{A}}, \mathcal{B}_{\mathrm{A}}, \mathcal{J}_{\mathrm{A}})$ define the reference cosmology. The adopted functions are the convex local kinetic profile $\widetilde{\mathcal{K}}$, the smoothed acceleration function $\mathcal{J}_{\mathrm{A},\sigma}$, and the positive spatial coefficients $\nu, \ell, \tau_6, \eta_R$. The decomposition is

$$S_{\mathrm{SCFT-A}} = S_{\mathrm{EH}} + S_T + S_{\mathrm{vis}}, \tag{25}$$

$$S_{\mathrm{EH}} = \frac{M_{\mathrm{Pl}}^2}{2} \int \mathrm{d}^4x \sqrt{-g}\, R, \tag{26}$$

$$S_{\mathrm{vis}} = \sum_A S_A[\Psi_A, g_{\mu\nu}], \qquad A \in \{\text{baryons, photons, neutrinos, Standard Model fields}\}. \tag{27}$$

There is no S_{cdm}, no S_{DE}, no cosmological-constant term, and no metric other than $g_{\mu\nu}$. The action is invariant under spacetime diffeomorphisms and under the internal shift

$$T \longmapsto T + T_0. \tag{28}$$

The shift symmetry excludes an arbitrary clock potential and produces the conserved quantity that controls the homogeneous evolution.

A. Seed normalization, exterior branch, and exact-vacuum plateau

The seed exterior functions are normalized at the reference point $Q_m = 1$ by

$$\mathcal{K}_{\mathrm{A}}(1) = 0, \qquad \mathcal{K}_{\mathrm{A},Q}(1) = 0, \qquad \mathcal{K}_{\mathrm{A},QQ}(1) = \kappa_m > 0, \tag{29}$$

and a constant part of $\mathcal{B}_{\mathrm{A}}$ is fixed by

$$\mathcal{B}_{\mathrm{A}}(1) = 0. \tag{30}$$

For the galactic function we impose

$$\mathcal{J}_{\mathrm{A}}(0) = 0, \tag{31}$$

so the homogeneous FLRW background does not inherit an acceleration from an additive constant in the MOND sector. Within the seed operator set and its exact MOND normalization, finite stiffness at the exact flat vacuum gives the negative quadratic direction derived in Section XII J. The revised theory therefore replaces the seed function only inside a compact clock-norm neighborhood of $Q = 1$.

B. Operator roles

The exterior $\mathcal{K}$ sector controls clock stiffness, conserved charge, and the matter-like regime; $\mathcal{B}\Theta$ supplies expansion–clock braiding. The acceleration term modifies the stationary lapse constraint. The completed action replaces the old momentum-independent $-\lambda_{\rm M}\Theta^2$ repair by $-\nu(Q)D_i\Theta D^i\Theta$, retains $-\ell(Q)^{(3)}RD_i\mathcal{A}^i$, and adds $-\tau_6 D_i{}^{(3)}R_{jk}D^{i(3)}R^{jk}$. The last term supplies a positive sixth-order tensor restoring contribution. The additional $-\eta_R{}^{(3)}R^2$ term supplies a positive fourth-order scalar restoring contribution. These are spatial derivatives in the clock foliation; they introduce no lapse or shift time derivative.

C. Explicit benchmark SCFT-A

The functional freedom is reduced to one fixed benchmark family whose branch geometry is specified directly in the action. For $C_T > 0$ in the exterior seed region, the unbraided current gives $\mathcal{K}_{{\rm A},Q} = C_T a^{-3} > 0$ and hence $Q > Q_m$. A continuous trajectory carrying finite positive charge cannot cross a point at which $\mathcal{K}_{{\rm A},Q} = \mathcal{B}_{{\rm A},Q} = 0$, because the left-hand side of the current equation would vanish there. The displaced late point is placed on the same side of the seed condensate,

$$Q_m = 1, \qquad Q_d = 1 + \Delta Q, \qquad \Delta Q > 0. \tag{32}$$

Late braiding is confined to a compact clock interval so that it is absent both near Q_m and again at very high charge.

Define the standard flat switch

$$f(x) = \begin{cases} 0, & x \le 0, \\ \exp(-1/x), & x > 0, \end{cases} \qquad S(x) = \frac{f(x)}{f(x) + f(1-x)}, \tag{33}$$

and set

$$\xi(Q) = \frac{Q-1}{\Delta Q}, \qquad \nu_{\rm A} > \frac{1}{4}, \qquad W(Q) = S(4\xi - 2)S\left(\frac{1 + \nu_{\rm A} - \xi}{\nu_{\rm A} - \frac{1}{4}}\right). \tag{34}$$

The window is C^∞ and obeys

$$W(Q) = 0, \qquad Q \le Q_L \text{ or } Q \ge Q_R, \qquad Q_L \equiv 1 + \frac{\Delta Q}{2}, \qquad Q_R \equiv 1 + (1 + \nu_{\rm A})\Delta Q, \tag{35}$$

$$W(Q) = 1, \qquad 1 + \frac{3\Delta Q}{4} \le Q \le 1 + \frac{5\Delta Q}{4}. \tag{36}$$

The globally evolving benchmark in Section XVII fixes $\nu_{\rm A} = 30$ before the trajectory is integrated; it is not varied as a redshift-dependent fit function.

Let

$$\mathcal{K}_{\rm DBI}(Q) = \frac{\kappa_m}{\lambda_D}\left[1 - \sqrt{1 - \lambda_D (Q-1)^2}\right], \tag{37}$$

$$\mathcal{K}_d(Q) = -3H_d^2 - 3H_d b_d (Q - Q_d) + \frac{\kappa_d}{2}(Q - Q_d)^2, \tag{38}$$

with

$$\begin{gathered} H_d > 0, \qquad \kappa_m > 0, \qquad \lambda_D > 0, \qquad b_d > 0, \\ -\frac{3}{2}b_d^2 < \kappa_d < 0, \qquad 0 < Q_d b_d < 2H_d, \qquad \lambda_D\left[(1 + \nu_{\rm A})\Delta Q\right]^2 < 1. \end{gathered} \tag{39}$$

Define the real DBI interval and the final positive-clock action domain by

$$Q_- \equiv \max\left\{0, 1 - \lambda_D^{-1/2}\right\}, \qquad Q_+ \equiv 1 + \lambda_D^{-1/2}, \qquad \mathcal{D}_{\rm DBI} = (Q_-, Q_+), \qquad \mathcal{D}_Q = (Q_-, \infty). \tag{40}$$

On the low- and intermediate-charge part of the seed exterior function, $Q \le Q_R$, define

$$\mathcal{K}_{\rm A}(Q) = [1 - W(Q)]\mathcal{K}_{\rm DBI}(Q) + W(Q)\mathcal{K}_d(Q), \qquad Q \le Q_R, \tag{41}$$

$$\mathcal{B}_{\rm A}(Q) = b_d (Q - Q_d) W(Q), \qquad Q \in \mathcal{D}_Q. \tag{42}$$

The kinetic function matches the DBI profile to all orders at Q_R and is continued smoothly for $Q > Q_R$ by the primordial definition in Section XVI B; the finite DBI boundary is therefore not part of the final SCFT-A action domain.

D. An exact convex kinetic interpolation

The local construction fixes $\lambda_D = 1$, as in the displayed cosmological benchmark. It is given first for $Q > 1$. Set

$$Q_a = \frac{1001}{1000}, \qquad Q_b = \frac{101}{100}, \qquad L = Q_b - Q_a = \frac{9}{1000}, \qquad \epsilon = \frac{1}{10^6}. \tag{43}$$

Write $U = \kappa_m u$, where $\kappa_m > 0$, and use the local exterior function

$$u_e(Q) = 1 - \sqrt{1-(Q-1)^2}. \tag{44}$$

The step agrees with Equation (33); define the accompanying bump by

$$S(z) = \begin{cases} 0, & z \le 0, \\ [1+\exp(1/z - 1/(1-z))]^{-1}, & 0 < z < 1, \\ 1, & z \ge 1, \end{cases}$$
$$b(z) = \begin{cases} e^{-1/[z(1-z)]}, & 0 < z < 1, \\ 0, & \text{otherwise}. \end{cases} \tag{45}$$

The endpoint data, ramp, and two moments are

$$F_b = u_e'(Q_b) = \frac{1}{\sqrt{9999}}, \qquad u_b = u_e(Q_b) = \frac{1}{100(100+\sqrt{9999})},$$
$$g_R(Q) = u_e''(Q) S\left(\frac{Q - Q_b + \epsilon}{\epsilon}\right), \qquad G_j = \int_{Q_a}^{Q_b} Q^j g_R(Q)\mathrm{d}Q \quad (j = 0, 1),$$
$$F_0 = F_b - G_0, \qquad \bar{Q} = \frac{Q_b F_b - u_b - G_1}{F_0}. \tag{46}$$

For $\phi_\theta(Q) = b((Q-Q_a)/L)e^{\theta(Q-Q_a)/L}$, choose the unique real θ and the positive constant c satisfying

$$\frac{\int_{Q_a}^{Q_b} Q\phi_\theta(Q)\mathrm{d}Q}{\int_{Q_a}^{Q_b} \phi_\theta(Q)\mathrm{d}Q} = \bar{Q}, \qquad c = \frac{F_0}{\int_{Q_a}^{Q_b} \phi_\theta(Q)\mathrm{d}Q}. \tag{47}$$

Define

$$u(Q) = \begin{cases} 0, & Q \le Q_a, \\ \displaystyle\int_{Q_a}^{Q} (Q-r)[g_R(r) + c\phi_\theta(r)]\mathrm{d}r, & Q_a < Q < Q_b, \\ u_e(Q), & Q \ge Q_b \text{ in the local DBI region}. \end{cases} \tag{48}$$

Lemma V.1 (Existence, convexity, and all-orders matching)**.** *Equations* (47)–(48) *define a* C^∞ *function. Its derivatives* $F = u'$ *and* $g = u''$ *are strictly positive on* (Q_a, Q_b)*. All derivatives match the zero plateau and the local exterior function.*

Proof. On the ramp support, $0 < u_e'' < 2$, and hence $0 < G_0 < 2\epsilon$. The exact rational bounds

$$\frac{1}{100} < F_b < \frac{1}{99}, \qquad \frac{1}{20000} < u_b < \frac{1}{19900} \tag{49}$$

give

$$F_0 > \frac{1}{100} - 2\epsilon > 0,$$
$$u_b - (Q_b G_0 - G_1) > \frac{1}{20000} - 2\epsilon^2 > 0,$$
$$L F_b - u_b - (G_1 - Q_a G_0) > \frac{L}{100} - \frac{1}{19900} - 2L\epsilon > 0. \tag{50}$$

The last two inequalities say $Q_a < \bar{Q} < Q_b$. The derivative of the weighted mean in (47) is $\mathrm{Var}_\theta(Q)/L > 0$; its limiting values are Q_a and Q_b. Thus θ exists uniquely. The total mass of $g_R + c\phi_\theta$ is F_b, and its first moment is $Q_b F_b - u_b$. These give the value and first derivative at the right endpoint. The ramp matches u_e'' to every order there; the bump is flat at both ends. At the left endpoint every derivative vanishes. Finally $g > 0$ inside, and $F(Q) = \int_{Q_a}^{Q} g(r)\mathrm{d}r > 0$. □

An even extension about $Q = 1$ defines the lower local coefficient profiles: replace their argument by $1 + |Q - 1|$. The central functions are constant, so the absolute value creates no nonsmoothness. Outside $|Q - 1| < 1/100$, retain the original full exterior SCFT-A kinetic, braid, and acceleration-prefactor functions. The spatial completion operators retain the positive coefficients (322); consequently the homogeneous exterior solution is unchanged, while its inhomogeneous perturbation action contains the uniform completion. The positive floors are part of the action at every clock norm. No source-free flat expanding branch is asserted on the lower side: there $QU' - U < 0$.

$$\widetilde{\mathcal{K}}(Q) = \begin{cases} \kappa_m u(1 + |Q - 1|), & |Q - 1| < 1/100, \\ \mathcal{K}_{\mathrm{A}}(Q), & |Q - 1| \geq 1/100, \end{cases} \qquad d_1 = \frac{1}{1000}, \quad d_2 = \frac{1}{100}. \tag{51}$$

The plateau is $|Q - 1| \leq d_1$, and the matching surfaces are $|Q - 1| = d_2$. In particular,

$$d_2 = \frac{1}{100} < Q_L - 1 = \frac{3}{200} < Q_d - 1 = \frac{3}{100}. \tag{52}$$

The parameter κ_m remains the exterior seed stiffness; it is not $\widetilde{\mathcal{K}}_{,QQ}(1)$, which vanishes exactly.

The acceleration function is fixed by a constraint-safe MOND interpolation. Introduce one dimensionless high-acceleration transition parameter

$$s_{\mathrm{N}} > 1, \qquad \gamma_{\mathrm{N}} \equiv 1 + \frac{1}{s_{\mathrm{N}}}, \tag{53}$$

and define, for $s \geq 0$,

$$\boxed{\mu_{\mathrm{A}}(s) \equiv 1 - \frac{1}{(1 + s)\,(1 + s^2/s_{\mathrm{N}}^2)}.} \tag{54}$$

The seed acceleration function is the unique normalization with $\mathcal{J}_{\mathrm{A}}(0) = 0$ and

$$\boxed{\mathcal{J}_{\mathrm{A},Y}(Y) = \frac{\mu_{\mathrm{A}}(\sqrt{Y})}{\gamma_{\mathrm{N}}} - 1, \qquad \mathcal{J}_{\mathrm{A}}(Y) = \int_0^Y \left[\frac{\mu_{\mathrm{A}}(\sqrt{z})}{\gamma_{\mathrm{N}}} - 1\right] \mathrm{d}z, \qquad Y \geq 0.} \tag{55}$$

A closed elementary form for this seed is given in Supplemental Material, Eq. (D23). With $G_* \equiv (8\pi M_{\mathrm{Pl}}^2)^{-1}$, the locally measured high-acceleration Newton constant is

$$G_{\mathrm{N}} = \gamma_{\mathrm{N}} G_*. \tag{56}$$

The base acceleration operator is

$$\widehat{\mathcal{J}}_{\mathrm{A}}(Q, Y) \equiv \Sigma_{\mathrm{A}}(Q) \mathcal{J}_{\mathrm{A}}(Y), \tag{57}$$

where the positive clock-norm profile $\Sigma_{\mathrm{A}}(Q)$ is specified exactly in Equations (452) and (453). It equals unity throughout the vacuum, late-time, and stationary galactic sectors.

E. Smooth acceleration tip

The adopted acceleration function regularizes the seed tip exactly. For $\sigma > 0$ first let

$$\begin{aligned} \widehat{\mu}_\sigma(Y) &= [1 - S((Y - \sigma^2)/(3\sigma^2))] \frac{\mu(\sigma)}{\sigma^2} Y + S((Y - \sigma^2)/(3\sigma^2)) \mu(\sqrt{Y}), \\ A_\sigma &= \frac{\displaystyle\int_0^{4\sigma^2} [\mu(\sqrt{z}) - \widehat{\mu}_\sigma(z)]\,\mathrm{d}z}{\displaystyle\int_0^{4\sigma^2} b(z/(4\sigma^2))\,\mathrm{d}z}, \qquad \mu_\sigma(Y) = \widehat{\mu}_\sigma(Y) + A_\sigma b(Y/(4\sigma^2)), \\ \mathcal{J}_{\mathrm{A},\sigma}(Y) &= \int_0^Y \left[\frac{\mu_\sigma(z)}{\gamma_{\mathrm{N}}} - 1\right] \mathrm{d}z. \end{aligned} \tag{58}$$

Here $\mu(s) = \mu_{\mathrm{A}}(s)$, and S, b are defined in Section V D. The denominator defining A_σ is positive. The moment condition makes $\mathcal{J}_{\mathrm{A},\sigma} = \mathcal{J}_{\mathrm{A}}$ exactly for $Y \geq 4\sigma^2$, while both vanish at $Y = 0$. Near $Y = 0$, $\mu_\sigma(Y) = \mu(\sigma)Y/\sigma^2$ plus a smooth function flat at zero, so $\mathcal{J}_{\mathrm{A},\sigma}$ is C^∞ as a function of the Cartesian components q_i. The subscript σ denotes the adopted regularization; the seed function remains $\mathcal{J}_{\mathrm{A}}$.

TABLE I. Parameter ledger for the revised SCFT-A benchmark. The locally measured Newton constant fixes the action-level Planck scale only after $s_{\rm N}$ fixes $\gamma_{\rm N}$. The spatial coefficients have exact positive floors and are fixed by the construction.

Symbol	Dimension	Restriction/status	Function in the benchmark
$M_{\rm Pl}$	time^{-1}	$G_* = (8\pi M_{\rm Pl}^2)^{-1}$	Tensor/action gravitational normalization; $G_{\rm N} = \gamma_{\rm N} G_*$.
H_d	time^{-1}	$H_d > 0$	Sets the late self-accelerating fixed-point scale.
a_0	time^{-1}	$a_0 > 0$	Fixed low-acceleration scale in $Y = \mathcal{A}^2/a_0^2$; it is not promoted to $a_0(H)$ in SCFT-A.
$s_{\rm N}$	1	$s_{\rm N} > 1$	Transition to the s^{-3} Newtonian tail and sufficient lapse-Hessian offset.
ΔQ	1	$\Delta Q > 0$ and Equation (39)	Places $Q_d = 1 + \Delta Q$ and fixes the lower switch and late plateau.
$\nu_{\rm A}$	1	$\nu_{\rm A} > 1/4$; fixed to 30 in Section XVII	Controls the upper return from the late plateau to the unbraided high-charge completion.
λ_D	1	$\lambda_D > 0$	Controls the exterior DBI profile and all-orders matching data at Q_R; the asymptotic high-charge slope is $\lambda_\infty = 8$.
κ_m	time^{-2}	$\kappa_m > 0$	Curvature of the exterior seed $\mathcal{K}_{\rm A}$ near $Q = 1$; it is not $\widetilde{\mathcal{K}}_{,QQ}(1)$.
δ	1	Exact positive value in Equation (339)	Fixes the uniform trace-gradient and curvature-gradient coefficients.
ℓ, ν	time^2	Equation (321)	Uniform spatial operators; $\tau_6 = \delta^2/\kappa_m^2$.
η_R	time^2	$1/(2\kappa_m)$	Constant intrinsic-curvature coefficient; positive endpoint restoring completion.
b_d	time^{-1}	$b_d > 0$ and $Q_d b_d < 2H_d$	Late braiding slope; the upper bound keeps the infrared endpoint momentum coefficient positive.
κ_d	time^{-2}	$-3b_d^2/2 < \kappa_d < 0$	Late curvature; the chosen curvature satisfies $\Xi_d > 0$; the reciprocal sign uses the full finite-charge limit in Equation (182).
C_T	time^{-2}	initial data, normally $C_T > 0$	Conserved homogeneous clock charge; fixes the amplitude of the exterior matter-like clock contribution.
Visible data	model dependent	initial densities and perturbations	Baryons, photons, neutrinos, and Standard Model fields in $S_{\rm vis}$; no cold-dark-matter density is added.

F. Adopted action and the analytic reference truncation

$$\boxed{\begin{aligned} S_{\rm SCFT-A} = \frac{M_{\rm Pl}^2}{2}\int {\rm d}^4x\sqrt{-g}\Big[&R + 2\widetilde{\mathcal{K}}(Q) + 2\mathcal{B}_{\rm A}(Q)\Theta - 2a_0^2\Sigma_{\rm A}(Q)\mathcal{J}_{{\rm A},\sigma}(Y) \\ &- \nu(Q)D_i\Theta D^i\Theta - \ell(Q)\,{}^{(3)}\!R D_i\mathcal{A}^i \\ &- \tau_6 D_i{}^{(3)}\!R_{jk}D^{i\,(3)}\!R^{jk} - \eta_R\,{}^{(3)}\!R^{\,2}\Big] + S_{\rm vis}. \end{aligned}} \tag{59}$$

All spatial contractions are intrinsic to the clock leaf. The coefficient dimensions and exact floors are

$$[\nu] = [\ell] = [\eta_R] = \text{time}^2, \quad [\tau_6] = \text{time}^4, \qquad \nu \geq \frac{\delta}{2\kappa_m} > 0, \quad \ell \geq \frac{1}{2\kappa_m} > 0, \quad \tau_6 = \frac{\delta^2}{\kappa_m^2} > 0, \quad \eta_R = \frac{1}{2\kappa_m} > 0. \tag{60}$$

The ordered profiles and the exact positive choice of δ are Equations (321) and (339); the regulator is Equation (157). These are fixed action data, not functions fitted to an evolution. No momentum-independent trace-square repair term is present. The floors persist in the exterior; their homogeneous values cannot be used to omit their perturbations. We denote by S_0 the reference action obtained by setting $\nu = \ell = \tau_6 = \eta_R = 0$, restoring the seed kinetic function $\mathcal{K}_{\rm A}$ in place of the local plateau $\widetilde{\mathcal{K}}$, and restoring $\mathcal{J}_{\rm A}$ in place of $\mathcal{J}_{{\rm A},\sigma}$. In the exterior the completed and base actions share exactly the same spatially flat homogeneous solutions.

Equivalently, after $G_{\rm N}$ and $s_{\rm N}$ fix $M_{\rm Pl}$, the independent action information may be recorded as one dimensional scale and eight dimensionless ratios,

$$\boldsymbol{\theta}_{\rm A} = \left(H_d, \frac{a_0}{H_d}, s_{\rm N}, \Delta Q, \nu_{\rm A}, \lambda_D, \frac{\kappa_m}{H_d^2}, \frac{b_d}{H_d}, \frac{\kappa_d}{H_d^2}\right). \tag{61}$$

Here $\lambda_D = 1$ in the integrated local construction; $\delta = 10^{-140}$ and $\sigma = 10^{-6}$ are fixed rational choices certified by sufficient bounds. For the revised point $a_0/H_d = 1$ and $s_{\rm N} = 10$.

Proposition V.2 (SCFT-A endpoint and vacuum identities)**.** *The low/intermediate seed functions* (41) *and* (42) *are* C^∞ *through the matching point* Q_R*; the high-charge definition in Section XVI B extends* $\mathcal{K}_\mathrm{A}$ *smoothly over the full* $\mathcal{D}_Q$*. The repaired functions satisfy*

$$\widetilde{\mathcal{K}}(1) = \widetilde{\mathcal{K}}_{,Q}(1) = \widetilde{\mathcal{K}}_{,QQ}(1) = 0, \qquad \mathcal{K}_{\mathrm{A},QQ}(1) = \kappa_m, \qquad \frac{\mathrm{d}^n \mathcal{B}_\mathrm{A}}{\mathrm{d}Q^n}(1) = 0 \quad (n \geq 0), \tag{62}$$

$$\widetilde{\mathcal{K}}(Q_d) = \mathcal{K}_\mathrm{A}(Q_d) = -3H_d^2, \qquad \widetilde{\mathcal{K}}_{,Q}(Q_d) = -3H_d b_d, \qquad \widetilde{\mathcal{K}}_{,QQ}(Q_d) = \kappa_d, \tag{63}$$

$$\mathcal{B}_\mathrm{A}(Q_d) = 0, \qquad \mathcal{B}_{\mathrm{A},Q}(Q_d) = b_d, \qquad \mathcal{B}_{\mathrm{A},QQ}(Q_d) = 0. \tag{64}$$

Consequently the zero-charge de Sitter equations are identities at (Q_d, H_d)*, while*

$$\mathcal{D}(Q_d, H_d) = \kappa_d < 0, \qquad \left.\frac{\mathcal{B}_{,Q}}{\mathcal{D}}\right|_d = \frac{b_d}{\kappa_d} < 0, \qquad \Phi_{,Q}(Q_d) = \Xi_d = \kappa_d + \frac{3}{2}b_d^2 > 0. \tag{65}$$

Thus the benchmark has a simple algebraic late endpoint, a positive combined Dirac/scalar rank coefficient, a repaired exact zero-charge Minkowski state, and the reciprocal source-free approach established by Equation (182)*. The endpoint and differentiability identities are proved in Supplemental Material, Appendix F; the exact local-vacuum positivity is proved in Section XIII.*

G. Intrinsic spatial curvature completion

The final action contains the local foliation invariant

$$\Delta S_R = -\frac{M_\mathrm{Pl}^2 \eta_R}{2} \int \mathrm{d}^4x \sqrt{-g}\, {}^{(3)}\!R^2, \qquad \boxed{\eta_R = \frac{1}{2\kappa_m}}, \qquad \eta_R H_d^2 = \frac{1}{2 \cdot 10^{30}}. \tag{66}$$

Here ${}^{(3)}\!R$ is the intrinsic scalar curvature of the leaves of the existing clock T. It is not the four-dimensional Ricci scalar. Intrinsic spatial curvature operators belong to the established spatially covariant operator basis [18, 36]. The coefficient is constant, is fixed in the action, and adds no free parameter to the displayed benchmark.

On a spatially flat homogeneous state ${}^{(3)}\!R = 0$, so this term and its first variation vanish. The background clock current, Friedmann equations, reciprocal branch, and late self-acceleration therefore remain unchanged. In the clock slicing ${}^{(3)}\!R$ depends only on the spatial metric and its spatial derivatives. The term has no metric, lapse, or shift velocity. For the scalar perturbation, $\delta^{(3)}\!R = -4a^{-2}\partial^2\zeta$, giving

$$\frac{\Delta L_R^{(2)}}{M_\mathrm{Pl}^2 a^3} = -8\eta_R p^4 \zeta^2, \qquad \Delta K = 0, \qquad \Delta V = 8\eta_R p^4 > 0. \tag{67}$$

It also leaves the flat-FLRW tensor quadratic action unchanged, because the first-order intrinsic scalar curvature of a transverse-traceless tensor is zero. These facts allow the endpoint to be corrected without changing the background solution or introducing a higher-time-derivative mode. The full nonlinear Hamiltonian acquires the potential and lapse source displayed in Equation (83); the stationary and interaction equations below retain the same operator.

H. Relation of the braiding term to kinetic gravity braiding

The term $\mathcal{B}(Q)\Theta$ contains second derivatives of T in covariant notation, but it belongs to a degenerate, second-order scalar–tensor structure. The vacuum repair operators are not part of this kinetic-braiding map; they are spatial foliation operators on the clock leaves and are audited separately in Section XIII. Define

$$X \equiv -\frac{1}{2}\nabla_\mu T \nabla^\mu T = \frac{Q^2}{2}. \tag{68}$$

Using $u^\mu = -\nabla^\mu T/Q$ and discarding a boundary term,

$$\begin{aligned} \mathcal{B}(Q)\Theta &= -\frac{\mathcal{B}}{Q}\Box T + \frac{\mathcal{B}}{Q^2}\nabla_\mu T \nabla^\mu Q \\ &\doteq \frac{\mathcal{B}_{,Q}}{Q}\nabla_\mu T \nabla^\mu Q = \frac{\mathcal{B}_{,Q}}{Q^2}\nabla_\mu T \nabla^\mu X, \end{aligned} \tag{69}$$

where $\doteq$ denotes equality up to a total divergence. If $G_3(X)$ is defined by

$$G_{3,X}(X) = \frac{\mathcal{B}_{,Q}}{Q^2}, \qquad \frac{\mathrm{d}G_3}{\mathrm{d}Q} = \frac{\mathcal{B}_{,Q}}{Q}, \tag{70}$$

then

$$\mathcal{B}(Q)\Theta \doteq -G_3(X)\Box T. \tag{71}$$

This is the standard shift-symmetric kinetic-gravity-braiding sector [6]. The acceleration operator contributes spatial lapse derivatives. The four additional spatial operators require the separate Legendre and constraint analysis below.

Remark V.3. Equation (71) is an identity of the action up to a boundary term. It does not prove that every choice of $\mathcal{K}$, $\mathcal{B}$, and $\mathcal{J}$ is stable. It establishes that the higher-derivative covariant appearance of the braiding operator is degenerate in the standard kinetic-braiding sense.

I. Metric and clock equations

The metric equation can be written without concealing any source:

$$M_{\rm Pl}^2 G_{\mu\nu} = T_{\mu\nu}^{\rm vis} + T_{\mu\nu}^{T}, \qquad T_{\mu\nu}^{T} \equiv -\frac{2}{\sqrt{-g}}\frac{\delta S_T}{\delta g^{\mu\nu}}. \tag{72}$$

The $\mathcal{K}$ contribution is exactly

$$T_{\mu\nu}^{(\mathcal{K})} = M_{\rm Pl}^2\left[\mathcal{K}\, g_{\mu\nu} + Q\mathcal{K}_{,Q} u_\mu u_\nu\right]. \tag{73}$$

The braiding and acceleration contributions are most compactly defined by

$$\mathcal{E}_{\mu\nu}^{(\mathcal{B})} \equiv -\frac{2}{\sqrt{-g}}\frac{\delta}{\delta g^{\mu\nu}}\int \mathrm{d}^4x\sqrt{-g}\,\mathcal{B}(Q)\Theta, \tag{74}$$

$$\mathcal{E}_{\mu\nu}^{(\mathcal{J})} \equiv -\frac{2}{\sqrt{-g}}\frac{\delta}{\delta g^{\mu\nu}}\int \mathrm{d}^4x\sqrt{-g}\,a_0^2\mathcal{J}(Y), \tag{75}$$

so that

$$T_{\mu\nu}^{T} = T_{\mu\nu}^{(\mathcal{K})} + M_{\rm Pl}^2\mathcal{E}_{\mu\nu}^{(\mathcal{B})} - M_{\rm Pl}^2\mathcal{E}_{\mu\nu}^{(\mathcal{J})} + T_{\mu\nu}^{(\rm sp)}. \tag{76}$$

Here the acceleration variation uses $\Sigma_{\rm A}(Q)\mathcal{J}_{{\rm A},\sigma}(Y)$ and $T_{\mu\nu}^{(\rm sp)} = -2(\sqrt{-g})^{-1}\delta S_{\rm sp}/\delta g^{\mu\nu}$ includes all four spatial operators of Equation (59). The explicit FLRW and weak-field components are derived below and in the appendices. Keeping the covariant equation in variational form avoids hiding integrations by parts or branch assumptions inside an overcompressed expression.

Because the action is shift symmetric, the clock equation is a conservation law,

$$\nabla_\mu \mathscr{J}_T^\mu = 0. \tag{77}$$

For a Lagrangian with second derivatives, the exact Noether current may be represented as

$$\mathscr{J}_T^\mu = \frac{\partial \mathcal{L}_T}{\partial(\nabla_\mu T)} - \nabla_\nu\left[\frac{\partial \mathcal{L}_T}{\partial(\nabla_\mu\nabla_\nu T)}\right], \tag{78}$$

This second-derivative representation applies to the base clock Lagrangian. The completed current also contains the higher spatial-jet terms obtained by repeated integration by parts, or equivalently by promoting $T \mapsto T + \epsilon(x)$ in the full action and collecting the coefficient of $\nabla_\mu\epsilon$. Those contributions vanish on a spatially flat homogeneous background. The acceleration contribution is therefore included once. On FLRW it vanishes because $Y = 0$ and $\mathcal{J}(Q,0) = 0$, including for the regulated operator. With this convention $\mathscr{J}_T^0 = M_{\rm Pl}^2\mathcal{F}$ on the background. The conserved current J_{KB}^μ in Supplemental Material, Eq. (B4) uses the opposite overall sign and omits $M_{\rm Pl}^2$, so $\mathscr{J}_T^\mu = -M_{\rm Pl}^2 J_{KB}^\mu$ when the acceleration term is absent.

Diffeomorphism invariance gives the Noether identity

$$\nabla^\mu\left(M_{\rm Pl}^2 G_{\mu\nu} - T_{\mu\nu}^{\rm vis} - T_{\mu\nu}^{T}\right) = \left(\nabla_\mu \mathscr{J}_T^\mu\right)\nabla_\nu T. \tag{79}$$

Thus the clock equation and metric Bianchi identity are mutually consistent, while universal matter coupling gives $\nabla^\mu T_{\mu\nu}^{\rm vis} = 0$ on the matter equations of motion.

VI. NONLINEAR HAMILTONIAN AND CONSTRAINT STRUCTURE

A. Operator Legendre map for the completed action

Use clock coordinates $T = x^0$, $Q = N^{-1}$, $q_i = D_i \ln N$, $d = D_i q^i$, and the canonical momentum density π^{ij}. Set $P = \pi/(M_{\rm Pl}^2\sqrt{h})$ and $P^{ij}_{\rm TF} = (\pi^{ij} - \pi h^{ij}/3)/(M_{\rm Pl}^2\sqrt{h})$. The full metric velocity variation of Equation (59) is

$$\pi^{ij} = \frac{M_{\rm Pl}^2\sqrt{h}}{2}\left[K^{ij} - K h^{ij} + \mathcal{B}_{\rm A} h^{ij} + \frac{h^{ij}}{N} D_k(N\nu D^k K)\right],$$
$$K^{ij}_{\rm TF} = 2P^{ij}_{\rm TF}, \qquad \mathscr{A}_N K = -P + \frac{3}{2}\mathcal{B}_{\rm A}, \qquad \mathscr{A}_N = 1 - \frac{3}{2N} D_i(N\nu D^i\,\cdot\,). \tag{80}$$

There is no $\dot{N}$ or $\dot{N}^i$. The metric Legendre map is a spatial elliptic operator, not the algebraic DeWitt inverse of S_0. The positive mass and positive floor give

$$\langle f, \mathscr{A}_N f\rangle_N = \int \sqrt{h}\, N\left(f^2 + \frac{3}{2}\nu |Df|^2\right) > 0 \quad (f \neq 0), \qquad \langle f, g\rangle_N = \int \sqrt{h}\, N f g. \tag{81}$$

This identity uses a closed leaf or the stated no-flux trace boundary condition. Keeping K as an auxiliary variable gives the exact canonical Hamiltonian

$$\frac{\widetilde{H}}{M_{\rm Pl}^2} = \int \sqrt{h}\, N\Big[2P^{ij}_{\rm TF}P^{\rm TF}_{ij} + \left(\frac{2}{3}P - \mathcal{B}_{\rm A}\right)K + \frac{1}{3}K^2 + \frac{\nu}{2}|DK|^2 - \widetilde{\mathcal{K}} - \frac{{}^{(3)}R}{2}$$
$$+ a_0^2 \Sigma_{\rm A}\mathcal{J}_{{\rm A},\sigma} + \frac{\ell}{2}{}^{(3)}R d + \frac{\tau_6}{2}|D^{(3)}R_{ij}|^2 + \frac{\eta_R}{2}{}^{(3)}R^2\Big] + \frac{1}{M_{\rm Pl}^2}\int N^i \mathcal{H}_i + \frac{H_{\rm vis}}{M_{\rm Pl}^2}. \tag{82}$$

The curvature term contributes exactly

$$\Delta H_R = \frac{M_{\rm Pl}^2 \eta_R}{2}\int \sqrt{h}\, N^{(3)}R^2, \quad \Delta\mathcal{C}_N = \frac{M_{\rm Pl}^2\sqrt{h}\,\eta_R}{2}{}^{(3)}R^2, \quad \left.\frac{\delta(\Delta\mathcal{C}_N)}{\delta N}\right|_{h,\pi} = 0. \tag{83}$$

It has no shift dependence. Thus the metric Legendre operator, momentum constraints, and full fixed-(h,π) lapse Hessian below retain their form. The regular-domain gravitational mode count is unchanged. For completeness its spatial-metric variation is

$$\frac{1}{\sqrt{h}}\frac{\delta}{\delta h^{ij}}\int \sqrt{h}\, N^{(3)}R^2 = N(2^{(3)}R^{(3)}R_{ij} - \tfrac{1}{2}h_{ij}{}^{(3)}R^2) + 2(h_{ij}\Delta_h - D_iD_j)(N^{(3)}R). \tag{84}$$

This fourth-order spatial contribution must be retained in metric evolution. Its K equation is Equation (80); eliminating K is an operator Schur reduction. Define $r_\nu = \nu - Q\nu'$ and $r_\ell = \ell - Q\ell'$. At fixed h, π, the envelope derivative with respect to N gives

$$\frac{\mathcal{C}_N}{M_{\rm Pl}^2\sqrt{h}} = 2P^{ij}_{\rm TF}P^{\rm TF}_{ij} + \left(\frac{2}{3}P - \mathcal{B}_{\rm A} + Q\mathcal{B}_{{\rm A},Q}\right)K + \frac{1}{3}K^2 + \frac{r_\nu}{2}|DK|^2 + Q\widetilde{\mathcal{K}}' - \widetilde{\mathcal{K}} - \frac{{}^{(3)}R}{2}$$
$$+ a_0^2\left[(\Sigma_{\rm A} - Q\Sigma'_{\rm A})\mathcal{J}_{{\rm A},\sigma} - 2\Sigma_{\rm A} Y \mathcal{J}_{{\rm A},\sigma,Y}\right] - 2D_i(\Sigma_{\rm A}\mathcal{J}_{{\rm A},\sigma,Y}q^i) + \frac{\tau_6}{2}|D^{(3)}R_{ij}|^2 + \frac{\eta_R}{2}{}^{(3)}R^2$$
$$+ \frac{1}{2}\left[r_\ell{}^{(3)}R d + N^{-1}\Delta_h(N\ell^{(3)}R)\right] + \frac{\mathcal{H}_\perp^{\rm vis}}{M_{\rm Pl}^2\sqrt{h}} = 0. \tag{85}$$

For a relative lapse variation $\delta N = N\varphi$ write $z = \delta K$. Differentiating the full Legendre equation, including the braid, gives

$$\mathscr{A}_N z = \frac{3}{2}r_\nu D_i K D^i\varphi - \frac{3\varphi}{2N}D_i(\nu' D^i K) - \frac{3}{2}Q\mathcal{B}_{{\rm A},Q}\varphi. \tag{86}$$

Set

$$\mathsf{G}^{ij} = -\mathcal{J}_{{\rm A},\sigma,Y}h^{ij} - 2a_0^{-2}\mathcal{J}_{{\rm A},\sigma,YY}q^iq^j, \qquad \mathsf{G}^{ij}_{\rm full} = \Sigma_{\rm A}\mathsf{G}^{ij} + \frac{1}{2}r_\ell{}^{(3)}R h^{ij},$$
$$\mathfrak{M}_{\rm full} = Q(\widetilde{\mathcal{K}}'' + \mathcal{B}_{{\rm A},QQ}K) + \frac{1}{2}\left[\Delta_h(\ell'^{(3)}R) - Q\ell''^{(3)}R d\right] - \frac{Q}{2}\nu''|DK|^2$$
$$- a_0^2 Q\Sigma''_{\rm A}\mathcal{J}_{{\rm A},\sigma} - 2D_i(\Sigma'_{\rm A}\mathcal{J}_{{\rm A},\sigma,Y}q^i). \tag{87}$$

The full relative-lapse derivative, before contracting with a second variation, is

$$\delta\left(\frac{\mathcal{C}_N}{M_{\rm Pl}^2\sqrt{h}}\right)[N\varphi] = \frac{2}{N}D_i(N\mathsf{G}^{ij}_{\rm full}D_j\varphi) - \frac{\mathfrak{M}_{\rm full}}{N}\varphi + \left[\frac{2}{3}(P+K) - \mathcal{B}_{\rm A} + Q\mathcal{B}_{{\rm A},Q}\right]z + r_\nu D_i K D^i z. \tag{88}$$

After elimination of K, its negative Hessian is exactly

$$-\frac{\delta^2 H_C[N\varphi,N\varphi]}{M_{\rm Pl}^2} = \int\sqrt{h}\left[2N\mathsf{G}^{ij}_{\rm full}D_i\varphi D_j\varphi + \mathfrak{M}_{\rm full}\varphi^2\right] + \frac{2}{3}\langle z, \mathscr{A}_N z\rangle_N. \tag{89}$$

The final term is nonnegative and is required by the inverse Legendre operator; it is not reproduced by substituting a momentum-dependent parameter in the old algebraic Hessian. The acceleration terms follow by varying $N\Sigma_{\rm A}(Q)\mathcal{J}_{{\rm A},\sigma}(Y)$ twice, and the braid contributes $Q\mathcal{B}_{{\rm A},QQ}K$ at fixed auxiliary K. The Hamiltonian is linear in canonical visible lapse and shift, so standard minimally coupled visible matter has zero lapse–lapse second derivative.

On homogeneous flat data the canonical relative-lapse symbol, in the normalization of the quadratic form above, is

$$\mathscr{L}^{\rm full}_{N,p} = Q\left[\widetilde{\mathcal{K}}'' + 3H\mathcal{B}_{{\rm A},QQ} + \frac{3\mathcal{B}^2_{{\rm A},Q}}{2(1+3\nu p^2/2)}\right] + \frac{2\Sigma_{\rm A}p^2}{Q}. \tag{90}$$

This reduces to the old $Q\Xi + 2\Sigma_{\rm A}p^2/Q$ only when $\nu = 0$. In the local unbraided interval it reduces exactly to $QU'' + 2p^2/Q$. Coercivity for general inhomogeneous data requires the bounds on $\mathsf{G}_{\rm full}$ and $\mathfrak{M}_{\rm full}$ in the chosen function space. A positive homogeneous symbol alone does not prove nonlinear evolution; Theorem XIV.3 instead assumes the full coercive strong-regularity margin and proves local evolution while that margin remains positive.

B. Base-action canonical derivation

The following algebraic derivation is the base-action S_0 analysis; the completed operator Legendre map is Equation (80). On each constant-$\Sigma_{\rm A}$ component, use $\mathcal{J}_{\rm A} \mapsto \Sigma_{\rm A}\mathcal{J}_{\rm A}$. The clock-norm transition and the full-action lapse operator are treated in Section XVI C.

On a domain where T is monotonic, it may be used as the time coordinate. This is an admissible gauge choice for a physical scalar, not the definition of the scalar. Write

$$ds^2 = -N^2 dT^2 + h_{ij}(dx^i + N^i dT)(dx^j + N^j dT). \tag{91}$$

In this gauge,

$$Q = \frac{1}{N}, \qquad u_\mu = (-N,0,0,0), \qquad \Theta = K, \qquad \mathcal{A}_i = D_i \ln N, \qquad Y = \frac{D_i \ln N D^i \ln N}{a_0^2}, \tag{92}$$

where

$$K_{ij} = \frac{1}{2N}\left(\dot{h}_{ij} - D_iN_j - D_jN_i\right), \qquad K = h^{ij}K_{ij}. \tag{93}$$

Up to the standard Einstein–Hilbert boundary term, the action becomes

$$S_{\rm SC} = \frac{M_{\rm Pl}^2}{2}\int dT d^3x\, N\sqrt{h}\left[{}^{(3)}R + K_{ij}K^{ij} - K^2 + 2\mathcal{K}\left(\frac{1}{N}\right) + 2\mathcal{B}\left(\frac{1}{N}\right)K - 2a_0^2\mathcal{J}\left(\frac{D_i\ln N D^i \ln N}{a_0^2}\right)\right] + S_{\rm vis}. \tag{94}$$

There is no time derivative of N or N^i. The six-dimensional velocity Hessian in the h_{ij} sector is the nondegenerate DeWitt metric of general relativity; the term $\mathcal{B}K$ translates the trace momentum but does not lower its rank. The canonical brackets are

$$\{h_{ij}(\boldsymbol{x}), \pi^{kl}(\boldsymbol{y})\} = \delta^k_{(i}\delta^l_{j)}\delta^{(3)}(\boldsymbol{x}-\boldsymbol{y}),$$
$$\{N(\boldsymbol{x}), p_N(\boldsymbol{y})\} = \delta^{(3)}(\boldsymbol{x}-\boldsymbol{y}), \qquad \{N^i(\boldsymbol{x}), p_j(\boldsymbol{y})\} = \delta^i_j\delta^{(3)}(\boldsymbol{x}-\boldsymbol{y}). \tag{95}$$

The visible sector is assumed to have completed its own Legendre and internal Dirac analysis. After any purely matter second-class pairs are reduced, standard minimally coupled matter has the ADM form

$$H_{\mathrm{vis}} = \int_{\Sigma_T} \mathrm{d}^3x \left(N\mathcal{H}_\perp^{\mathrm{vis}} + N^i \mathcal{H}_i^{\mathrm{vis}} + \lambda^a \chi_a \right), \tag{96}$$

where the χ_a are the remaining internal gauge constraints and neither $\mathcal{H}_\perp^{\mathrm{vis}}$ nor $\mathcal{H}_i^{\mathrm{vis}}$ depends on N or N^i. This is the canonical meaning of universal minimal coupling used below. It implies that visible matter contributes to $\mathcal{C}_N$ through $\mathcal{H}_\perp^{\mathrm{vis}}$ but does not contribute to the lapse Hessian Δ_N. The internal constraints are assumed to have their standard closed algebra and $\mathcal{C}_N$ is an internal-gauge scalar. Their constraint blocks and physical degrees of freedom are counted separately from the gravitational–clock block.

C. Exact Legendre map and canonical Hamiltonian

The momentum conjugate to h_{ij} is

$$\pi^{ij} = \frac{M_{\mathrm{Pl}}^2\sqrt{h}}{2} \left(K^{ij} - Kh^{ij} + \mathcal{B}h^{ij} \right). \tag{97}$$

Its trace and inverse Legendre map are

$$\pi = M_{\mathrm{Pl}}^2\sqrt{h}\left(-K + \frac{3}{2}\mathcal{B} \right), \tag{98}$$

$$K = \frac{3}{2}\mathcal{B} - \frac{\pi}{M_{\mathrm{Pl}}^2\sqrt{h}}, \tag{99}$$

$$K_{ij} = \frac{2}{M_{\mathrm{Pl}}^2\sqrt{h}}\left(\pi_{ij} - \frac{1}{2}\pi h_{ij} \right) + \frac{1}{2}\mathcal{B}h_{ij}. \tag{100}$$

No relation among the six π^{ij} is generated. The only gravitational primary constraints are therefore

$$p_N \approx 0, \qquad p_i \approx 0. \tag{101}$$

After the shift term is integrated by parts, the total Hamiltonian is

$$H_T = \int_{\Sigma_T} \mathrm{d}^3x \left[N\mathcal{H}_\perp + N^i\mathcal{H}_i + \lambda_N p_N + \lambda^i p_i + \lambda^a \chi_a \right] + H_{\partial\Sigma}, \tag{102}$$

where $H_{\partial\Sigma}$ is the boundary functional required by the chosen asymptotics and

$$\mathcal{H}_\perp = \mathcal{H}_0 + \pi\mathcal{B} - \frac{3M_{\mathrm{Pl}}^2\sqrt{h}}{4}\mathcal{B}^2 - M_{\mathrm{Pl}}^2\sqrt{h}\,\mathcal{K} + M_{\mathrm{Pl}}^2\sqrt{h}\,a_0^2\mathcal{J}, \tag{103}$$

$$\mathcal{H}_0 = \frac{2}{M_{\mathrm{Pl}}^2\sqrt{h}}\left(\pi_{ij}\pi^{ij} - \frac{1}{2}\pi^2 \right) - \frac{M_{\mathrm{Pl}}^2\sqrt{h}}{2}\,{}^{(3)}R + \mathcal{H}_\perp^{\mathrm{vis}}, \tag{104}$$

$$\mathcal{H}_i = -2D_j\pi^j{}_i + \mathcal{H}_i^{\mathrm{vis}}. \tag{105}$$

All unlabelled functions in these equations are evaluated at $Q = N^{-1}$ and $Y = D_i \ln N D^i \ln N/a_0^2$. Equation (103) is the fully expanded form of the shifted-momentum expression and displays every N dependence needed by the Dirac algorithm.

D. Secondary constraints

Preservation of the shift momenta gives

$$\dot{p}_i = -\mathcal{H}_i \approx 0. \tag{106}$$

Preservation of p_N gives one local scalar constraint,

$$\dot{p}_N = -\mathcal{C}_N \approx 0, \qquad \mathcal{C}_N(\boldsymbol{x}) \equiv \frac{\delta H_C}{\delta N(\boldsymbol{x})}, \tag{107}$$

where H_C is equation (102) without the primary multipliers. Introduce

$$q_i \equiv D_i \ln N, \qquad Y = \frac{q_i q^i}{a_0^2}. \tag{108}$$

Direct functional differentiation gives the exact density

$$\boxed{\begin{aligned}\mathcal{C}_N = \mathcal{H}_0 + \pi\big(\mathcal{B} - Q\mathcal{B}_{,Q}\big) \\ + M_{\rm Pl}^2\sqrt{h}\Big[Q\mathcal{K}_{,Q} - \mathcal{K} - \frac{3}{4}\mathcal{B}^2 + \frac{3}{2}Q\mathcal{B}\mathcal{B}_{,Q} \\ + a_0^2\big(\mathcal{J} - 2Y\mathcal{J}_{,Y}\big) - 2D_i\big(\mathcal{J}_{,Y}q^i\big)\Big] \approx 0.\end{aligned}} \tag{109}$$

No minisuperspace or stationarity assumption has entered equation (109). On FLRW it reduces to the Friedmann constraint in Equation (168); the check is shown in Supplemental Material, Appendix D 2.

E. Exact functional lapse operator

For a lapse variation $\eta = \delta N$, define

$$\mathsf{P}^{ij} \equiv \mathcal{J}_{,Y}h^{ij} + \frac{2\mathcal{J}_{,YY}}{a_0^2}q^i q^j, \tag{110}$$

where the value at $q_i = 0$ is the continuous acceleration-component Hessian, not a separated divergent $\mathcal{J}_{,YY}(0)$. The scalar controlling the local part of the Hessian is

$$\boxed{\Xi(Q,K) \equiv \mathcal{K}_{,QQ} + K\mathcal{B}_{,QQ} + \frac{3}{2}\mathcal{B}_{,Q}^2.} \tag{111}$$

The full model-specific lapse operator is

$$\boxed{\begin{aligned}\Delta_N\eta \equiv \frac{\delta\mathcal{C}_N}{\delta N}\eta = & -M_{\rm Pl}^2\sqrt{h}\,Q^3\Xi\,\eta \\ & - \frac{2M_{\rm Pl}^2\sqrt{h}}{N}D_i\Big[N\mathsf{P}^{ij}D_j\Big(\frac{\eta}{N}\Big)\Big].\end{aligned}} \tag{112}$$

Equation (112) includes the complete local dependence of $\mathcal{K}$ and $\mathcal{B}$, the complete nonlinear differential contribution of $\mathcal{J}$, and all terms generated by the N dependence of the shifted momentum. Its derivation from the exact second variation is given in Supplemental Material, Appendix D 3. In particular, no unspecified "principal part" remains.

On the $\Sigma_{\rm A} = 1$ SCFT-A plateau, set

$$\mathsf{G}^{ij} \equiv -\mathsf{P}^{ij}. \tag{113}$$

The Dirac audit in Supplemental Material, Appendix D 4 proves the uniform bound

$$\mathsf{G}^{ij}v_i v_j \geq g_{\rm N}\,h^{ij}v_i v_j, \qquad g_{\rm N} \equiv \frac{1 - 9/(8\sqrt{3})}{s_{\rm N}+1} > 0 \tag{114}$$

for every finite acceleration and every spatial covector v_i.

It is useful to remove the kinematic factors associated with the variable N. Write $\eta = N\varphi$ and define the scalar operator

$$\boxed{\mathscr{L}_N\varphi \equiv -\frac{N}{M_{\rm Pl}^2\sqrt{h}}\Delta_N(N\varphi) = Q\Xi\,\varphi - 2D_i\left(N\mathsf{G}^{ij}D_j\varphi\right).} \tag{115}$$

Its symmetric closed form is

$$\mathfrak{b}_N[\varphi,\psi] = \int_{\Sigma_T} \mathrm{d}^3x\sqrt{h}\,\left[Q\Xi\,\varphi\psi + 2N\mathsf{G}^{ij}D_i\varphi D_j\psi\right] + 2\int_{\partial\Sigma_T} \mathrm{d}^2x\sqrt{\sigma}\,\sigma_R\varphi\psi. \tag{116}$$

The boundary integral is absent on a closed or asymptotically decaying leaf, vanishes for Dirichlet data, and has $\sigma_R = 0$ for the no-flux case. For nonnegative Robin data it is the positive boundary contribution generated by equation (118).

F. Dirac-regular domain and boundary conditions

Definition VI.1 (Dirac-regular component)**.** A connected phase-space component $\mathfrak{R}$ is called *Dirac regular* if

$$0 < N_{\min} \le N \le N_{\max} < \infty, \qquad \overline{Q(\Sigma_T)} \Subset \mathcal{D}_Q, \qquad \Xi(Q,K) \ge \xi_0 > 0, \tag{117}$$

the spatial metric is smooth and uniformly positive definite relative to the reference geometry of the selected function space, the coefficients $Q\Xi$ and $N\mathsf{G}^{ij}$ are essentially bounded above, and the lapse variations belong to one of the following domains:

1. a compact leaf without boundary;
2. a bounded leaf with Dirichlet data $\varphi|_{\partial\Sigma} = 0$;
3. a bounded leaf with no-flux or nonnegative Robin data
$$n_iN\mathsf{G}^{ij}D_j\varphi + \sigma_R\varphi = 0, \qquad \sigma_R \ge 0; \tag{118}$$
4. an asymptotically homogeneous leaf with $h_{ij} \to a^2(T)\delta_{ij}$, $N \to \bar{N}(T) > 0$, $q_i \to 0$, and $\varphi \to 0$ in the weighted energy space defined by the norm associated with equation (116). Asymptotically flat data are the special case $a = \bar{N} = 1$.

At a physical boundary, the corresponding condition is imposed both on allowed variations and on the multiplier equation. Spatial-diffeomorphism smearings are restricted to preserve these data; transformations with nonvanishing boundary charges are global symmetries and are not included in the local constraint count.

On $\mathfrak{R}$, equations (114) and (117) imply

$$\mathfrak{b}_N[\varphi,\varphi] \ge \int \mathrm{d}^3x\sqrt{h}\left[\frac{\xi_0}{N_{\max}}\varphi^2 + 2N_{\min}g_{\mathrm{N}}D_i\varphi D^i\varphi\right]. \tag{119}$$

Thus $\mathscr{L}_N$ is uniformly strongly elliptic and coercive, and the symmetric closed form defines its positive self-adjoint Friedrichs realization on the stated domain. The Lax–Milgram theorem gives a unique weak inverse from the energy-space dual to the energy space; standard elliptic regularity applies on subdomains where the coefficients possess the required additional regularity. The C^2 but non-C^3 MOND point is sufficient for the Hessian and for this weak inverse; no third derivative of the action is used by the regular Dirac chain. This is the same structural role played by the elliptic lapse equation in nonprojectable Hořava gravity, but equation (112) is specific to SCFT-A [17, 18].

G. Constraint algebra and termination of the Dirac chain

The exact generator of spatial diffeomorphisms is most cleanly written in smeared form,

$$\mathcal{D}[\boldsymbol{\xi}] = \int \mathrm{d}^3x\left[\pi^{ij}\mathcal{L}_{\boldsymbol{\xi}}h_{ij} + p_N\mathcal{L}_{\boldsymbol{\xi}}N + p_i\mathcal{L}_{\boldsymbol{\xi}}N^i + \sum_A p_A\mathcal{L}_{\boldsymbol{\xi}}\Psi^A\right]. \tag{120}$$

After integration by parts, its local density is the primary-extended momentum constraint

$$\widetilde{\mathcal{H}}_i = \mathcal{H}_i + p_ND_iN + p_jD_iN^j + D_j(p_iN^j), \tag{121}$$

up to the standard primary extensions associated with any constrained visible-matter variables. Thus $\mathcal{D}[\boldsymbol{\xi}] = \int \mathrm{d}^3x\, \xi^i \widetilde{\mathcal{H}}_i$ and $\widetilde{\mathcal{H}}_i \approx \mathcal{H}_i$ on the primary surface. By construction,

$$\{F, \mathcal{D}[\boldsymbol{\xi}]\} = \mathcal{L}_{\boldsymbol{\xi}} F \tag{122}$$

for every canonical tensor or tensor density F. It follows that the three p_i and the three primary-extended constraints $\widetilde{\mathcal{H}}_i$ are first class and satisfy the spatial-diffeomorphism algebra. Replacing the secondary $\mathcal{H}_i$ by $\widetilde{\mathcal{H}}_i$ is an equivalent change of constraint basis because their difference is proportional to primary constraints.

For the lapse chain define

$$P_N[\alpha] = \int \mathrm{d}^3x\, \alpha p_N, \qquad C[\beta] = \int \mathrm{d}^3x\, \beta \mathcal{C}_N. \tag{123}$$

Then

$$\{P_N[\alpha], C[\beta]\} = -\int \mathrm{d}^3x\, \beta\, \Delta_N \alpha. \tag{124}$$

The antisymmetric secondary–secondary kernel is not an additional assumption. It is the exact functional

$$\begin{aligned} \Omega(\boldsymbol{x},\boldsymbol{y}) &\equiv \{\mathcal{C}_N(\boldsymbol{x}), \mathcal{C}_N(\boldsymbol{y})\} \\ &= \int \mathrm{d}^3z \left[\frac{\delta \mathcal{C}_N(\boldsymbol{x})}{\delta h_{ij}(\boldsymbol{z})} \frac{\delta \mathcal{C}_N(\boldsymbol{y})}{\delta \pi^{ij}(\boldsymbol{z})} - (\boldsymbol{x} \leftrightarrow \boldsymbol{y})\right] + \Omega_{\mathrm{vis}}(\boldsymbol{x},\boldsymbol{y}), \end{aligned} \tag{125}$$

where Ω_{vis} is the analogous sum over the reduced visible-matter canonical pairs. The momentum derivative entering this expression is explicit:

$$\begin{aligned} \frac{\delta \mathcal{C}_N(\boldsymbol{x})}{\delta \pi^{ij}(\boldsymbol{z})} &= \left[\frac{4}{M_{\mathrm{Pl}}^2 \sqrt{h}} \left(\pi_{ij} - \frac{1}{2}\pi h_{ij}\right) + h_{ij}(\mathcal{B} - Q\mathcal{B}_{,Q})\right]_{\boldsymbol{x}} \delta^{(3)}(\boldsymbol{x}-\boldsymbol{z}) \\ &= (2K_{ij} - Q\mathcal{B}_{,Q} h_{ij})_{\boldsymbol{x}}\, \delta^{(3)}(\boldsymbol{x}-\boldsymbol{z}). \end{aligned} \tag{126}$$

The remaining metric derivative follows directly from the displayed local density (109); equation (125) therefore fixes every coefficient and derivative-of-delta term even though expanding that distributional expression is unnecessary for the rank classification.

On the common self-adjoint domain, the complete scalar constraint matrix is

$$\mathbb{C} = \begin{pmatrix} 0 & -\Delta_N \\ \Delta_N & \Omega \end{pmatrix}. \tag{127}$$

Because Δ_N is invertible on $\mathfrak{R}$, this matrix is invertible for the exact antisymmetric operator Ω; an explicit two-sided inverse is

$$\mathbb{C}^{-1} = \begin{pmatrix} \Delta_N^{-1}\Omega\Delta_N^{-1} & \Delta_N^{-1} \\ -\Delta_N^{-1} & 0 \end{pmatrix}. \tag{128}$$

Direct block multiplication proves the identity. Consequently no special cancellation or closure ansatz for $\{\mathcal{C}_N, \mathcal{C}_N\}$ is required: $(p_N, \mathcal{C}_N)$ is a definitive second-class pair whenever Δ_N^{-1} exists.

Preservation of the secondary scalar constraint takes the form

$$\dot{\mathcal{C}}_N = \mathcal{S} + \Delta_N \lambda_N \approx 0, \qquad \mathcal{S} \equiv \{\mathcal{C}_N, H_C\}\big|_{\lambda_N=0}, \tag{129}$$

where the shift contribution is its spatial Lie derivative and is weakly zero. Invertibility gives the unique multiplier

$$\lambda_N = -\Delta_N^{-1}\mathcal{S}. \tag{130}$$

Equivalently, writing $\lambda_N = N\chi$,

$$\mathscr{L}_N \chi = \frac{N}{M_{\mathrm{Pl}}^2\sqrt{h}}\mathcal{S}. \tag{131}$$

No tertiary constraint is generated on $\mathfrak{R}$. Equations (128) and (130) complete the Dirac–Bergmann algorithm rather than stopping at a conditional count.

H. Reference-action regular-branch degree-of-freedom count

Theorem VI.2 (Complete regular-branch Dirac classification)**.** *For the reference action S_0 on any constant-$\Sigma_{\rm A}$ component $\mathfrak{R}$ satisfying Definition VI.1, the full gravitational–clock constraint set is*

$$
\begin{array}{ll}
\textit{primary:} & p_N \approx 0, \quad p_i \approx 0, \\
\textit{secondary:} & \mathcal{C}_N \approx 0, \quad \mathcal{H}_i \approx 0, \\
\textit{equivalent spatial basis:} & \widetilde{\mathcal{H}}_i \approx 0, \\
\textit{tertiary:} & \textit{none.}
\end{array} \tag{132}
$$

The six constraints $(p_i, \widetilde{\mathcal{H}}_i)$ are first class and generate the three time-dependent spatial diffeomorphisms. The pair $(p_N, \mathcal{C}_N)$ is second class. Hence the twenty-dimensional gravitational–clock phase space per spatial point has

$$\dim \Gamma_{\rm phys} = 20 - 2(6) - 2 = 6, \qquad N_{\rm dof} = 3 = 2_{\rm tensor} + 1_{\rm clock}. \tag{133}$$

No vector degree of freedom is added by the hypersurface-orthogonal clock.

Proof. The Legendre map (100) proves that equation (101) is the complete gravitational primary set. Equations (106) and (107) give the complete secondary set. Spatial covariance and equations (120) and (121) make the shift chains first class. Coercivity (119) makes Δ_N invertible; equations (127)–(128) therefore make the lapse chain second class, and equation (130) fixes its multiplier without a tertiary condition. The standard phase-space count then gives equation (133). □

I. FLRW specialization and SCFT-A regular components

On a homogeneous leaf $q_i = 0$, $K = 3H$, and $\mathsf{G}^{ij} = h^{ij}$. Therefore

$$\Xi_{\rm FLRW} = \mathcal{K}_{,QQ} + 3H\mathcal{B}_{,QQ} + \frac{3}{2}\mathcal{B}_{,Q}^2, \tag{134}$$

and a Fourier mode with comoving wavenumber k has

$$\mathscr{L}_{N,k} = Q\Xi_{\rm FLRW} + \frac{2Nk^2}{a^2}. \tag{135}$$

The homogeneous mode is invertible precisely when $\Xi_{\rm FLRW} \neq 0$, and it is positive on the regular component when $\Xi_{\rm FLRW} > 0$. In the condensate-side unbraided DBI region of SCFT-A,

$$\Xi_{\rm A} = \mathcal{K}_{{\rm DBI},QQ} = \frac{\kappa_m}{[1 - \lambda_D(Q-1)^2]^{3/2}} > 0. \tag{136}$$

On the complete late plateau

$$\mathcal{I}_d \equiv \left[1 + \frac{3\Delta Q}{4}, 1 + \frac{5\Delta Q}{4}\right], \qquad W = 1, \tag{137}$$

one has $\mathcal{K}_{{\rm A},QQ} = \kappa_d$, $\mathcal{B}_{{\rm A},Q} = b_d$, and $\mathcal{B}_{{\rm A},QQ} = 0$, hence

$$\Xi_{\rm A}(Q, K) = \kappa_d + \frac{3}{2}b_d^2 > 0, \qquad Q \in \mathcal{I}_d, \tag{138}$$

independently of the value of the extrinsic trace K. Thus the condensate-side DBI region and the entire late plateau lie inside open Dirac-regular regions; the completed high-charge sector is checked separately in Section XVI C.

Within the low/intermediate core, only the two compact switch bands can contain an SCFT-A rank surface. Their exact diagnostic is

$$\Xi_{\rm A}(Q, K) = \mathcal{K}_{{\rm A},QQ}(Q) + K\mathcal{B}_{{\rm A},QQ}(Q) + \frac{3}{2}\mathcal{B}_{{\rm A},Q}(Q)^2, \tag{139}$$

with all derivatives displayed in Supplemental Material, Appendix D 7. For a proposed branch satisfying $|K| \le K_{\max}$ through the switch bands, the explicit sufficient condition

$$\xi_{\rm sw}(K_{\max}) \equiv \min_{Q\in\mathcal{I}_{\rm sw}} \left[\mathcal{K}_{{\rm A},QQ} + \frac{3}{2}\mathcal{B}_{{\rm A},Q}^2 - K_{\max}|\mathcal{B}_{{\rm A},QQ}|\right] > 0 \tag{140}$$

places the entire branch segment in $\mathfrak{R}$. This is a finite inequality in the SCFT-A parameters. Along any homogeneous solution, equation (139) is evaluated on $Q(a), H(a)$. For the homogeneous $k = 0$ lapse mode, $\Xi_{\rm A} = 0$ is an actual zero eigenvalue by equation (135); for general inhomogeneous data, loss of the strict $\Xi > 0$ margin ends this reference-action coercive certificate and requires the spectrum of its lapse operator to be examined directly.

J. Rank-changing and gauge-boundary loci

The exact rank criterion is spectral:

$$0 \notin \operatorname{spec}(\mathscr{L}_N) \quad \Longleftrightarrow \quad \Delta_N^{-1} \text{ exists as a bounded map on the selected domain.} \tag{141}$$

On compact or Fredholm domains, an isolated crossing is equivalently signaled by $\ker \Delta_N \neq \{0\}$. The complete analysis identifies, rather than hides, every structural way in which the regular theorem can cease to apply:

1. a reference DBI chart reaches Q_- or Q_+, where its stiffness diverges; the adopted high-charge continuation leaves that chart before Q_+ and removes this upper boundary from the final action;
2. $Q \le 0$, $N = 0$, or $N = \infty$, where the clock ceases to define the regular timelike unitary-gauge patch;
3. the sufficient margin $\Xi \ge \xi_0 > 0$ fails. This is the boundary of the coercive certificate, not by itself a general inhomogeneous rank change; the exact event is zero entering the spectrum in equation (141);
4. the principal matrix G^{ij} loses positive definiteness, so ellipticity changes type. The chosen $\mathcal{J}_{\rm A}$ excludes this event at every finite s;
5. the operator domain or boundary data admit a zero spectral value, for example pure Neumann data combined with a vanishing local term.

If an isolated finite-dimensional kernel is spanned by z_A, equation (129) has the Fredholm conditions

$$\mathcal{T}_A \equiv \langle z_A, \mathcal{S}\rangle \approx 0. \tag{142}$$

They are genuine tertiary constraints when satisfied nontrivially; if they are not satisfied, the putative branch is dynamically inconsistent. If zero enters the essential or continuous spectrum on a noncompact domain, the bounded inverse is lost without a finite Fredholm projector and that non-Fredholm branch requires a separate evolution analysis. Further preservation must therefore be redone branch by branch. None of these bifurcations occurs on $\mathfrak{R}$.

K. Covariant interpretation

The local mode count follows from the constraint analysis with its specified lapse domain. Clock gauge is admissible when $\nabla_\mu T$ is timelike. Removing lapse and shift time derivatives does not, by itself, prove well-posedness of the remaining spatial differential equations. The action-specific nonlinear Cauchy theorem in Section XIV C adds the gauge reduction, exact symmetrizer, and loss-free energy needed for that conclusion on its strongly regular boundaryless domain.

L. Exact nonlinear metric Legendre map and lapse constraint

Specialize the completed action to the local interval, where $\mathcal{B}_{\rm A} = 0$, $\Sigma_{\rm A} = 1$, and $U = \widetilde{\mathcal{K}}$. Use dimensionful variables and the clock coordinate T. All primes now mean $\mathrm{d}/\mathrm{d}Q$. Define

$$P^{ij}_{\rm TF} = \frac{\pi^{ij} - \pi h^{ij}/3}{M_{\rm Pl}^2\sqrt{h}}, \qquad P = \frac{\pi}{M_{\rm Pl}^2\sqrt{h}}, \qquad \mathscr{A}_N f = f - \frac{3}{2N} D_i(N\nu D^i f). \tag{143}$$

With vanishing trace flux at a boundary, or on a closed leaf, variation of the full velocity terms gives

$$\pi^{ij} = \frac{M_{\rm Pl}^2\sqrt{h}}{2}\left[K^{ij} - Kh^{ij} + \frac{h^{ij}}{N}D_k(N\nu D^k K)\right],$$
$$K_{\rm TF}^{ij} = 2P_{\rm TF}^{ij}, \qquad \mathscr{A}_N K = -P. \tag{144}$$

The operator is positive in $\langle f,g\rangle_N = \int \sqrt{h}\,Nfg$:

$$\langle f, \mathscr{A}_N f\rangle_N = \int \sqrt{h}\,N\left(f^2 + \frac{3}{2}\nu|Df|^2\right) \geq \|f\|^2_{L^2_N}. \tag{145}$$

The floor (322) makes $\mathscr{A}_N$ uniformly elliptic. On a closed leaf, or with the displayed no-flux condition, elliptic regularity gives, for every integer $j \geq 0$ in the coefficient regularity range,

$$\|f\|_{H^{j+2}} \leq C_j\big(\|\mathscr{A}_N f\|_{H^j} + \|f\|_{L^2}\big), \qquad \|\mathscr{A}_N^{-1}\|_{H^j\to H^j} \leq C_j. \tag{146}$$

The constants are uniform on bounded sets with $N \geq N_0 > 0$, $h \geq c_h\widehat{h}$, and $\nu \geq \rho\delta/\kappa_m$. The resolvent identity $A^{-1} - B^{-1} = A^{-1}(B-A)B^{-1}$ gives the corresponding tame Lipschitz and Fréchet estimates. This is the estimate that the vanishing compact profile lacked.

It is convenient to keep K temporarily as an auxiliary variable in the canonical Hamiltonian:

$$\frac{\widetilde{H}}{M_{\rm Pl}^2} = \int \sqrt{h}\,N\Bigg[2P_{\rm TF}^{ij}P^{\rm TF}_{ij} + \frac{2}{3}PK + \frac{1}{3}K^2 + \frac{\nu}{2}|DK|^2 - U - \frac{{}^{(3)}\!R}{2}$$
$$+ a_0^2\mathcal{J}_{{\rm A},\sigma} + \frac{\ell}{2}{}^{(3)}\!Rd + \frac{\tau_6}{2}|D^{(3)}R_{ij}|^2 + \frac{\eta_R}{2}{}^{(3)}\!R^2\Bigg] + \frac{1}{M_{\rm Pl}^2}\int N^i\mathcal{H}_i, \qquad \mathcal{H}_i = -2D_j\pi^j{}_i. \tag{147}$$

Its K equation is (144). Eliminating it replaces the three trace terms by $-\langle P, \mathscr{A}_N^{-1}P\rangle_N/3$ under the integral. No new propagating field is being added by this auxiliary representation.

At fixed (h_{ij}, π^{ij}) the envelope derivative gives

$$\mathfrak{c}_N \equiv \frac{\mathcal{C}_N}{M_{\rm Pl}^2\sqrt{h}} = 2P_{\rm TF}^{ij}P^{\rm TF}_{ij} + \frac{2}{3}PK + \frac{1}{3}K^2 + \frac{1}{2}(\nu - Q\nu')|DK|^2 + QU' - U - \frac{{}^{(3)}\!R}{2}$$
$$+ a_0^2(\mathcal{J}_{{\rm A},\sigma} - 2Y\mathcal{J}_{{\rm A},\sigma,Y}) - 2D_i(\mathcal{J}_{{\rm A},\sigma,Y}q^i)$$
$$+ \frac{\tau_6}{2}|D^{(3)}R_{ij}|^2 + \frac{\eta_R}{2}{}^{(3)}\!R^2$$
$$+ \frac{1}{2}\left[(\ell - Q\ell')^{(3)}Rd + \frac{1}{N}\Delta_h(N\ell^{(3)}R)\right]. \tag{148}$$

The lapse constraint is $\mathfrak{c}_N = 0$, evaluated with $K = -\mathscr{A}_N^{-1}P$. It is not the old trace-repair constraint with a Fourier-dependent parameter substituted into it.

1. *Full lapse linearization, including the inverse operator*

For a relative variation $\delta N = N\varphi$, let $z = \delta K$. Define

$$r_\nu = \nu - Q\nu', \qquad r_\ell = \ell - Q\ell',$$
$$\mathsf{G}^{ij} = -\mathcal{J}_{{\rm A},\sigma,Y}h^{ij} - \frac{2\mathcal{J}_{{\rm A},\sigma,YY}}{a_0^2}q^iq^j, \qquad \mathsf{G}_R^{ij} = \mathsf{G}^{ij} + \frac{1}{2}r_\ell{}^{(3)}\!Rh^{ij},$$
$$M_R = QU'' + \frac{1}{2}[\Delta_h(\ell'^{(3)}R) - Q\ell''^{(3)}Rd]. \tag{149}$$

At $q_i = 0$ this is the grouped acceleration Hessian. For the adopted smooth tip all derivatives are finite; the grouped definition also has a continuous seed limit. Exact differentiation of (144) gives

$$\mathscr{A}_N z = \frac{3}{2}r_\nu D_iKD^i\varphi - \frac{3\varphi}{2N}D_i(\nu'D^iK). \tag{150}$$

Together with (150), the complete Fréchet derivative is

$$\delta\mathfrak{c}_N[N\varphi] = \frac{2}{N}D_i(N\mathsf{G}_R^{ij}D_j\varphi) - \frac{M_R}{N}\varphi + \frac{1}{2}Q^2\nu''|DK|^2\varphi + \frac{2}{3}(P+K)z + r_\nu D_iKD^iz. \tag{151}$$

The last line, which comes from varying the inverse metric Legendre operator, must not be dropped. The spatial-switch contribution contains third derivatives when expanded:

$$\Delta_h(\ell'{}^{(3)}R) - Q\ell''{}^{(3)}Rd = \ell'\Delta_h{}^{(3)}R - 2Q\ell''(q^iD_i{}^{(3)}R + {}^{(3)}Rd) + (Q\ell'' + Q^2\ell''')^{(3)}Rq_iq^i. \tag{152}$$

Also $D_i(\nu' D^iK) = \nu'\Delta_hK - Q\nu''q^iD_iK$. Thus all switch derivatives are explicit or retained inside their displayed differential operators.

2. *Exact lapse Hessian and a regular constraint domain*

Define

$$M_* = M_R - \frac{Q}{2}\nu''|DK|^2. \tag{153}$$

At an auxiliary solution, the negative canonical lapse Hessian is

$$-\frac{\delta^2H_C[N\varphi,N\varphi]}{M_{\rm Pl}^2} = \int\sqrt{h}\,[2N\mathsf{G}_R^{ij}D_i\varphi D_j\varphi + M_*\varphi^2] + \frac{2}{3}\langle z,\mathscr{A}_Nz\rangle_N. \tag{154}$$

To see its sign, the auxiliary K–K Hessian is the positive operator $(2/3)N\mathscr{A}_N$. Eliminating K subtracts $H_{NK}H_{KK}^{-1}H_{KN}$ from the lapse Hessian. After sign reversal this is precisely the last, nonnegative term in (154). The N–N Hessian at fixed K yields the first line. This also gives an independent check of (151).

For the seed MOND function, the acceleration Hessian obeys

$$\mathsf{G}_{\rm seed} \geq g_{\rm N}h^{-1}, \qquad g_{\rm N} = \frac{1-9/(8\sqrt{3})}{s_{\rm N}+1} > 0. \tag{155}$$

Indeed its transverse and longitudinal eigenvalues are $1-\mu/\gamma_{\rm N}$ and $1-(\mu+s\mu')/\gamma_{\rm N}$. With $t = s/s_{\rm N}$, $\mu + s\mu' \leq 1 + 2t/[s_{\rm N}(1+t^2)^2]$ and $\max_{t\geq0} 2t/(1+t^2)^2 = 9/(8\sqrt{3})$, which proves (155).

For the smooth tip define the exact margin

$$g_\sigma = \inf_{Y\geq0}\min\left\{1-\frac{\mu_\sigma(Y)}{\gamma_{\rm N}}, 1-\frac{\mu_\sigma(Y)+2Y\mu_\sigma'(Y)}{\gamma_{\rm N}}\right\}. \tag{156}$$

There is a positive admissible σ. Indeed, on $0 \leq Y \leq 4\sigma^2$, $\mu(\sqrt{Y}) = O(\sigma)$, $\widehat{\mu}_\sigma + 2Y\widehat{\mu}_\sigma' = O(\sigma)$, the numerator defining A_σ is $O(\sigma^3)$, and its denominator is $4\sigma^2\int_0^1 b(z)\,\mathrm{d}z$. Hence $A_\sigma = O(\sigma)$ and both quantities subtracted in (156) converge uniformly to zero on the modified interval. Outside it they are the seed quantities. For the adopted regulator the stronger explicit choice is

$$\boxed{\sigma = 10^{-6}}, \qquad \mathsf{G}_\sigma \geq g_{\rm N}h^{-1}. \tag{157}$$

The companion proves the uniform tip bound by elementary inequalities and the seed margin outside the modified interval. No minimum over an uncertified numerical function defines σ.

Proposition VI.3 (A nonlinear no-kernel domain for the lapse constraint)**.** *On a smooth bounded leaf, take zero Dirichlet lapse variations and the trace no-flux condition. Suppose the background coefficients in* (150)–(154) *are bounded and*

$$N \geq N_0 > 0, \quad \mathsf{G}_R \geq g_0h^{-1}, \quad M_* \geq -m_0, \quad \|\varphi\|_2 \leq C_P\|D\varphi\|_2, \quad 2N_0g_0 - m_0C_P^2 > 0. \tag{158}$$

Then the full canonical lapse Hessian has a unique weak Dirichlet inverse. The lapse second-class pair has no kernel on this domain.

Proof. Equation (154) bounds the negative Hessian from below by $(2N_0 g_0 - m_0 C_P^2)\|D\varphi\|_2^2$. Its form is bounded: the right-hand side of (150) is bounded from H_0^1 to L_N^2, and (145) controls $\langle z, \mathscr{A}_N z\rangle_N$ by the squared L_N^2 norm of that source. Lax–Milgram gives the stated inverse. □

A sufficient spatial-symbol margin is $|r_\ell {}^{(3)}R| \le g_{\mathrm{N}}/2$, giving $\mathsf{G}_R \ge (g_{\mathrm{N}}/4)h^{-1}$. The separate bound on M_* must still be imposed. On homogeneous flat data, $D_i K = {}^{(3)}R = 0$, so $z = 0$ and the scalar lapse operator reduces exactly to

$$\mathscr{L}_p = QU'' + \frac{2p^2}{Q} > 0 \quad (p \neq 0). \tag{159}$$

It stays positive throughout both switch regions and at their positive floors. With the regular Legendre inverse and the lapse inverse above, the usual local count is

$$N_{\text{physical}} = \frac{20 - 2(6) - 2}{2} = 3: \quad \text{two tensors and one scalar.} \tag{160}$$

Spatial-diffeomorphism generators are extended to act on lapse and shift. The global lapse mode on a closed plateau leaf is excluded from this Dirichlet statement; its time-reparametrization constraint must be treated separately, as in related nonprojectable theories [41].

VII. HOMOGENEOUS SPACE-CLOCK DYNAMICS

Consider a spatially flat homogeneous metric in an arbitrary parameter λ,

$$\mathrm{d}s^2 = -N^2(\lambda)\mathrm{d}\lambda^2 + a^2(\lambda)\mathrm{d}\boldsymbol{x}^2, \qquad T = T(\lambda), \qquad Q = \frac{\dot T}{N} > 0, \tag{161}$$

where the dot in this subsection initially denotes $\mathrm{d}/\mathrm{d}\lambda$. The matter proper time is $\mathrm{d}t = N\mathrm{d}\lambda$ and

$$H = \frac{1}{N}\frac{\dot a}{a}. \tag{162}$$

Homogeneity gives $\mathcal{A}_\mu = 0$, $Y = 0$, and $\Theta = 3H$. With $\mathcal{J}(0) = 0$, the minisuperspace Lagrangian per unit coordinate volume, after the Einstein boundary term is removed, is

$$L_{\text{mini}} = -\frac{3M_{\text{Pl}}^2 a\dot a^2}{N} + M_{\text{Pl}}^2 N a^3 \mathcal{K}(Q) + 3M_{\text{Pl}}^2 a^2 \dot a\, \mathcal{B}(Q) + L_{\text{vis}}. \tag{163}$$

The three homogeneous equations below follow directly from varying T, N, and a before fixing $N = 1$.

A. Conserved clock charge

Shift symmetry implies

$$\frac{\mathrm{d}}{\mathrm{d}\lambda}\left[\frac{\partial L_{\text{mini}}}{\partial \dot T}\right] = 0. \tag{164}$$

Because $\partial Q/\partial \dot T = N^{-1}$,

$$\frac{\partial L_{\text{mini}}}{\partial \dot T} = M_{\text{Pl}}^2 a^3\left(\mathcal{K}_{,Q} + 3H\mathcal{B}_{,Q}\right). \tag{165}$$

Absorbing the constant factor M_{Pl}^2 into the definition of the charge gives the exact first integral

$$\boxed{a^3\mathcal{F}(Q,H) = C_T, \qquad \mathcal{F}(Q,H) \equiv \mathcal{K}_{,Q}(Q) + 3H\mathcal{B}_{,Q}(Q).} \tag{166}$$

The quantity C_T is initial data for the one clock field rather than the abundance of a second particle species. It sets the amplitude of the clock's matter-like contribution and plays the same phenomenological role as a dark-matter abundance parameter.

If $\mathcal{B}_{,Q} \neq 0$, equation (166) may be written as

$$H(Q,a) = \frac{C_T a^{-3} - \mathcal{K}_{,Q}(Q)}{3\mathcal{B}_{,Q}(Q)}. \tag{167}$$

If instead $\mathcal{B}_{,Q} = 0$ on an interval, the charge equation reduces to the purely kinetic relation $\mathcal{K}_{,Q} = C_T a^{-3}$. In either case the clock norm is determined dynamically.

B. Clock energy density and pressure

Variation with respect to the lapse and scale factor yields

$$3M_{\rm Pl}^2 H^2 = \rho_{\rm vis} + \rho_T, \tag{168}$$

$$-2M_{\rm Pl}^2 \dot{H} = \rho_{\rm vis} + p_{\rm vis} + \rho_T + p_T, \tag{169}$$

where dots now denote matter proper-time derivatives and

$$\boxed{\rho_T = M_{\rm Pl}^2 \left[Q\mathcal{K}_{,Q} - \mathcal{K} + 3HQ\mathcal{B}_{,Q}\right] = M_{\rm Pl}^2 \left[Q\frac{C_T}{a^3} - \mathcal{K}(Q)\right],} \tag{170}$$

$$\boxed{p_T = M_{\rm Pl}^2 \left[\mathcal{K}(Q) - \mathcal{B}_{,Q}(Q)\dot{Q}\right].} \tag{171}$$

The second form of equation (170) uses the clock current. It makes the two contributions transparent: QC_T/a^3 is the charge contribution, while $-\mathcal{K}$ is the displacement energy of the clock state.

The continuity equation is not independent. Differentiating equation (170) and using

$$\dot{\mathcal{F}} + 3H\mathcal{F} = 0 \tag{172}$$

gives

$$\dot{\rho}_T + 3H(\rho_T + p_T) = 0. \tag{173}$$

The clock equation-of-state parameter is

$$w_T = \frac{\mathcal{K} - \mathcal{B}_{,Q}\dot{Q}}{QC_T a^{-3} - \mathcal{K}}. \tag{174}$$

Acceleration occurs when

$$\rho_{\rm tot} + 3p_{\rm tot} < 0, \tag{175}$$

or, when the clock dominates,

$$Q\frac{C_T}{a^3} + 2\mathcal{K} - 3\mathcal{B}_{,Q}\dot{Q} < 0. \tag{176}$$

This is genuine acceleration of the one physical metric. It is not an apparent acceleration obtained by reparametrizing a decelerating Einstein solution.

C. Exact reciprocal response

Equation (166) makes the clock norm a dynamical function of the expansion and conserved charge. Differentiating it with respect to $\ln a$ gives

$$\mathcal{D}(Q,H)Q' + 3\mathcal{B}_{,Q}H' = -3\mathcal{F}, \qquad \mathcal{D}(Q,H) \equiv \mathcal{K}_{,QQ} + 3H\mathcal{B}_{,QQ}, \tag{177}$$

where a prime denotes $\mathrm{d}/\mathrm{d}\ln a$. Therefore

$$Q' = -\frac{3\mathcal{F} + 3\mathcal{B}_{,Q}H'}{\mathcal{D}}. \tag{178}$$

Equivalently, the scale-factor evolution of the clock conversion is

$$\frac{\mathrm{d}\ln\mathcal{N}_T}{\mathrm{d}\ln a} = -\frac{Q'}{Q} = \frac{3}{Q\mathcal{D}}\left(\mathcal{F} + \mathcal{B}_{,Q}H'\right). \tag{179}$$

Since $\mathcal{N}_T = Q^{-1}$,

$$\frac{\mathrm{d}\mathcal{N}_T}{\mathrm{d}H} = -\frac{1}{Q^2}\frac{Q'}{H'} = \frac{3}{Q^2\mathcal{D}}\left(\frac{\mathcal{F}}{H'} + \mathcal{B}_{,Q}\right), \qquad H' \neq 0. \tag{180}$$

Equation (180) is an exact branch diagnostic. The reciprocal space-clock condition is

$$\frac{\mathcal{F}/H' + \mathcal{B}_{,Q}}{\mathcal{D}} < 0. \tag{181}$$

In an exactly unbraided positive-charge regime, $\mathcal{F} > 0$, $H' < 0$, and $\mathcal{D} > 0$, so Equation (181) holds. For a nonzero braid the finite charge term must be retained, including near a late endpoint. On a source-free trajectory,

$$H_{,Q} = \frac{Q\mathcal{D} + 3H\mathcal{B}_{,Q}}{3\mathcal{W}_s}, \qquad \frac{\mathcal{F}}{H'} = -\frac{2H\Xi_s}{Q\mathcal{D} + 3H\mathcal{B}_{,Q}}, \qquad \frac{\mathrm{d}\mathcal{N}_T}{\mathrm{d}H} = -\frac{3\mathcal{W}_s}{Q^2(Q\mathcal{D} + 3H\mathcal{B}_{,Q})}. \tag{182}$$

These identities follow by differentiating both the current and Friedmann constraints. They remain the appropriate diagnostic across a zero of $\mathcal{D}$ whenever the undivided system and the displayed remaining denominators are regular. Equations (178)–(181), when written with $1/\mathcal{D}$, require $\mathcal{D} \neq 0$.

For the fixed parameters in Equation (469), the source-free limits are exactly

$$\boxed{\lim_{a\to\infty} \frac{\mathcal{F}}{H'} = -\frac{5600}{7519}H_d, \qquad \lim_{a\to\infty} H_d\frac{\mathrm{d}\mathcal{N}_T}{\mathrm{d}H} = -\frac{11250}{7519} < 0.} \tag{183}$$

Both $\mathcal{F}$ and H' vanish, but their ratio does not. Dropping it would give a different response and an invalid sign argument.

The approach is also loading dependent. If visible nonrelativistic matter satisfies $\rho_b/M_{\mathrm{Pl}}^2 = r_b\mathcal{F}$ with constant r_b and radiation decays faster, linearization about the endpoint gives

$$\begin{aligned} Q - Q_d &= \frac{1 - b_d(Q_d + r_b)/(2H_d)}{\Xi_d}\mathcal{F} + o(\mathcal{F}), \\ H - H_d &= \frac{\kappa_d(Q_d + r_b) + 3H_d b_d}{6H_d\Xi_d}\mathcal{F} + o(\mathcal{F}). \end{aligned} \tag{184}$$

The source-free result sets $r_b = 0$; the representative loaded benchmark has $r_b = 3/20$. Thus a partial derivative on the zero-charge constraint curve is not the reciprocal derivative along a finite-charge cosmological approach.

D. An explicit contracting branch of the same action

Theorem VII.1 (Clock-rate reciprocity in an unbraided contraction)**.** *On any compact interval inside $Q_a < Q < Q_L$ with $U' > 0$, $U'' > 0$, the completed action admits source-free expanding and contracting flat FLRW solutions at any fixed charge $C_T > 0$. On the contracting solution $\dot{a} < 0$ and $\dot{Q} > 0$: the field clock advances faster per unit matter proper time as the physical spatial volume decreases.*

Proof. All spatial completion operators and their first variations vanish on flat FLRW, while $\mathcal{B}_{\mathrm{A}} = 0$ on this interval. Set

$$a(Q) = \left(\frac{C_T}{U'(Q)}\right)^{1/3}, \qquad H_\pm(Q) = \pm\sqrt{\frac{QU'(Q) - U(Q)}{3}}, \qquad \dot{Q} = -3H_\pm\frac{U'}{U''}. \tag{185}$$

Here $QU' - U = \int_{Q_a}^{Q} rU''(r)\,\mathrm{d}r > 0$. The right-hand side is smooth and nonzero on the chosen compact interval. Equivalently,

$$t(Q) - t(Q_i) = -\int_{Q_i}^{Q} \frac{U''(r)}{3H_\pm(r)U'(r)}\,\mathrm{d}r, \qquad T(Q) - T(Q_i) = \int_{Q_i}^{Q} r\frac{\mathrm{d}t}{\mathrm{d}r}\,\mathrm{d}r. \tag{186}$$

These quadratures give local existence and uniqueness for this homogeneous family. Differentiation verifies $a^3U' = C_T$, $3H^2 = QU' - U$, and $\dot{H} = -QU'/2$. On H_-, both $\dot{Q} > 0$ and $\dot{a} = aH_- < 0$ follow exactly. ☐

In the exact exterior DBI interval $Q_b \le Q \le Q_L$, put $Z = C_T/(\kappa_m a^3)$ and $R = \sqrt{1 + Z^2}$. The construction is elementary:

$$Q = 1 + Z/R, \qquad H_- = -\sqrt{\frac{\kappa_m}{3}(Z + R - 1)}, \qquad \dot{Q} = -\frac{3H_- Z}{(1 + Z^2)^{3/2}} > 0. \tag{187}$$

The data archive tabulates this branch with exact rational Q inputs. Its charge is specified separately from the expanding numerical example. The response derivative distinguishes the two branches:

$$\frac{\mathrm{d}\mathcal{N}_T}{\mathrm{d}H} = -\frac{6H}{Q^3U''}, \qquad \frac{\mathrm{d}\ln Q}{\mathrm{d}\ln a} = -\frac{3U'}{QU''} < 0. \tag{188}$$

Thus $\mathrm{d}\mathcal{N}_T/\mathrm{d}H < 0$ is the expanding-branch diagnostic; it is positive on this contraction, although $\dot{Q} > 0$ realizes the stated clock-rate interpretation. The unbraided local quadratic spectra also survive time reversal: H and the mixed coefficient B_p change sign together, and $a^{-3}(a^3B_p)^{\cdot}$ is unchanged. This does not construct a contracting continuation through the nonzero braid: the term $\mathcal{B}(Q)\Theta$ is not invariant under reversal with $Q > 0$ fixed.

E. One scale factor and two physical descriptions

Combining equations (13) and (166), the clock-field expansion rate is

$$H_T = \frac{H}{Q}, \qquad Q = Q(H, a; C_T), \tag{189}$$

where $Q(H, a; C_T)$ is an implicit solution of the current equation. Both derivatives refer to the same scale factor and metric.

VIII. EXTERIOR MATTER-LIKE CLOCK REGIME

The following calculation identifies a matter-like stress in an unbraided exterior regime. It does not establish a cold-dark-matter transfer function. In the fixed action the exact DBI interval is $Q_b \le Q \le Q_L < Q_d$, whereas the displayed cosmological trajectory approaches Q_d from above. Thus this low-charge interval is not an early stage of that selected trajectory; its early behavior is governed by the high-charge continuation in Sec. XVI B.

A. Expansion around a clock condensate

Let the exterior seed point Q_m satisfy equation (29), and write

$$Q = Q_m + \delta Q, \qquad |\delta Q| \ll Q_m. \tag{190}$$

Assume that braiding is switched off sufficiently rapidly in this regime,

$$|3H\mathcal{B}_{,Q}| \ll |\mathcal{K}_{,Q}|, \qquad |3H\mathcal{B}_{,QQ}| \ll \mathcal{K}_{,QQ}, \tag{191}$$

and expand

$$\mathcal{K}(Q) = \frac{\kappa_m}{2}(\delta Q)^2 + \frac{\kappa_3}{6}(\delta Q)^3 + \mathcal{O}((\delta Q)^4). \tag{192}$$

The current equation then gives

$$\delta Q = \frac{C_T}{\kappa_m a^3} - \frac{\kappa_3 C_T^2}{2\kappa_m^3 a^6} + \mathcal{O}(a^{-9}) + \mathcal{O}(\mathcal{B}_{,Q}). \tag{193}$$

Substitution into equations (170) and (171) yields

$$\rho_T = M_{\rm Pl}^2\left[\frac{Q_m C_T}{a^3} + \frac{C_T^2}{2\kappa_m a^6} + \mathcal{O}(a^{-9})\right] + \mathcal{O}(\mathcal{B}_{,Q}), \tag{194}$$

$$p_T = M_{\rm Pl}^2\left[\frac{C_T^2}{2\kappa_m a^6} + \mathcal{O}(a^{-9})\right] - M_{\rm Pl}^2\mathcal{B}_{,Q}\dot{Q}. \tag{195}$$

The leading term is exactly proportional to a^{-3}. The first correction is stiff and is suppressed whenever

$$\epsilon_m(a) \equiv \frac{C_T}{\kappa_m Q_m a^3} \ll 1. \tag{196}$$

For $C_T > 0$, $Q_m > 0$, and $\kappa_m > 0$, the leading energy density is positive.

Proposition VIII.1 (Matter-like clock asymptotics). *Suppose equations* (29), (191), *and* (196) *hold on an interval. Then the homogeneous clock stress satisfies*

$$\rho_T = \rho_{T0}^{(m)} a^{-3} \left[1 + \mathcal{O}(\epsilon_m)\right], \qquad w_T = \frac{\epsilon_m}{2} + \mathcal{O}(\epsilon_m^2) + \mathcal{O}(\mathcal{B}_{,Q}), \tag{197}$$

with $\rho_{T0}^{(m)} = M_{\rm Pl}^2 Q_m C_T$, *and the reciprocal condition is satisfied for the usual matter-era sign* $H' < 0$.

B. Adiabatic sound speed before braiding

When $\mathcal{B} = 0$, the homogeneous clock is a purely kinetic scalar and its adiabatic sound speed is

$$c_{\rm ad}^2 = \frac{\dot{p}_T}{\dot{\rho}_T} = \frac{\mathcal{K}_{,Q}}{Q\mathcal{K}_{,QQ}}. \tag{198}$$

Near Q_m,

$$c_{\rm ad}^2 = \frac{\delta Q}{Q_m} + \mathcal{O}((\delta Q)^2) = \epsilon_m + \mathcal{O}(\epsilon_m^2). \tag{199}$$

This is the Scherrer-type unified-dark-matter mechanism: a scalar near a kinetic extremum behaves as dust with a tunably small sound speed [19]. The present theory differs by embedding that regime in a clock-defined foliation and by activating $\mathcal{B}$ and $\mathcal{J}$ for late acceleration and galaxies.

The adiabatic derivative is a background quantity. The propagation frequency of the completed theory follows from its constrained quadratic action, including the spatial operators. The formal condensate series is restricted to the exterior interval where the kinetic template is actually used; it cannot be extrapolated through the replaced plateau.

C. Clock charge as initial data

The coefficient C_T is a Noether charge and therefore an integration constant rather than an action parameter. It fixes the gravitating amplitude of the matter-like clock contribution without introducing a second particle species.

D. Exact condensate-side DBI sector of SCFT-A

In the exterior condensate-side interval $Q_b \leq Q \leq Q_L$, equations (41) and (42) reduce exactly to $\mathcal{K} = \mathcal{K}_{\rm DBI}$ and $\mathcal{B} = 0$. For $C_T > 0$, define

$$Z(a) \equiv \frac{C_T}{\kappa_m a^3} > 0, \qquad R(a) \equiv \sqrt{1 + \lambda_D Z^2}. \tag{200}$$

Whenever the physical trajectory lies in this condensate-side DBI sector, the current equation is solved exactly by

$$Q(a) = 1 + \frac{Z}{R}, \qquad Q_b \leq Q \leq Q_L. \tag{201}$$

Substitution into the exact stress tensor gives

$$\mathcal{K}(Q(a)) = \frac{\kappa_m}{\lambda_D}\left(1 - \frac{1}{R}\right), \tag{202}$$

$$\rho_T(a) = M_{\rm Pl}^2 \kappa_m \left[Z + \frac{R-1}{\lambda_D}\right], \tag{203}$$

$$p_T(a) = M_{\rm Pl}^2 \frac{\kappa_m}{\lambda_D}\left(1 - \frac{1}{R}\right), \tag{204}$$

$$c_{\rm ad}^2(a) = \frac{Z}{(1 + \lambda_D Z^2)\,[R + Z]}. \tag{205}$$

The condensate limit $Z \ll 1$ is

$$w_T = \frac{Z}{2} + \mathcal{O}(Z^2), \qquad c_{\rm ad}^2 = Z + \mathcal{O}(Z^2), \qquad \rho_T = M_{\rm Pl}^2 \kappa_m \left[Z + \frac{1}{2} Z^2 + \mathcal{O}(Z^4) \right]. \tag{206}$$

These are dust-like exterior asymptotics of the DBI template. They are not an extension of that template into the replaced plateau $|Q-1| \leq d_1$, nor a completed finite-momentum propagation speed. The separate primordial high-charge asymptote of the final theory is the exponential continuation in Equations (461) and (463); it is not the finite-domain DBI extrapolation.

IX. LATE ACCELERATION FROM CLOCK–EXPANSION BRAIDING

The selected positive-charge trajectory approaches a displaced constant-clock state from $Q > Q_d$. The algebraic de Sitter conditions below establish a solution supported by clock stress. They do not establish a trajectory departing from the separate low-charge DBI interval.

A. Charge dilution and the late branch

As the universe expands, C_T/a^3 decreases. The current equation approaches

$$\mathcal{K}_{,Q} + 3H\mathcal{B}_{,Q} = 0. \tag{207}$$

If visible matter is negligible and the solution tends to a constant pair (Q_d, H_d) with $H_d > 0$, the Friedmann equation and current condition become

$$3H_d^2 + \mathcal{K}(Q_d) = 0, \tag{208}$$

$$\mathcal{K}_{,Q}(Q_d) + 3H_d\mathcal{B}_{,Q}(Q_d) = 0. \tag{209}$$

Thus

$$\mathcal{K}(Q_d) = -3H_d^2 < 0. \tag{210}$$

The acceleration is supported by the displaced clock state. The scale H_d is specified in the action through $\mathcal{K}_d$; its observed magnitude is not predicted by the construction. At the exact fixed point, $\dot{Q} = 0$ and equations (170)–(171) give

$$\rho_T = 3M_{\rm Pl}^2 H_d^2, \qquad p_T = -3M_{\rm Pl}^2 H_d^2, \qquad w_T = -1. \tag{211}$$

A time-dependent approach generally has $w_T \neq -1$ and a varying clock conversion $\mathcal{N}_T = 1/Q$.

Theorem IX.1 (Algebraic self-acceleration condition)**.** *Let $\mathcal{K}$ and $\mathcal{B}$ be differentiable and let $Q_d > 0$. A clock-dominated de Sitter solution with no bare cosmological constant exists at (Q_d, H_d) if and only if equations* (208) *and* (209) *hold for some $H_d > 0$. A constant part of $\mathcal{B}$ is irrelevant, whereas $\mathcal{B}_{,Q}(Q_d)$ permits the current condition to be satisfied without requiring $\mathcal{K}_{,Q}(Q_d) = 0$.*

B. Regularity of the fixed point

Define the reduced late-branch function

$$\Phi(Q) \equiv \mathcal{K}_{,Q}(Q) + 3\sqrt{-\frac{\mathcal{K}(Q)}{3}}\,\mathcal{B}_{,Q}(Q), \tag{212}$$

where the positive square root is used on $\mathcal{K} < 0$. A simple fixed point satisfies $\Phi(Q_d) = 0$ and

$$\Phi_{,Q}(Q_d) = \mathcal{K}_{,QQ} + 3H_d\mathcal{B}_{,QQ} + \frac{3}{2}\mathcal{B}_{,Q}^2 \neq 0. \tag{213}$$

Then the implicit-function theorem gives a unique nearby branch for sufficiently small C_T/a^3 and visible density. Equation (213), together with the scalar coefficients derived in Section XIII, determines the local regularity and stability of that branch.

For SCFT-A, the endpoint identities make this homogeneous branch simple. The signs $\kappa_d < 0$, $b_d > 0$, $\Xi_d > 0$, and $Q_d b_d < 2H_d$ give a positive infrared scalar coefficient in Section XIII. They do not prove finite-momentum stability of the completed action. The independent all-momentum positive endpoint certificate for the curvature-completed action is established in Section XII B.

C. No hidden cosmological constant

Three distinct statements must be separated:

1. $\mathcal{K}(Q_m) = 0$ and $\mathcal{J}(0) = 0$ mean that no constant has been inserted on the matter-like cosmological branch.
2. $\mathcal{K}(Q_d) < 0$ means that a dynamically selected clock state carries vacuum-like stress at late times.
3. Quantum vacuum contributions from visible fields still renormalize the gravitational action and are not cancelled by equations (208)–(209).

The theory replaces an additive cosmological constant in the classical background equations by vacuum-like stress of a displaced clock state. It does not provide a radiative sequestering mechanism for quantum vacuum energy.

D. A correlated, not arbitrary, equation of state

The same functions that determine the early clustering regime determine the late pressure. Combining the continuity equation with the Friedmann system gives

$$1 + w_T = -\frac{1}{3H\rho_T}\frac{\mathrm{d}\rho_T}{\mathrm{d}t}, \tag{214}$$

where ρ_T is fixed by equation (170) and $Q(a)$ by equation (166). Consequently $w_T(a)$, the clock sound speed, and $\mathcal{N}_T(a)$ are not independent fit functions. This correlation is one of the principal falsifiable contents of Space-Clock Field Theory. A complete fixed-parameter realization, including the dynamically traversed upper switch, the late plateau, and all scalar sign diagnostics, is given in Section XVII.

X. GALACTIC GRAVITY FROM THE CLOCK ACCELERATION INVARIANT

The seed stationary derivation in this section identifies the MOND/AQUAL limit. For the completed action it applies outside the acceleration tip and only when spatial completion terms are negligible. The coupled completed weak-field equations are Equations (495) and (496).

The invariant Y is built from the clock congruence. The next calculation identifies a stationary operator limit. For the revised benchmark, Sec. XX C establishes a local scale hierarchy. This operator ordering by itself does not establish a sourced galactic solution with cosmological boundary data.

A. Stationary weak-field limit

To isolate the structural weak-field operator, first consider the formal stationary zero-charge reference branch generated by nonrelativistic baryons,

$$\mathrm{d}s^2 = -(1+2\Phi)\mathrm{d}t^2 + (1-2\Psi)\delta_{ij}\mathrm{d}x^i\mathrm{d}x^j + \mathcal{O}(v^3, \Phi^2), \tag{215}$$

and choose $T = t$ at leading order. Then

$$N = 1 + \Phi + \mathcal{O}(\Phi^2), \qquad Q = 1 - \Phi + \mathcal{O}(\Phi^2), \qquad \mathcal{A}_i = \partial_i\Phi + \mathcal{O}(\Phi^2), \tag{216}$$

so that

$$Y = \frac{|\boldsymbol{\nabla}\Phi|^2}{a_0^2} + \mathcal{O}(\Phi^3). \tag{217}$$

This calculation fixes the stationary AQUAL/MOND operator. In a local quasi-static patch of a homogeneous state $T = \bar{T}(t)$ with $\bar{Q}(t) > 1$, one has $Q = \bar{Q}(1 - \Phi) + \mathcal{O}(\Phi^2, HL)$ and $\mathcal{A}_i = \partial_i \Phi + \mathcal{O}(\Phi^2, HL)$, so the acceleration operator has the same form if the clock-flow perturbation is consistently negligible. This is a conditional kinematic substitution. The clock and momentum equations must also be solved, as shown in Section XX.

Define the *derived clock-rate contrast*

$$\mathcal{R}_T(T, \boldsymbol{x}) \equiv \frac{N(T, \boldsymbol{x})}{\bar{N}(T)} = \frac{\bar{Q}(T)}{Q(T, \boldsymbol{x})}, \tag{218}$$

where the bar denotes the homogeneous clock state on the same leaf. Because $\bar{N}$ has no spatial gradient,

$$D_i \ln \mathcal{R}_T = D_i \ln N = \mathcal{A}_i, \qquad Y = \frac{D_i \ln \mathcal{R}_T D^i \ln \mathcal{R}_T}{a_0^2}. \tag{219}$$

Thus spatial clock-rate contrast is a relational observable constructed from the single clock norm Q, not an additional field.

This also gives a precise single-metric meaning to the statement that clock gradients give rise to gravitational motion. For a massive test body minimally coupled to $g_{\mu\nu}$,

$$S_{\mathrm{pp}} = -m \int \mathrm{d}s \simeq \int \mathrm{d}t \left(\frac{1}{2} m \boldsymbol{v}^2 - m\Phi \right) \tag{220}$$

up to an irrelevant rest-mass constant and higher weak-field orders. The geodesic equation therefore becomes

$$\frac{\mathrm{d}\boldsymbol{v}}{\mathrm{d}t} = -\boldsymbol{\nabla}\Phi = -\boldsymbol{\nabla} \ln \mathcal{R}_T + \mathcal{O}(\Phi^2, v^2\Phi). \tag{221}$$

Here $c = 1$ as in the manuscript conventions; restoring units gives $\Phi_{\mathrm{N}} = c^2 \ln \mathcal{R}_T$ at leading order. Equation (221) is not an additional fifth force: matter remains geodesic. The clock sector changes the metric constraint that determines Φ, and the resulting metric guides the motion.

On the stationary slicing the trace of the extrinsic curvature vanishes, while the $\mathcal{K}$ sector can generate a long-distance Helmholtz term through its expansion about the local clock state.

At leading post-Newtonian order the two metric potentials obey

$$\Phi = \Psi + \text{post-Newtonian corrections}, \tag{222}$$

provided the selected stationary clock branch carries no leading anisotropic stress. Before calibrating the locally measured Newton constant, the 00 equation has the action-level form

$$\boldsymbol{\nabla} \cdot \left[\bar{\mu}\left(\frac{|\boldsymbol{\nabla}\Phi|}{a_0} \right) \boldsymbol{\nabla}\Phi \right] + \widehat{m}_{\mathrm{loc}}^2 \Phi = 4\pi G_* \rho_b, \qquad \bar{\mu}(s) = 1 + \mathcal{J}_{,Y}(s^2). \tag{223}$$

For SCFT-A, Supplemental Material, Eq. (D24) and (56) convert this exactly to

$$\boxed{\boldsymbol{\nabla} \cdot \left[\mu_{\mathrm{A}}\left(\frac{|\boldsymbol{\nabla}\Phi|}{a_0} \right) \boldsymbol{\nabla}\Phi \right] + m_{\mathrm{loc}}^2 \Phi = 4\pi G_{\mathrm{N}} \rho_b,} \tag{224}$$

where

$$G_{\mathrm{N}} = \gamma_{\mathrm{N}} G_*, \qquad m_{\mathrm{loc}}^2 = \gamma_{\mathrm{N}} \widehat{m}_{\mathrm{loc}}^2. \tag{225}$$

The coefficient m_{loc}^2 is a calculable combination of local derivatives of $\mathcal{K}$ and, away from an exactly static branch, braiding corrections. The AQUAL limit applies on scales satisfying

$$|m_{\mathrm{loc}}^2| r^2 \ll \min\{\mu_{\mathrm{A}}, \mu_{\mathrm{A}} + s\mu_{\mathrm{A}}'\} \tag{226}$$

through the weak-field region under consideration, with the right-hand side evaluated at the local acceleration. In the deep-MOND regime this is stronger than $|m_{\mathrm{loc}}^2| r^2 \ll 1$; see Section XX.

B. Dirac-regular MOND function and regularity at $Y = 0$

The seed interpolation, recovered exactly by the completed acceleration function for $s \geq 2\sigma$, is

$$\boxed{\mu_{\rm A}(s) = 1 - \frac{1}{(1+s)(1+s^2/s_{\rm N}^2)}.} \tag{227}$$

It is strictly increasing for $s > 0$ and obeys

$$\mu_{\rm A}(s) = s + \left(s_{\rm N}^{-2} - 1\right) s^2 + \mathcal{O}(s^3), \qquad s \ll 1, \tag{228}$$

$$\mu_{\rm A}(s) = 1 - \frac{s_{\rm N}^2}{s^3} + \frac{s_{\rm N}^2}{s^4} + \mathcal{O}(s^{-5}), \qquad s \gg s_{\rm N}. \tag{229}$$

Thus, when the local mass term is negligible, equation (224) becomes

$$\boldsymbol{\nabla} \cdot \left(\frac{|\boldsymbol{\nabla}\Phi|}{a_0} \boldsymbol{\nabla}\Phi \right) = 4\pi G_{\rm N} \rho_b \tag{230}$$

in the deep-MOND regime and approaches the Newtonian Poisson equation with an s^{-3} correction above the transition $s_{\rm N}$ [20, 21].

The parameter $s_{\rm N}$ has two linked roles. It places the crossover to the rapid Newtonian tail at the physical acceleration $s_{\rm N} a_0$, and it fixes the finite renormalization $G_{\rm N}/G_* = \gamma_{\rm N} = 1 + s_{\rm N}^{-1}$. It is not an independently adjusted coupling. Large $s_{\rm N}$ makes the difference between the tensor/action coupling and the Cavendish coupling small.

A careful regularity statement distinguishes differentiability in Y from differentiability in the underlying acceleration components. From Supplemental Material, Eq. (D25),

$$\mathcal{J}_{\rm A}(Y) = -Y + \frac{2s_{\rm N}}{3(s_{\rm N}+1)} Y^{3/2} + \mathcal{O}(Y^2), \tag{231}$$

so $\mathcal{J}_{,YY} \propto Y^{-1/2}$ when treated in isolation. In a local orthonormal frame define

$$v_i \equiv \frac{\mathcal{A}_i}{a_0}, \qquad r \equiv (\delta^{ij} v_i v_j)^{1/2}, \qquad Y = r^2. \tag{232}$$

The composite entering the action satisfies

$$\widehat{\mathcal{J}}_{\rm A}(\boldsymbol{v}) \equiv \mathcal{J}_{\rm A}(r^2) = -r^2 + \frac{2s_{\rm N}}{3(s_{\rm N}+1)} r^3 + \mathcal{O}(r^4). \tag{233}$$

For $r > 0$ its Hessian is

$$\frac{\partial^2 \widehat{\mathcal{J}}_{\rm A}}{\partial v_i \partial v_j} = 2\mathcal{J}_{{\rm A},Y} \delta_{ij} + 4\mathcal{J}_{{\rm A},YY} v_i v_j. \tag{234}$$

The grouped second term is $\mathcal{O}(r)$ and the Hessian tends to $-2\delta_{ij}$ as $\boldsymbol{v} \to 0$. Hence the composite is C^2 but not C^3 at the homogeneous point.

Proposition X.1 (Acceleration-sector regularity and definiteness)**.** *The first and second variations of the revised SCFT-A acceleration action are finite and continuous at $\mathcal{A}_i = 0$. More strongly, the negative lapse-gradient Hessian $\mathsf{G}^{ij} = -\mathsf{P}^{ij}$ obeys the global lower bound* (114)*. Therefore the acceleration sector has no finite-Y principal-symbol rank change.*

The physical MOND equation (224) is degenerate elliptic only at its expected zero-field point because $\mu_{\rm A}(0) = 0$. This is distinct from the Dirac lapse Hessian, whose finite action-level asymptotic coefficient and Newton calibration make it uniformly definite. The Sobolev domain, boundary form, and inverse of the full lapse operator are established in Definition VI.1 and Supplemental Material, Appendix D 5.

C. Lensing

Because photons and baryons couple to the same metric, the lensing potential is

$$\Phi_{\rm lens} = \frac{\Phi + \Psi}{2}. \tag{235}$$

If equation (222) holds, the same potential that produces the enhanced nonrelativistic acceleration bends light. This is the central advantage of a relativistic single-metric completion over a purely modified-inertia law: the force and lensing potentials are not independently adjustable.

D. The cosmology–galaxy consistency relation

The same fixed functions control the cosmological and galactic limits. The curvature of $\mathcal{K}(Q)$ determines the clock sound-speed hierarchy and contributes to $m^2_{\rm loc}$, while $\mathcal{J}(Y)$ fixes both the MOND interpolation and the lapse-gradient principal symbol. The clustering and weak-field scales are therefore correlated rather than independently tunable.

XI. TENSOR SECTOR OF THE COMPLETED ACTION

On spatially flat FLRW write

$$h_{ij} = a^2(e^{\gamma})_{ij}, \qquad \partial_i\gamma_{ij} = 0, \qquad \gamma_{ii} = 0. \tag{236}$$

The first-order trace and scalar curvature vanish for a tensor perturbation, while $\delta^{(3)}R_{ij} = -\partial^2\gamma_{ij}/2$. Consequently the completed quadratic action is

$$S_T^{(2)} = \frac{M_{\rm Pl}^2}{8}\int {\rm d}t{\rm d}^3x\, a^3\left[\dot\gamma_{ij}^2 - a^{-2}(\partial\gamma_{ij})^2 - \tau_6 a^{-6}(\partial_k\partial^2\gamma_{ij})^2\right]. \tag{237}$$

For physical momentum $p = k/a$,

$$Q_T = \frac{M_{\rm Pl}^2}{4} > 0, \qquad \omega_T^2 = p^2 + \tau_6 p^6 > 0, \qquad m_T^2 = 0. \tag{238}$$

The phase and group velocities in the local frozen-background approximation are

$$v_{\rm ph} = \sqrt{1+\tau_6 p^4}, \qquad v_{\rm gr} = \frac{1+3\tau_6 p^4}{\sqrt{1+\tau_6 p^4}}, \qquad \lim_{p\to 0} v_{\rm ph} = \lim_{p\to 0} v_{\rm gr} = c_\gamma = 1. \tag{239}$$

Universal metric coupling of matter therefore gives the same low-momentum limit, but not an exact common tensor–photon cone at finite momentum. Multimessenger observations constrain the dispersive coefficient in their frequency band [22–25]; compatibility of the fixed coefficient $\tau_6 = \delta^2/\kappa_m^2$ has not been established by the local mathematical construction.

XII. SCALAR PERTURBATIONS AND PHYSICAL-BRANCH INFRARED STABILITY

A. Exact completed quadratic action at general clock norm

For $p^2 = k^2/a^2$, $z = \dot\zeta$, and $\chi = \Delta\psi/a^2$, let

$$\begin{aligned} W_s &= 2H - Q\mathcal{B}_{{\rm A},Q}, \qquad D_s = \widetilde{\mathcal{K}}'' + 3H\mathcal{B}_{{\rm A},QQ}, \\ A_k &= Q^2 D_s - 6H^2 + 6HQ\mathcal{B}_{{\rm A},Q} + 2\Sigma_{\rm A}p^2, \quad b = \nu p^2, \quad A = 2+3b, \\ C &= p^2(1+\ell p^2), \qquad J = W_s + 3bH, \qquad \mathcal{D} = W_s^2 + b(A_k + 6HW_s). \end{aligned} \tag{240}$$

Here W_s is the same background combination as $\mathcal{W}_s$ below; J is an auxiliary scalar coefficient, not the acceleration function. The completed gravity–clock quadratic density is

$$\begin{aligned}\frac{L^{(2)}}{M_{\rm Pl}^2 a^3} =& -3z^2 + W_s\alpha(3z-\chi) + 2z\chi + \frac{1}{2}A_k\alpha^2 + 2C\alpha\zeta + (p^2 - 8\eta_R p^4 - 3\tau_6 p^6)\zeta^2 \\ & -\frac{b}{2}(3z-\chi-3H\alpha)^2. \end{aligned} \tag{241}$$

In particular, the correction to the displayed base quadratic action is

$$\frac{\Delta L^{(2)}}{M_{\rm Pl}^2 a^3} = -\frac{\nu p^2}{2}(3\dot\zeta - \chi - 3H\alpha)^2 + 2\ell p^4 \alpha\zeta - 8\eta_R p^4\zeta^2 - 3\tau_6 p^6\zeta^2. \tag{242}$$

The smooth acceleration tip has $\mathcal{J}_{{\rm A},\sigma,Y}(0) = -1$, so it leaves the quadratic acceleration coefficient equal to $\Sigma_{\rm A}$. Spatial background gradients vanish: derivatives of ν and ℓ do not add terms to Equation (241), but time derivatives of their background values must be retained after the auxiliary reduction.

Where $\mathcal{D} \neq 0$, direct solution gives

$$\begin{aligned} \alpha &= \frac{2Jz - 2bC\zeta}{\mathcal{D}}, \qquad \chi = Kz + \frac{2JC}{\mathcal{D}}\zeta, \\ K &= \frac{AA_k + 3W_s^2 + 18bH(W_s - H)}{\mathcal{D}}, \qquad B = \frac{2JC}{\mathcal{D}}, \\ V_{\rm full} &= \frac{2bC^2}{\mathcal{D}} - p^2 + 8\eta_R p^4 + 3\tau_6 p^6 + \frac{1}{a^3}\frac{\rm d}{{\rm d}t}(a^3 B), \qquad \frac{L^{(2)}_{\rm red}}{M_{\rm Pl}^2 a^3} = K\dot\zeta^2 - V_{\rm full}\zeta^2. \end{aligned} \tag{243}$$

The (α,χ) Hessian determinant is $-\mathcal{D}$. The derivative in $V_{\rm full}$ is at fixed comoving momentum, so $\dot p = -Hp$. These formulas are exact for the completed source-free action. They also define the gravity block of the matter-loaded unreduced action when the full background equations are used. In the local interval $W_s = 2H$, $D_s = U''$, and $\Sigma_{\rm A} = 1$, they give precisely Equations (326) and (328). There $\mathcal{D}, K, V_{\rm full} > 0$ by Theorem XIII.1. The braided de Sitter endpoint and a nearby source-free collar are covered by Theorems XII.1 and XII.3. No global matter-loaded positivity theorem is inferred from those results.

For fixed regular background coefficients and positive floors,

$$\lim_{p\to\infty} K = 3, \qquad \lim_{p\to\infty}\frac{V_{\rm full}}{p^6} = \frac{\ell^2}{\Sigma_{\rm A}} + 3\tau_6 > 0. \tag{244}$$

Thus the reference saturating scalar frequency and its ultraviolet matter-loading criterion cannot be imported by continuity in momentum. Setting the completion to zero and taking $p\to\infty$ are different limits.

B. Positive scalar spectrum at the braided de Sitter endpoint

Write $\mathfrak{k} = \kappa_m/H_d^2$. The revised exact coefficient point is $\mathfrak{k} = 10^{30}$ and $\delta = 10^{-140}$. The following calculation keeps $\mathfrak{k}$ symbolic; it therefore audits the change of hierarchy without importing the old endpoint spectrum. Put $X = p^2/H_d^2$. Then

$$W_s/H_d = 6/5, \quad Q_d^2 D_s/H_d^2 = -8/125, \quad \nu H_d^2 = \frac{\delta}{2\mathfrak{k}}, \quad \ell H_d^2 = \eta_R H_d^2 = \frac{1}{2\mathfrak{k}}, \quad \tau_6 H_d^4 = \frac{\delta^2}{\mathfrak{k}^2}. \tag{245}$$

Define $Z = 180\mathfrak{k} + 125\delta X^2 + 371\delta X$. Exact elimination gives

$$\begin{aligned} \overline{\mathcal{D}} &= \mathcal{D}/H_d^2 = Z/(125\mathfrak{k}), \\ K_d &= \frac{500\mathfrak{k}X + 224\mathfrak{k} + 375\delta X^2 - 12\delta X}{Z}, \\ \overline{B}_d &= \frac{2(6/5 + 3\delta X/(2\mathfrak{k}))X(1 + X/(2\mathfrak{k}))}{\overline{\mathcal{D}}}, \\ \overline{V}_d \equiv V_d/H_d^2 &= \frac{\delta X^3(1+X/(2\mathfrak{k}))^2}{\mathfrak{k}\overline{\mathcal{D}}} - X + \frac{4X^2}{\mathfrak{k}} + \frac{3\delta^2 X^3}{\mathfrak{k}^2} + 3\overline{B}_d - 2X\partial_X\overline{B}_d. \end{aligned} \tag{246}$$

The derivative uses $\dot X = -2H_d X$ at fixed comoving momentum.

Theorem XII.1 (Continuum endpoint positivity at the revised coefficient point)**.** *For $\mathfrak{k} = 10^{30}$, $\delta = 10^{-140}$, and every $X > 0$,*

$$\mathcal{D}_d > 0, \qquad K_d > 0, \qquad V_d > 0. \tag{247}$$

Proof. The denominator and kinetic numerator have positive coefficients, since $500\mathfrak{k} > 12\delta$. Direct differentiation of Equation (246) gives the exact polynomial certificate

$$\overline{V}_d = \frac{X}{4\mathfrak{k}^2 Z^2} \sum_{j=0}^{6} a_j X^j, \tag{248}$$

with

$$\begin{aligned}
a_0 &= 86400\mathfrak{k}^4, \\
a_1 &= 4320\mathfrak{k}^3(123\delta + 95), \\
a_2 &= 16\mathfrak{k}^2\delta(41250\mathfrak{k} + 24671\delta + 122160), \\
a_3 &= 2\mathfrak{k}\delta(188500\mathfrak{k}\delta + 517500\mathfrak{k} + 801360\delta^2 + 962003\delta), \\
a_4 &= 6\delta(90000\mathfrak{k}\delta^2 + 293875\mathfrak{k}\delta + 3750\mathfrak{k} + 275282\delta^3), \\
a_5 &= 125\delta^2(2500\mathfrak{k} + 8904\delta^2 + 371), \\
a_6 &= 15625\delta^2(12\delta^2 + 1).
\end{aligned} \tag{249}$$

All seven coefficients are positive. This proves the statement for the entire continuum, independently of floating-point arithmetic or a cutoff. □

At fixed X the exact limiting expression is

$$\lim_{\delta \to 0^+} \overline{V}_d = \frac{2}{3}X + \frac{19X^2}{6\mathfrak{k}}. \tag{250}$$

The revised action retains $\delta > 0$. The old numerical witness at $\mathfrak{k} = 120$ is not a value of the revised benchmark.

C. A decreasing energy for every endpoint scalar mode

Theorem XII.2 (Endpoint energy monotonicity)**.** *For every comoving scalar mode on the expanding de Sitter solution, define*

$$\mathcal{E}_k = K_d(X)|\dot{\zeta}_k|^2 + V_d(X)|\zeta_k|^2. \tag{251}$$

At the revised coefficient point, $\dot{\mathcal{E}}_k \le 0$ for every solution and every $k \neq 0$. The result also holds after a convergent sum with time-independent, nonnegative comoving Sobolev weights.

Proof. The exact equation $(a^3 K_d \dot{\zeta}_k)^{\cdot} + a^3 V_d \zeta_k = 0$ implies

$$\dot{\mathcal{E}}_k = -2H_d(3K_d - XK_{d,X})|\dot{\zeta}_k|^2 - 2H_d X V_{d,X}|\zeta_k|^2. \tag{252}$$

The numerator of $3K_d - XK_{d,X}$ over Z^2 is

$$\begin{aligned}
&140625\delta^2 X^4 + 250\delta(1000\mathfrak{k} + 1089\delta)X^3 + 4\delta(191000\mathfrak{k} - 3339\delta)X^2 \\
&\qquad + 32\mathfrak{k}(5625\mathfrak{k} + 10253\delta)X + 120960\mathfrak{k}^2 > 0.
\end{aligned} \tag{253}$$

Write $V_{d,X}/H_d^2 = P_8(X)/(4\mathfrak{k}^2 Z^3)$. All coefficients of P_8 are manifestly positive except the coefficient whose expanded form contains a negative monomial. That coefficient is

$$\begin{aligned}
[X^4]P_8 = 4\mathfrak{k}\delta\big[&5062500\mathfrak{k} - 20625000\mathfrak{k}^2\delta + 179098000\mathfrak{k}\delta^2 + 527643750\mathfrak{k}\delta \\
&+ 668935260\delta^3 + 356903113\delta^2\big] > 0.
\end{aligned} \tag{254}$$

The inequality follows from $\mathfrak{k}\delta = 10^{-110} < 1/10$. The complete polynomial is provided in the exact-check data and verified by symbolic differentiation. Both coefficients in Equation (252) therefore have the required sign. □

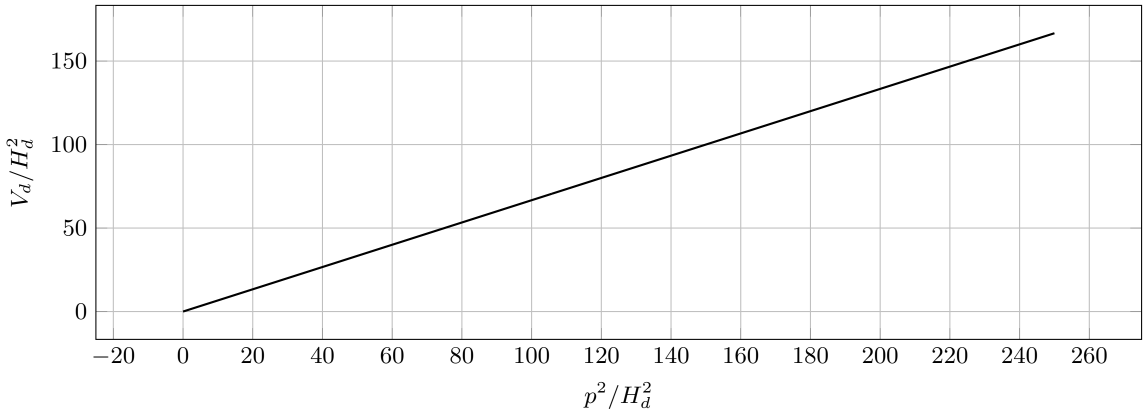

FIG. 1. Recomputed endpoint restoring coefficient at the revised coefficient point. The exact positivity and energy results use the polynomial identities, not the plotted finite momentum interval.

This is an all-initial-data linear energy result on a time-dependent background, stronger than instantaneous positivity. It excludes growth in the displayed energy. It does not prove nonlinear stability, nor a uniform-in-time bound on ζ obtained by dividing by V_d, because $X \to 0$ and $V_d \to 0$ along expansion. A canonical pump term is not being discarded: the proof uses the exact nonautonomous equation.

Corollary XII.3 (An open positive source-free exterior collar)**.** *For the revised fixed positive coefficients, a sufficiently small source-free collar $Q_d < Q < Q_d + \varepsilon$ has $\mathcal{D}, K, V_{\rm full} > 0$ for every nonzero momentum.*

Proof. Compactify momentum with $y = X/(1+X)$ and normalize the three symbols as $\mathcal{D}/[H_d^2(1+X^2)]$, K, and $V/[H_d^2 X(1+X^2)]$. Their endpoint limits are positive: $K_d(0) = 56/45$, $K_d(\infty) = 3$, $V_d/(H_d^2 X) \to 2/3$ at zero, and the ultraviolet restoring coefficient is positive. Smoothness in the constant-coefficient late plateau and compactness give a common positive margin on a sufficiently small collar. This does not assign its width or extend the energy-monotonicity theorem to a general evolving background. □

D. Base-action scalar derivation and seed instability diagnostic

The following reduction through the matter-point no-go concerns S_0. The completed local-vacuum proof is in Section XIII.

For comparison, the following reference-action calculation isolates the finite-stiffness seed's flat-vacuum problem. The completed coefficients are those above. The auxiliary expansion is recorded in Supplemental Material, Appendix J; relevant operator precedents are [6–8, 26].

The visible-fluid extension of the completed action is derived in Section XV.

E. FLRW variables and invariant background combinations

Choose matter proper time on the background, $\bar{N} = 1$, and use the physical clock as the unitary-gauge slicing field,

$$T = \bar{T}(t), \qquad Q(t) = \dot{\bar{T}}(t) > 0. \tag{255}$$

For the nonzero scalar Fourier modes write

$$N = 1 + \alpha, \qquad N_i = \partial_i \psi, \qquad h_{ij} = a^2(t) e^{2\zeta} \delta_{ij}, \qquad x \equiv \frac{k^2}{a^2}. \tag{256}$$

The homogeneous $k = 0$ perturbation is a variation of the background solution and is not counted as a separate oscillator.

Four combinations control the entire reduction:

$$\sigma_J \equiv -\widehat{\mathcal{J}}_{,Y}(\bar{Q},0) = \Sigma_{\mathrm{A}}(\bar{Q}), \tag{257}$$

$$\sigma_J = 1 \quad \text{on the matter/late plateau,} \qquad \sigma_J = \frac{1}{16} \quad \text{on the primordial plateau,}$$

$$\mathcal{W}_s \equiv 2H - Q\mathcal{B}_{,Q}, \tag{258}$$

$$\mathcal{D}_s \equiv \mathcal{K}_{,QQ} + 3H\mathcal{B}_{,QQ}, \qquad \Xi_s \equiv \mathcal{D}_s + \frac{3}{2}\mathcal{B}_{,Q}^2, \tag{259}$$

$$\begin{aligned} \mathcal{C}_s &\equiv -\dot{\mathcal{W}}_s + H\mathcal{W}_s - \frac{1}{2}\mathcal{W}_s^2 \\ &= -2\dot{H} + \dot{Q}\big(\mathcal{B}_{,Q} + Q\mathcal{B}_{,QQ}\big) + HQ\mathcal{B}_{,Q} - \frac{1}{2}Q^2\mathcal{B}_{,Q}^2. \end{aligned} \tag{260}$$

The quantity Ξ_s is exactly the homogeneous specialization of the Dirac rank scalar in Equation (134). The quantity $\mathcal{W}_s$ is the coefficient of the scalar momentum constraint; it is unrelated to the compact benchmark window $W(Q)$. The coefficient $\mathcal{C}_s$ controls the reduced spatial-gradient energy.

F. Complete unreduced quadratic action

After expanding the action through second order, using the background equations, and discarding boundary terms, the gravity–clock scalar action is

$$\begin{aligned} S^{(2)}_{s,\mathrm{unred}} = M_{\mathrm{Pl}}^2 \int \mathrm{d}t\mathrm{d}^3x\, a^3 \Bigg\{ & -3\dot{\zeta}^2 + \mathcal{W}_s\alpha\left(3\dot{\zeta} - \frac{\partial^2\psi}{a^2}\right) + 2\dot{\zeta}\frac{\partial^2\psi}{a^2} \\ & + \frac{1}{2}\left(Q^2\mathcal{D}_s - 6H^2 + 6HQ\mathcal{B}_{,Q}\right)\alpha^2 - 2\alpha\frac{\partial^2\zeta}{a^2} + \frac{(\partial\zeta)^2}{a^2} + \sigma_J\frac{(\partial\alpha)^2}{a^2} \Bigg\}. \end{aligned} \tag{261}$$

Equation (261) contains every quadratic term of the base action S_0. The completed action adds Equation (242). In particular, the acceleration operator does not introduce a new time derivative: because Y begins quadratically in the lapse gradient when the background acceleration vanishes, it contributes only the last term. The action is second order in time even though the reduced kinetic coefficient will depend on k.

Varying with respect to the scalar shift gives the exact momentum constraint

$$\mathcal{W}_s\alpha - 2\dot{\zeta} = 0. \tag{262}$$

Varying with respect to the lapse gives

$$0 = \left[Q^2\mathcal{D}_s - 6H^2 + 6HQ\mathcal{B}_{,Q} - 2\sigma_J\frac{\partial^2}{a^2}\right]\alpha + 3\mathcal{W}_s\dot{\zeta} - \mathcal{W}_s\frac{\partial^2\psi}{a^2} - 2\frac{\partial^2\zeta}{a^2}. \tag{263}$$

On a curvature-gauge patch with $\mathcal{W}_s \neq 0$, the two nondynamical variables are therefore

$$\alpha = \frac{2\dot{\zeta}}{\mathcal{W}_s}, \tag{264}$$

$$\frac{\partial^2\psi}{a^2} = \frac{2}{\mathcal{W}_s^2}\left(Q^2\Xi_s - 2\sigma_J\frac{\partial^2}{a^2}\right)\dot{\zeta} - \frac{2}{\mathcal{W}_s}\frac{\partial^2\zeta}{a^2}. \tag{265}$$

Equivalently, for a Fourier mode,

$$-\frac{k^2}{a^2}\psi_{\boldsymbol{k}} = \frac{2\left(Q^2\Xi_s + 2\sigma_J x\right)}{\mathcal{W}_s^2}\dot{\zeta}_{\boldsymbol{k}} + \frac{2x}{\mathcal{W}_s}\zeta_{\boldsymbol{k}}. \tag{266}$$

The only possible algebraic denominators in this reduction are $\mathcal{W}_s$ and the positive kinetic combination displayed below. No function has been reconstructed from a desired perturbation history.

G. Exact reduced action, characteristic factor, and Hamiltonian

Substituting Equations (264) and (265) into Equation (261) and integrating the single $\zeta\dot{\zeta}$ term by parts gives

$$\boxed{S_s^{(2)} = \frac{1}{2}\int \mathrm{d}t \frac{\mathrm{d}^3k}{(2\pi)^3}\, a^3 \left[Q_s(t,k)|\dot{\zeta}_{\boldsymbol{k}}|^2 - F_s(t)\frac{k^2}{a^2}|\zeta_{\boldsymbol{k}}|^2\right],} \tag{267}$$

where

$$\boxed{Q_s(t,k) = \frac{4M_{\rm Pl}^2}{\mathcal{W}_s^2}\left(Q^2\Xi_s + 2\sigma_J\frac{k^2}{a^2}\right),} \tag{268}$$

$$\boxed{F_s(t) = \frac{4M_{\rm Pl}^2}{\mathcal{W}_s^2}\mathcal{C}_s, \qquad c_s^2(t,k) \equiv \frac{F_s}{Q_s} = \frac{\mathcal{C}_s}{Q^2\Xi_s + 2\sigma_J k^2/a^2}.} \tag{269}$$

There is no algebraic ζ^2 mass term on an exact source-free FLRW solution:

$$\mathcal{M}_s^2(t,k) = 0 \qquad \text{in the curvature variable } \zeta. \tag{270}$$

Time dependence nevertheless produces the usual pump term after canonical normalization. Defining

$$z_k^2 \equiv a^3 Q_s(t,k), \qquad v_{\boldsymbol{k}} \equiv z_k\zeta_{\boldsymbol{k}}, \tag{271}$$

the canonical mode satisfies

$$\ddot{v}_{\boldsymbol{k}} + \Omega_k^2 v_{\boldsymbol{k}} = 0, \qquad \Omega_k^2 = c_s^2\frac{k^2}{a^2} - \frac{\ddot{z}_k}{z_k}. \tag{272}$$

The pump contribution is a background-growth or tachyonic diagnostic; it is not a ghost criterion.

Freezing the background coefficients over a time interval short compared with their evolution gives the complete physical scalar characteristic factor

$$\boxed{\mathcal{P}_s(\omega,k) = Q_s(t,k)\omega^2 - F_s(t)\frac{k^2}{a^2} = 0, \qquad \omega^2(k) = \frac{\mathcal{C}_s\, k^2/a^2}{Q^2\Xi_s + 2\sigma_J k^2/a^2}.} \tag{273}$$

Thus

$$\omega^2 = \frac{\mathcal{C}_s}{Q^2\Xi_s}\frac{k^2}{a^2} + \mathcal{O}(k^4/a^4), \qquad\qquad k/a \longrightarrow 0, \tag{274}$$

$$\omega^2 \longrightarrow \frac{\mathcal{C}_s}{2\sigma_J}, \qquad \frac{\omega}{k/a} \longrightarrow 0, \qquad\qquad k/a \longrightarrow \infty. \tag{275}$$

The lapse-gradient operator therefore produces a dispersive scalar whose high-k frequency saturates rather than a mode with an arbitrarily large propagation speed. The time evolution remains second order.

The momentum conjugate to $\zeta_{\boldsymbol{k}}$ is

$$\Pi_{\boldsymbol{k}} = a^3 Q_s\dot{\zeta}_{-\boldsymbol{k}}, \tag{276}$$

and the fully reduced quadratic Hamiltonian is

$$\boxed{H_s^{(2)} = \frac{1}{2}\int \frac{\mathrm{d}^3k}{(2\pi)^3}\left[\frac{|\Pi_{\boldsymbol{k}}|^2}{a^3Q_s} + a^3F_s\frac{k^2}{a^2}|\zeta_{\boldsymbol{k}}|^2\right].} \tag{277}$$

This expression answers the infrared-energy question on every expanding FLRW patch for which the reduction is valid.

Theorem XII.4 (Quadratic FLRW stability criterion)**.** *For a source-free spatially flat FLRW solution of the reference action S_0, suppose*

$$Q > 0, \qquad \Xi_s > 0, \qquad \sigma_J > 0, \qquad \mathcal{W}_s \neq 0, \qquad \mathcal{C}_s > 0. \tag{278}$$

Then every nonzero Fourier mode of the unique gravity–clock scalar has $Q_s > 0$, $F_s > 0$, $c_s^2 > 0$, a real frozen-coefficient frequency, no lapse/shift pole, and a positive instantaneous quadratic Hamiltonian in the stated curvature variables. Conversely, within this curvature-gauge patch, $\Xi_s < 0$ produces an infrared ghost, $\mathcal{C}_s < 0$ produces a gradient and negative-energy instability, and $\mathcal{C}_s = 0$ is a marginal quadratic surface requiring a higher-order analysis.

The condition $\mathcal{W}_s \neq 0$ states that the momentum constraint can be solved in the curvature variable. A zero of $\mathcal{W}_s$ is a "braiding crossing" of this gauge reduction and is not, by itself, a proof of a physical singularity; another nonsingular perturbation variable must be used there. The signs of Q_s and F_s give the stated quadratic kinetic and gradient test in this valid reduction. Time-dependent pump terms, matter mixing, and higher-order interactions require separate tests.

H. Exact unbraided DBI branch

In the condensate-side unbraided SCFT-A DBI region,

$$\mathcal{B}_{,Q} = \mathcal{B}_{,QQ} = 0, \qquad \mathcal{W}_s = 2H, \qquad \Xi_s = \mathcal{K}_{,QQ}, \qquad \mathcal{C}_s = -2\dot{H}. \tag{279}$$

For a source-free clock background, the Raychaudhuri equation gives $-2\dot{H} = Q\mathcal{K}_{,Q}$. Equations (268) and (269) reduce exactly to

$$Q_s = \frac{M_{\rm Pl}^2}{H^2}\left(Q^2\mathcal{K}_{,QQ} + 2\frac{k^2}{a^2}\right), \tag{280}$$

$$F_s = \frac{M_{\rm Pl}^2}{H^2} Q\mathcal{K}_{,Q}, \tag{281}$$

$$c_s^2(t,k) = \frac{Q\mathcal{K}_{,Q}}{Q^2\mathcal{K}_{,QQ} + 2k^2/a^2}. \tag{282}$$

At $k/a \to 0$ this reproduces the intrinsic kinetic-fluid result,

$$c_s^2(t,0) = \frac{\mathcal{K}_{,Q}}{Q\mathcal{K}_{,QQ}} = c_{\rm ad}^2. \tag{283}$$

For the explicit DBI function and the positive-charge branch $Q > 1$, both $\mathcal{K}_{,Q}$ and $\mathcal{K}_{,QQ}$ are positive. Therefore every expanding source-free DBI mode of S_0 passes its quadratic ghost, gradient, and Hamiltonian tests, while the long-wavelength sound speed tends to zero toward the condensate limit derived in Section VIII D. This is an exact consistency check on the reduction.

I. Reference-action late fixed point and the infrared sign sector

At the SCFT-A de Sitter endpoint,

$$\mathcal{W}_{s,d} = 2H_d - Q_d b_d, \qquad \Xi_{s,d} = \kappa_d + \frac{3}{2}b_d^2, \qquad \mathcal{C}_{s,d} = \frac{1}{2}Q_d b_d\left(2H_d - Q_d b_d\right). \tag{284}$$

The opposite sign choice $b_d < 0$, $\kappa_d > 0$ makes $\mathcal{W}_{s,d} > 0$ but necessarily gives $\mathcal{C}_{s,d} < 0$ and therefore a scalar gradient instability for every nonzero k.

For S_0, a nonempty sufficient endpoint region satisfying Dirac regularity, scalar quadratic positivity, and the source-free reciprocal response is

$$\boxed{b_d > 0, \qquad -\frac{3}{2}b_d^2 < \kappa_d < 0, \qquad 0 < Q_d b_d < 2H_d.} \tag{285}$$

Indeed, $\Xi_{s,d} > 0$, $\mathcal{W}_{s,d} > 0$, and $\mathcal{C}_{s,d} > 0$ hold simultaneously. Reciprocity follows from $Q_d\kappa_d + 3H_d b_d > 0$ in Equation (182), not from b_d/κ_d. The choice $\kappa_d < 0$ selects this benchmark; it is not necessary for reciprocity on every stable endpoint. It is useful to parameterize this open set by

$$r_d \equiv \frac{Q_d b_d}{H_d} \in (0,2), \qquad \chi_d \equiv -\frac{\kappa_d}{b_d^2} \in \left(0, \frac{3}{2}\right). \tag{286}$$

Then

$$\mathcal{W}_{s,d} = H_d(2 - r_d), \qquad \Xi_{s,d} = b_d^2\left(\frac{3}{2} - \chi_d\right), \qquad \mathcal{C}_{s,d} = \frac{1}{2}r_d(2 - r_d)H_d^2, \tag{287}$$

$$c_{s,d}^2(0) = \frac{2 - r_d}{r_d(3 - 2\chi_d)}. \tag{288}$$

If one additionally requires the long-wavelength scalar cone to lie inside or on the metric cone at the endpoint, the exact condition is

$$r_d \geq \frac{1}{2-\chi_d}. \tag{289}$$

Because $0 < \chi_d < 3/2$, the interval defined by Equations (286) and (289) is nonempty. These restrictions fix the infrared endpoint of the benchmark in Equation (39) and Table I. The all-momentum positivity of the final spatial completion follows independently from Theorem XII.1.

J. Unrepaired strict Minkowski boundary: two independent quadratic derivations

This subsection audits the finite-stiffness seed action, not the adopted repaired action at $Q = 1$. Its role in the revised manuscript is diagnostic: it identifies the sign obstruction that forces the compact vacuum modification in Section XIII.

The FLRW curvature reduction cannot be continued by simply setting $H = 0$ at the matter point, because there

$$Q = 1, \qquad H = 0, \qquad \mathcal{W}_s = 0. \tag{290}$$

The exact seed Minkowski solution is also a homogeneous zero-charge sector: the unbraided current gives $C_T = a^3\mathcal{K}_{\mathrm{A},Q}(1) = 0$. In the seed action it is not a singular point of the nonlinear Dirac operator: $\Xi = \kappa_m > 0$ and the lapse operator remains coercive on the stated domains. What fails is the particular curvature-variable elimination that divides by $\mathcal{W}_s$. The nonlinear count remains one clock scalar, although its quadratic dynamics is degenerate in this representation. It must therefore be analyzed independently rather than inferred by substituting into a curvature-gauge formula whose momentum-constraint coefficient vanishes.

First retain the clock perturbation and write

$$\mathrm{d}s^2 = -(1+2\Phi)\mathrm{d}t^2 + (1-2\Psi)\delta_{ij}\mathrm{d}x^i\mathrm{d}x^j, \qquad T = t + \sigma, \qquad \Upsilon \equiv \dot{\sigma} - \Phi. \tag{291}$$

Near $Q = 1$ the unrepaired seed benchmark obeys

$$\mathcal{K} = \frac{\kappa_m}{2}(Q-1)^2 + \mathcal{O}[(Q-1)^4], \qquad \mathcal{B} = 0 \text{ with all } Q \text{ derivatives}, \qquad \mathcal{J} = -Y + \mathcal{O}(Y^{3/2}). \tag{292}$$

Define

$$\mu^2 \equiv \frac{\kappa_m}{2} > 0, \qquad \alpha_{\mathrm{M}} \equiv -\mathcal{J}_{,Y}(0) = 1. \tag{293}$$

A gauge-invariant expansion gives

$$S^{(2)}_{\mathrm{Mink}} = M_{\mathrm{Pl}}^2 \int \mathrm{d}t\mathrm{d}^3x \left[-3\dot{\Psi}^2 + (\partial\Psi)^2 + 2\Phi\partial^2\Psi + \alpha_{\mathrm{M}}(\partial\Upsilon)^2 + \mu^2\Upsilon^2\right]. \tag{294}$$

The exact linear constraint reduction yields

$$H^{(2)}_{\mathrm{Mink,dec}} = M_{\mathrm{Pl}}^2 \int \frac{\mathrm{d}^3k}{(2\pi)^3} \frac{(1-\alpha_{\mathrm{M}})k^2 - \mu^2}{\alpha_{\mathrm{M}}k^2 + \mu^2} k^2 |\Psi_{\boldsymbol{k}}|^2. \tag{295}$$

For the unrepaired finite-stiffness seed, $\alpha_{\mathrm{M}} = 1$, and hence

$$\boxed{H^{(2)}_{\mathrm{Mink,dec}} = -M_{\mathrm{Pl}}^2 \int \frac{\mathrm{d}^3k}{(2\pi)^3} \frac{\mu^2k^2}{k^2+\mu^2} |\Psi_{\boldsymbol{k}}|^2 < 0 \quad (k \neq 0).} \tag{296}$$

This statement concerns the quadratic second variation about the exactly homogeneous, zero-charge Minkowski configuration. It proves that this configuration is not a local minimum of the quadratic energy. It does *not* by itself prove that the complete nonlinear Hamiltonian is unbounded at every wavenumber, because the MOND contribution begins at cubic order in the acceleration. In the closest published khronon model, those nonlinear terms bound the high-k energy while a long-wavelength Jeans band remains [8].

The result is independently reproduced without restoring the clock perturbation. Set $H = 0$, $Q = 1$, and $a = 1$ directly in the unreduced ADM action (261). For one real Fourier mode,

$$\frac{L^{(2)}_{k,\mathrm{ADM}}}{M^2_{\mathrm{Pl}}} = -3\dot{\zeta}_k^2 - 2k^2\dot{\zeta}_k\psi_k + \frac{1}{2}\left(\kappa_m + 2\sigma_J k^2\right)\alpha_k^2 + 2k^2\alpha_k\zeta_k + k^2\zeta_k^2. \tag{297}$$

The shift and lapse equations give, respectively,

$$\dot{\zeta}_k = 0, \qquad \alpha_k = -\frac{2k^2}{\kappa_m + 2\sigma_J k^2}\,\zeta_k. \tag{298}$$

The reduced ADM Hamiltonian is therefore

$$\boxed{H^{(2)}_{k,\mathrm{ADM}} = M^2_{\mathrm{Pl}}k^2\,\frac{2(1-\sigma_J)k^2 - \kappa_m}{\kappa_m + 2\sigma_J k^2}\,|\zeta_k|^2.} \tag{299}$$

Using $\sigma_J = 1$, $\mu^2 = \kappa_m/2$, and $\zeta = -\Psi$ at linear order, equation (299) is exactly equation (296). Thus the negative quadratic direction is not a gauge artifact or a missed term in the first derivation.

K. Positive-charge DBI branch and the singular zero-charge limit

The independent Minkowski result does not determine the sign on the expanding cosmological solution. The conserved charge divides the two calculations into dynamically invariant sectors. For $C_T > 0$, define Z and R as in equation (200). At every finite scale factor,

$$Z = \frac{C_T}{\kappa_m a^3} > 0, \qquad Q = 1 + \frac{Z}{R} > 1, \qquad R = \sqrt{1 + \lambda_D Z^2}. \tag{300}$$

The exact DBI identities are

$$\mathcal{K}_{,Q} = \kappa_m Z, \qquad \mathcal{K}_{,QQ} = \kappa_m R^3, \qquad 3H^2 = \kappa_m\left[Z + \frac{R-1}{\lambda_D}\right], \qquad -2\dot{H} = Q\kappa_m Z. \tag{301}$$

Consequently,

$$\mathcal{W}_s = 2H > 0, \qquad \Xi_s = \kappa_m R^3 > 0, \qquad \mathcal{C}_s = Q\kappa_m Z > 0 \tag{302}$$

for every $Z > 0$. With physical wavenumber $p = k/a$, the exact reduced coefficients and frozen frequency are

$$Q_s = \frac{M^2_{\mathrm{Pl}}}{H^2}\left(Q^2\kappa_m R^3 + 2p^2\right) > 0, \tag{303}$$

$$F_s = \frac{M^2_{\mathrm{Pl}}}{H^2} Q\kappa_m Z > 0, \tag{304}$$

$$\omega^2(p) = \frac{Q\kappa_m Z\,p^2}{Q^2\kappa_m R^3 + 2p^2} > 0 \qquad (p \neq 0). \tag{305}$$

Proposition XII.5 (No open negative-energy interval on the positive-charge DBI branch)**.** *For the exact source-free unbraided DBI reference solution with $C_T > 0$, the displayed scalar kinetic and gradient coefficients and frozen frequency are positive wherever that reference solution is defined. Applying the statement to the completed action requires restricting to its DBI interval and using the completed coefficients.*

Proof. At finite a, equation (300) gives $Z > 0$. Equations (301)–(302) then satisfy all hypotheses of Theorem XII.4; equations (303)–(305) display the signs explicitly. □

The following zero-charge limit belongs to the unmodified unbraided DBI reference theory. The completed action leaves that template at Q_b and has a different plateau; the displayed late cosmological trajectory instead ends at Q_d.

In the reference theory, as $Z \to 0^+$,

$$H^2 = \frac{\kappa_m}{3} Z + \frac{\kappa_m}{6} Z^2 - \frac{\kappa_m \lambda_D}{24} Z^4 + \mathcal{O}(Z^6), \tag{306}$$

$$Q_s(t,0) = \frac{3M_{\rm Pl}^2}{Z} + \frac{9}{2} M_{\rm Pl}^2 + \mathcal{O}(Z), \tag{307}$$

$$F_s = 3M_{\rm Pl}^2 + \frac{3}{2} M_{\rm Pl}^2 Z + \mathcal{O}(Z^2), \tag{308}$$

$$c_s^2(t,0) = Z - Z^2 + \mathcal{O}(Z^3). \tag{309}$$

Thus the physical frequency tends to zero from above while the curvature-variable normalization diverges. Simultaneously $\mathcal{W}_s = 2H \to 0$, so the transformation used to solve the momentum constraint in curvature gauge loses rank. Taking $Z \to 0^+$ *after* reduction is therefore not equivalent to imposing the exact $C_T = 0$, $H = 0$ background *before* reduction. The latter is a boundary sector, not an open neighborhood crossed by a solution with fixed $C_T > 0$. The stable late endpoint lies instead at (Q_d, H_d) with $Q_d > 1$ and $H_d > 0$.

The unbraided result has an additional independent check. Using $4\pi G_*(\rho_T + p_T) = Q\mathcal{K}_{,Q}/2$ and $c_{\rm ad}^2 = \mathcal{K}_{,Q}/(Q\mathcal{K}_{,QQ})$, equation (282) becomes

$$c_s^2(t,k) = c_{\rm ad}^2 \left[1 + \frac{c_{\rm ad}^2 k^2}{4\pi G_* a^2(\rho_T + p_T)}\right]^{-1}, \tag{310}$$

which is the published generalized-dark-matter sound-speed expression for the unbraided relativistic khronon sector [8].

L. Matter-point braiding no-go

It is natural to ask whether one should turn on a small braid at $Q = 1$. The exact quadratic calculation answers this question negatively. Let

$$b_m \equiv \mathcal{B}_{,Q}(1) \tag{311}$$

while retaining the exact Minkowski background, $\mathcal{K}_{,QQ}(1) = \kappa_m > 0$, and $\mathcal{J}_{,Y}(0) = -1$. The FLRW invariants evaluated on that constant background are

$$\mathcal{W}_{s,m} = -b_m, \qquad \Xi_{s,m} = \kappa_m + \frac{3}{2} b_m^2, \qquad \mathcal{C}_{s,m} = -\frac{1}{2} b_m^2. \tag{312}$$

For every $b_m \neq 0$, curvature gauge is regular but

$$\boxed{F_{s,m} = \frac{4M_{\rm Pl}^2 \mathcal{C}_{s,m}}{\mathcal{W}_{s,m}^2} = -2M_{\rm Pl}^2 < 0.} \tag{313}$$

Turning on matter-point braiding would therefore replace the zero-frequency negative-energy direction by a genuine gradient instability. If $b_m = 0$, all higher Q derivatives of $\mathcal{B}$ are multiplied by H or $\dot{Q}$ on the exact constant Minkowski background and do not change the quadratic result.

Proposition XII.6 (Matter-point braid no-go within the SCFT operator set)**.** *Assume the action contains only the displayed $\mathcal{K}(Q)$, $\mathcal{B}(Q)\Theta$, and $\mathcal{J}(Y)$ operators, with $\mathcal{K}_{,QQ}(1) > 0$ and exact MOND normalization $-\mathcal{J}_{,Y}(0) = 1$. No choice of $\mathcal{B}_{,Q}(1)$ makes the exact zero-charge Minkowski scalar quadratic form positive: $\mathcal{B}_{,Q}(1) = 0$ gives equation* (296)*, whereas $\mathcal{B}_{,Q}(1) \neq 0$ gives equation* (313).

Accordingly, no choice of $\mathcal{B}_{,Q}(1)$ repairs the zero-charge Minkowski quadratic form within the operator set of Equation (4). A positive asymptotically flat zero-charge vacuum would require a different operator class or a changed assumption.

XIII. COMPLETED LOCAL-VACUUM TRANSITION AND ALL-MOMENTUM POSITIVITY

The local action is the specialization of Equation (59) with $\mathcal{B}_{\rm A} = 0$, $\Sigma_{\rm A} = 1$, and $U = \widetilde{\mathcal{K}}$. Its vacuum plateau has

$$U = U' = U'' = 0, \qquad \mathcal{B}_{\rm A} = 0, \qquad \Sigma_{\rm A} = 1, \quad \nu = \delta/\kappa_m, \quad \ell = 1/\kappa_m. \tag{314}$$

The exact vacuum remains

$$g_{\mu\nu} = \eta_{\mu\nu}, \quad T = t, \quad Q = 1, \quad H = 0, \quad C_T = 0. \tag{315}$$

Every added operator and its first variation vanish on this state.

A. Homogeneous equations and positive-floor switches

Use matter proper time t on the homogeneous background. Because $D_i K = 0$, $q_i = 0$, and ${}^{(3)}R = 0$, all four spatial completion operators and their first variations vanish on spatially flat homogeneous data. Thus

$$3H^2 = QU' - U, \qquad -2\dot{H} = QU', \qquad a^3 U' = C_T > 0. \tag{316}$$

Here $U = \widetilde{\mathcal{K}} = \kappa_m u$ and $\lambda_D = 1$. The lower extension uses $1 + |Q - 1|$; the following source-free expanding branch and its positivity proof are on the upper side.

Introduce dimensionless variables used through Section XIII D:

$$\begin{aligned}
&\tau = \sqrt{\kappa_m}\, t, && \mathcal{H} = H/\sqrt{\kappa_m}, && h = \mathcal{H}^2 = \frac{QF - u}{3}, \\
&x = \frac{p^2}{\kappa_m}, && m = Q^2 g, && q = -\frac{\dot{H}}{H^2} = \frac{QF}{2h}, \\
&\mathfrak{D} = \frac{\mathrm{d}}{\mathrm{d}\ln a}, && \mathfrak{D}Q = -\frac{3F}{g}, && m_N \equiv \mathfrak{D}m = -6QF - \frac{3Q^2 F g'}{g}.
\end{aligned} \tag{317}$$

The scalar h here is not the spatial metric h_{ij}. The symbol q without an index denotes deceleration, not the lapse-gradient vector q_i. The background identities give

$$\mathfrak{D}x = -2x, \qquad \mathfrak{D}h = -2qh, \qquad \frac{3}{2} \le q \le \frac{3Q_b}{2Q_a} = \frac{1515}{1001} < \frac{7}{4}. \tag{318}$$

Indeed $QF - u = \int_{Q_a}^{Q} r g(r)\mathrm{d}r$ lies between $Q_a F$ and QF.

Let

$$Q_1 = Q_a + L/3 = \frac{251}{250}, \qquad Q_2 = Q_a + 2L/3 = \frac{1007}{1000}. \tag{319}$$

Fix the exact floor

$$\rho = \frac{1}{2}. \tag{320}$$

The two ordered profiles and their positive-floor completions are

$$\begin{aligned}
&w(Q) = \left[1 - S\left(\frac{Q - Q_1}{Q_2 - Q_1}\right)\right]^3, && v(Q) = 1 - S\left(\frac{Q - Q_2}{Q_b - Q_2}\right), \\
&r(Q) = \rho + (1-\rho) w(Q), && \lambda(Q) = \rho + (1-\rho) v(Q), \\
&\nu(Q) = \frac{\delta}{\kappa_m} r(Q), && \ell(Q) = \frac{1}{\kappa_m}\lambda(Q), && \tau_6 = \frac{\delta^2}{\kappa_m^2}, \qquad \delta > 0.
\end{aligned} \tag{321}$$

Thus $\lambda = 1$ throughout the varying part of r; only after r has reached its floor does λ vary. Along expansion $r_N \equiv \mathfrak{D}r \ge 0$ and $\lambda_N \equiv \mathfrak{D}\lambda \ge 0$, since Q decreases. Crucially,

$$\nu \ge \frac{\rho\delta}{\kappa_m} > 0, \qquad \ell \ge \frac{\rho}{\kappa_m} > 0, \qquad \tau_6 = \frac{\delta^2}{\kappa_m^2} > 0. \tag{322}$$

The profiles still carry every switch derivative, but neither nonlinear operator changes order. The positive dimensionless coupling δ is fixed exactly in Section XIII C.

B. Complete scalar reduction

In proper-time coordinates use $N = 1 + \alpha$, $T = \bar{T}(t)$ with $\dot{\bar{T}} = Q$, and hence $\delta Q = -Q\alpha$. Equivalently, the clock-coordinate lapse is $\bar{N}(1+\alpha)$. Use $N_i = \partial_i \psi$, $h_{ij} = a^2 e^{2\zeta}\delta_{ij}$, and $\chi = \Delta\psi/a^2$. For one real nonzero Fourier mode put

$$b_p = \nu p^2, \qquad A_p = 2 + 3b_p, \qquad C_p = p^2(1 + \ell p^2), \qquad M = Q^2 U''. \tag{323}$$

The full background-on-shell quadratic Lagrangian is

$$\begin{aligned}\frac{L_p^{(2)}}{M_{\rm Pl}^2 a^3} = &-3\dot{\zeta}^2 + 2\dot{\zeta}\chi + 2H\alpha(3\dot{\zeta} - \chi) + \frac{1}{2}(M - 6H^2 + 2p^2)\alpha^2 \\ &+ 2C_p\alpha\zeta + p^2\zeta^2 - 8\eta_R p^4\zeta^2 - 3\tau_6 p^6\zeta^2 - \frac{b_p}{2}(3\dot{\zeta} - \chi - 3H\alpha)^2.\end{aligned} \tag{324}$$

The last term follows from $\delta K = 3\dot{\zeta} - \chi - 3H\alpha$. Background spatial gradients vanish, so perturbations of ν first contribute to this operator at cubic order. Its time-dependent background coefficient must nevertheless be differentiated in the reduced action.

Set

$$\mathcal{D}_p = 2H^2 A_p + b_p(M + 2p^2) = 4H^2 + b_p(6H^2 + M + 2p^2). \tag{325}$$

Direct solution of the two auxiliary equations gives

$$\begin{aligned}&\alpha = \frac{2HA_p\dot{\zeta} - 2b_pC_p\zeta}{\mathcal{D}_p}, && \chi = \frac{A_p[(M+2p^2)\dot{\zeta} + 2HC_p\zeta]}{\mathcal{D}_p}, \\ &K_p = \frac{A_p(M+2p^2)}{\mathcal{D}_p}, && B_p = \frac{2HC_pA_p}{\mathcal{D}_p}, \qquad V_{0p} = \frac{2b_pC_p^2}{\mathcal{D}_p} - p^2.\end{aligned} \tag{326}$$

In particular the determinant of the (α, χ) quadratic Hessian is $-\mathcal{D}_p$. After one time integration by parts,

$$\begin{aligned}\frac{L_{p,\rm red}^{(2)}}{M_{\rm Pl}^2 a^3} &= K_p\dot{\zeta}^2 - V_p^{\rm full}\zeta^2, \\ V_p^{(0)} &= \frac{2b_pC_p^2}{\mathcal{D}_p} - p^2 + \frac{1}{a^3}\frac{\mathrm{d}}{\mathrm{d}t}(a^3B_p).\end{aligned} \tag{327}$$

Here and in the positivity polynomial it is useful to denote this displayed quantity by $V_p^{(0)}$. The full completed potential is

$$V_p^{\rm full} = V_p^{(0)} + 8\eta_R p^4 + 3\tau_6 p^6 > V_p^{(0)}. \tag{328}$$

The derivative is taken at fixed comoving wave number, so $\dot{p} = -Hp$. Both switch derivatives are included.

1. *The two endpoint tests*

On the exact plateau $H = U'' = 0$, $\nu = \delta/\kappa_m > 0$, $\ell = 1/\kappa_m$, and every $p \neq 0$ has

$$\begin{aligned}&K_{p,\rm M} = 3 + \frac{2}{\nu p^2} > 0, \qquad V_{p,\rm M}^{\rm full} = (2\ell + 8\eta_R)p^4 + (\ell^2 + 3\tau_6)p^6 > 0, \\ &\omega_{p,\rm M}^2 = \frac{\nu p^2}{2 + 3\nu p^2}\left[(2\ell + 8\eta_R)p^4 + (\ell^2 + 3\tau_6)p^6\right] > 0.\end{aligned} \tag{329}$$

Thus $\omega^2/p^6 \to \nu(\ell + 4\eta_R)$ as $p \to 0$. This differs from the old momentum-independent trace repair; its Minkowski kinetic coefficient must not be reused.

For a fixed rolling background with $H > 0$,

$$\lim_{p\to 0}\frac{V_p^{\rm full}}{p^2} = q > 0. \tag{330}$$

This removes the earlier -1 infrared limit, but by itself it would not exclude a finite-momentum negative band. The next sections prove the all-momentum statement.

The tensor quadratic action on all these FLRW backgrounds is

$$S_T^{(2)} = \frac{M_{\rm Pl}^2}{8} \int \mathrm{d}t\, \mathrm{d}^3x\, a^3 [\dot\gamma_{ij}^2 - p^2\gamma_{ij}^2 - \tau_6 p^6 \gamma_{ij}^2]. \tag{331}$$

The first-order tensor trace and first-order scalar spatial curvature of a transverse-traceless perturbation vanish, while $\delta^{(3)}R_{ij} = -\Delta\gamma_{ij}/2$. Hence the trace-gradient and curvature–lapse operators do not alter this sector, and the final curvature-gradient term supplies the positive sixth-order contribution.

C. An exact positive choice of the coupling

All quantities in this section are dimensionless as in (317). The moment integrals and unique root (47) define the kinetic profile exactly. The coupling is an explicit rational number justified by uniform sufficient bounds, rather than a numerical extremum.

Put $s = Q - Q_a$. The flat bump endpoint gives

$$\begin{aligned} &g(Q_a + s) = ce^{-1}e^{-L/s}[1 + O(s)], \\ &\frac{F}{g} = \frac{s^2}{L}[1 + O(s)], \qquad \frac{u}{F} = \frac{s^2}{L}[1 + O(s)], \qquad a_m \equiv -\frac{m_N}{m} \longrightarrow 3. \end{aligned} \tag{332}$$

These follow by substituting $r = L/s$ in the endpoint integrals; the differentiated expansions have the corresponding orders. In particular

$$\frac{h}{m^2} \longrightarrow +\infty, \qquad \frac{h}{m^{3/2}} \longrightarrow +\infty. \tag{333}$$

Choose $n_0 = 16$. The companion proves

$$a_m(Q) \geq q(Q) + 1 \quad (Q_a < Q \leq Q_a + L/16). \tag{334}$$

Set $Q_0 = Q_a + L/16$, $I_0 = (Q_a, Q_0]$, and $I = [Q_0, Q_b]$. Define

$$d_0 = \inf_{I_0} \frac{8h}{m^2} > 0, \qquad d_1 = \inf_{I_0} \frac{h}{m^{3/2}} > 0, \qquad h_* = \min_I h > 0. \tag{335}$$

The infima are positive by (333), positivity in the interior, and compactness away from the left endpoint.

The step obeys $0 \leq S' \leq 40/9$; a direct bound is given below. Therefore

$$0 \leq r_N \equiv \mathfrak{D}r \leq R_*, \qquad R_* = \frac{40(1-\rho)}{Q_2 - Q_1} \max_{[Q_1,Q_2]} \frac{F}{g} < \infty. \tag{336}$$

For I set

$$\begin{aligned} A_1 &= \max_I \{m(q-1) + |m_N| + R_* m\}, \\ E_2 &= \max_I \{6h[m(q+1) + |m_N|] + m^2 + 4h[m(q-1) + |m_N|] + 4hR_*m + 8hR_*\}, \\ E_3 &= \max_I \{6h[m(q+1) + |m_N|] + 2m + 8hR_*\}, \\ c_* &= 4\rho h_*^2, \qquad d_* = 8\rho^3 h_*. \end{aligned} \tag{337}$$

All these constants are positive. A sufficient coupling condition is

$$2\delta \leq \min\left\{1, d_0, d_1, \frac{\rho h_*}{A_1}, \sqrt{\frac{27c_*^2 d_*}{32E_2^3}}, \frac{27c_* d_*^2}{32E_3^3}\right\}. \tag{338}$$

The adopted exact action coefficient is

$$\boxed{\delta = 10^{-140}}. \tag{339}$$

The companion gives an independent sufficient-bounds certificate:

$$d_0, d_1 \geq 10^{-12}, \quad h_* > 10^{-22}, \quad A_1, E_2 < 10^{20}, \quad E_3 < 10^{14}. \tag{340}$$

These strict bounds imply the displayed coupling condition by exact rational arithmetic. They use analytic estimates on the entire inner and compact intervals, with a rigorously enclosed moment integral to bound the bump tilt. They do not use the former binary64 extremum. The following proof uses only the sufficient inequalities, so it applies to this exact rational choice for every $\kappa_m > 0$.

Bound on the smooth step. For $1/4 \leq z \leq 3/4$, use $S(1-S) \leq 1/4$ and $z^{-2} + (1-z)^{-2} \leq 160/9$. For $0 < z \leq 1/4$, put $r = 1/z \geq 4$; then

$$S'(z) \leq e^{4/3-r}(r^2 + 16/9) \leq (160/9)e^{-8/3} < 2. \tag{341}$$

Reflection gives the other endpoint. Since $r_N = 9(1-\rho)(F/g)(1-S)^2 S'/(Q_2 - Q_1)$ on its support, (336) follows. □

D. All-momentum positivity theorem

For this proof put $k = \kappa_m \nu = \delta r$, $k_N = \mathfrak{D} k$, and

$$A = 2 + 3kx, \qquad D = 2hA + kx(m+2x), \qquad \widehat{V}^{(0)} = V_p^{(0)}/\kappa_m. \tag{342}$$

The symbol k in this section denotes a coupling, *not* a comoving wave number. With $C = x(1+\lambda x)$ and $\widehat{B} = B_p/\sqrt{\kappa_m}$,

$$K_p = \frac{A(m+2x)}{D}, \quad \widehat{B} = \frac{2\sqrt{h}\,CA}{D}, \quad \widehat{V}^{(0)} = \frac{2kxC^2}{D} - x + \sqrt{h}\,(\mathfrak{D}\widehat{B} + 3\widehat{B}). \tag{343}$$

The completed dimensionless potential is

$$\widehat{V}^{\text{full}} = \widehat{V}^{(0)} + 4x^2 + 3\delta^2 x^3. \tag{344}$$

Theorem XIII.1 (Positive scalar quadratic form for every nonzero momentum)**.** *For* (48), (321)*, and* (339)*, every source-free expanding upper-transition background $Q_a < Q \leq Q_b$ satisfies*

$$H^2 > 0, \qquad U'' > 0, \qquad \mathcal{D}_p > 0, \qquad K_p > 0, \qquad V_p^{\text{full}} > 0 \quad \textit{for every } p^2 > 0. \tag{345}$$

The exact Minkowski endpoint has (329)*. The tensor sector has a positive $p^2 + \tau_6 p^6$ quadratic action. The proof does not require a finite Fourier grid or an interchange of the Q and p limits.*

Proof. The background and kinetic statements follow from $h, m > 0$, $k \geq 0$ and $D = 4h + kx(6h + m + 2x) > 0$. It is enough to prove $\widehat{V}^{(0)} > 0$, because (344) then gives strict positivity of the completed potential.

Polynomial identity with both switch derivatives. Differentiating (343), including $\mathfrak{D}x = -2x$, yields

$$\frac{D^2 \widehat{V}^{(0)}}{x} = \sum_{j=0}^{6} c_j x^j, \tag{346}$$

where

$$\begin{aligned}
c_0 &= 16h^2 q, \\
c_1 &= 4h[12hkq + 4h\lambda(q-1) + 4h\lambda_N - km(q-1) - km_N - k_N m], \\
c_2 &= 36h^2k^2q + 48h^2k\lambda(q-1) + 48h^2k\lambda_N - 6hk^2[m(q+1) + m_N] \\
&\quad - 4hk\lambda[m(q-1) + m_N] + 4hk\lambda_N m + 8hk(4-q) - 4hk_N\lambda m - 8hk_N - k^2m^2, \\
c_3 &= 2\{18h^2k^2\lambda(q-1) + 18h^2k^2\lambda_N - 3hk^2\lambda[m(q+1) + m_N] \\
&\qquad + 3hk^2\lambda_N m + 6hk^2(2-q) + 4hk\lambda(5-q) + 4hk\lambda_N - 4hk_N\lambda - k^2 m\}, \\
c_4 &= 4k[3hk\lambda(3-q) + 3hk\lambda_N + 2h\lambda^2 + k\lambda m], \\
c_5 &= 2k^2\lambda(6h\lambda + \lambda m + 4), \qquad c_6 = 4k^2\lambda^2.
\end{aligned} \tag{347}$$

These formulas retain both $k_N = \delta r_N$ and λ_N exactly.

Inner interval I_0. Here $r = \lambda = 1$, $k = \delta$, and $k_N = \lambda_N = 0$. By (334), $m_N \le -(q+1)m$. Thus $c_1, c_4, c_5, c_6 \ge 0$ and

$$c_2 \ge 8h\delta(4-q) - \delta^2 m^2 \ge 8h\delta, \qquad c_3 \ge -2\delta^2 m, \qquad c_5 \ge 8\delta^2. \tag{348}$$

The middle inequality uses $q < 7/4$ and $\delta m^2 \le 8h$. For $a, b, z > 0$ the weighted arithmetic–geometric mean inequality gives

$$az^2 + bz^5 \ge \frac{3}{2^{2/3}} a^{2/3} b^{1/3} z^3. \tag{349}$$

Since $\delta^2 m^3 \le h^2$,

$$(2\delta^2 m)^3 \le 8h^2\delta^4 < \frac{27}{4}(8h\delta)^2(8\delta^2), \tag{350}$$

the positive $c_2x^2 + c_5x^5$ terms dominate the possible negative c_3x^3. Also $c_0 > 0$, so (346) is strictly positive.

Compact interval I. Equation (339) implies $0 < \delta \le 1$ and $\delta A_1 \le \rho h_*$. From (318), $\rho \le r, \lambda \le 1$, $0 \le r_N \le R_*$, and (347),

$$\begin{aligned} &c_1 \ge 4h(2\rho h - \delta A_1) \ge 4\rho h^2 \ge c_*, \\ &c_4 \ge 8hk\lambda^2 \ge d_*\delta, \\ &c_2 \ge -\delta E_2, \qquad\qquad c_3 \ge -\delta E_3, \qquad c_5, c_6 \ge 0. \end{aligned} \tag{351}$$

For the negative-part bounds use $k \le \delta$, $k_N \le \delta R_*$, $\delta^2 \le \delta$, and $|m_N|$ in each negative term. Every term proportional to λ_N has a nonnegative sign, and all other omitted terms are nonnegative because $1 < q < 2$.

For $a, b > 0$, another two weighted arithmetic–geometric mean inequalities are

$$\begin{aligned} \tfrac{1}{2}(ax + bx^4) &\ge \frac{3}{2^{5/3}} a^{2/3} b^{1/3} x^2, \\ \tfrac{1}{2}(ax + bx^4) &\ge \frac{3}{2^{5/3}} a^{1/3} b^{2/3} x^3. \end{aligned} \tag{352}$$

Use $a = c_*$, $b = d_*\delta$ for the two halves of $c_1x + c_4x^4$. The definitions of δ ensure

$$\begin{aligned} (\delta E_2)^3 &\le \frac{27}{32} c_*^2 d_* \delta, \\ (\delta E_3)^3 &\le \frac{27}{32} c_* d_*^2 \delta^2. \end{aligned} \tag{353}$$

Hence (352) absorbs both possible negative coefficients and $c_0 > 0$ supplies strict positivity. This covers the varying parts of both switches and their positive exterior floors. Equation (329) proves the separate exact-vacuum statement. □

Remark XIII.2 (Meaning and limits of the theorem). The result excludes a negative spatial-gradient term and a ghost in the complete on-shell source-free FLRW scalar quadratic action, including finite momenta. It is a classical result for the specified modified action. It does not imply uniform coercivity as $p \to 0$ or $Q \to Q_a$, nor does it bound the canonically normalized background pump term, parametric amplification, matter mixing, or the nonlinear strong-coupling scale. At positive charge, $Q \downarrow Q_a$ requires $a \to \infty$; it is not a finite-scale-factor passage into the exactly zero-charge vacuum.

Corollary XIII.3 (Exact Minkowski scalar quadratic energy)**.** *On the mean-zero sector of a flat torus, or for decaying data for which the displayed Fourier integral is finite, the completed exact vacuum has*

$$H^{(2)}_{\mathrm{M,s}} = M_{\mathrm{Pl}}^2 \int \frac{\mathrm{d}^3p}{(2\pi)^3} \left[K_{p,\mathrm{M}}|\dot{\zeta}_p|^2 + V^{\mathrm{full}}_{p,\mathrm{M}}|\zeta_p|^2\right] > 0 \tag{354}$$

for nonzero physical data. On a torus replace the integral by its Fourier sum. Here the exact coefficients and dispersion are Equation (329)*. The energy is conserved because the background coefficients are constant.*

Proof. Both coefficients are strictly positive for $p \ne 0$ by Equation (329). Hamilton's equations give energy conservation mode by mode. The stated summability assumptions permit summation or integration of the mode identities. □

XIV. LOCAL VACUUM AND FULL NONLINEAR CAUCHY EVOLUTION

The completed theory has a positive local-transition quadratic form and an exact Minkowski vacuum. The first subsections below explain positive-charge asymptotics and the finite-band linear packet construction. They are followed by the full nonlinear local Hadamard theorem on the open strongly regular vacuum Cauchy domain, including its exact loss-free energy, constraint propagation, explicit rolling neighborhood, and the retained inhomogeneous calculations needed to treat the homogeneous lapse mode.

A. A locally nearly flat metric retains the clock background

Start from an exact source-free expanding background with a regular timelike clock, and set $\boldsymbol{r} = a(t)\boldsymbol{x}$. Without making a weak-field expansion, the metric and clock become

$$\mathrm{d}s^2 = -(1 - H^2 r^2)\mathrm{d}t^2 - 2H\boldsymbol{r}\cdot \mathrm{d}\boldsymbol{r}\,\mathrm{d}t + \mathrm{d}\boldsymbol{r}^2, \qquad T = \bar{T}(t), \qquad \dot{\bar{T}} = \bar{Q}(t). \tag{355}$$

This is a coordinate description of the same FLRW solution, not a newly constructed inhomogeneous geometry. A patch of size L is nearly Minkowskian when $|H|L \ll 1$ and $|\dot{H}|L^2 \ll 1$. Nevertheless, the invariant clock expansion is $\Theta = 3H$, and the momentum-constraint coefficient is still $\mathcal{W}_s = 2H - \bar{Q}\mathcal{B}_{,Q}$. Local inertial coordinates do not set these physical quantities to zero.

B. Localized solutions of the linearized exterior vacuum equations

Choose a compact proper-time interval $I = [t_0, t_1]$ on which the exterior background is smooth and $\bar{Q} \geq q_* > 1$. On the selected nonzero Fourier annulus assume $K > 0$, $V_{\rm full} > 0$, and $|\mathcal{D}|$ bounded away from zero, using Equation (243). The endpoint and nearby source-free collar satisfy these signs by Theorems XII.1 and XII.3; other backgrounds require their own check. Let the Fourier initial data be smooth and supported in an annulus $0 < k_- \leq |\boldsymbol{k}| \leq k_+ < \infty$, with the usual reality condition. For each mode introduce

$$A_k(t) = 2M_{\rm Pl}^2 a^3 K(t,k) > 0, \qquad B_k(t) = 2M_{\rm Pl}^2 a^3 V_{\rm full}(t,k) > 0, \qquad P_k = A_k\dot{\zeta}_k. \tag{356}$$

The complete linear evolution is

$$\dot{\zeta}_k = \frac{P_k}{A_k}, \qquad \dot{P}_k = -B_k\zeta_k. \tag{357}$$

Here P_k is the momentum after the $B\zeta\dot{\zeta}$ boundary term is removed; it differs from the unshifted canonical momentum by $2M_{\rm Pl}^2 a^3 B\zeta_k$. No frozen-frequency approximation has entered. Compactness of I and the momentum annulus gives finite coefficient bounds and positive lower bounds. The inverse transforms are spatially decaying, inhomogeneous perturbations of the specified cosmological vacuum.

The lapse and shift are reconstructed from the constraints:

$$\alpha_k = \frac{2J\dot{\zeta}_k - 2bC\zeta_k}{\mathcal{D}}, \qquad \psi_k = -\frac{K\dot{\zeta}_k + B\zeta_k}{k^2/a^2}. \tag{358}$$

A transformation to Newtonian gauge gives

$$\Psi_{{\rm N},k} = -\zeta_k - H\psi_k, \qquad \Phi_{{\rm N},k} = \alpha_k + \dot{\psi}_k, \qquad \delta T_{{\rm N},k} = \bar{Q}\psi_k. \tag{359}$$

Thus the metric, clock perturbation, and both constraints are simultaneously determined. The construction does not set the clock perturbation or the time derivatives to zero in a local potential.

Proposition XIV.1 (Finite-band linear exterior-vacuum certificate)**.** *Under the preceding assumptions, every such packet has positive quadratic scalar energy at each time and a finite energy bound on I. Its metric and clock perturbations decay to the chosen positive-charge cosmological background at spatial infinity. An arbitrarily small nonzero amplitude can be chosen so that the unitary lapse remains positive and the local clock norm stays above unity throughout I.*

Proof. For a real mode set $E_k = (P_k^2/A_k + B_k\zeta_k^2)/2$. Direct differentiation gives

$$\dot{E}_k = -\frac{\dot{A}_k}{2}\dot{\zeta}_k^2 + \frac{\dot{B}_k}{2}\zeta_k^2, \qquad |\dot{E}_k| \le C_I E_k, \tag{360}$$

where $C_I = \sup_{I,[k_-,k_+]} \max\{|\dot{A}_k/A_k|, |\dot{B}_k/B_k|\} < \infty$. Hence $E_k(t) \le E_k(t_0)\exp[C_I(t-t_0)]$, with the same bound for the integrated packet energy. The smooth Fourier multipliers in Equation (358) preserve spatial decay. Scaling both initial data by ε scales all linear perturbations by ε. For sufficiently small $|\varepsilon|$,

$$\|\alpha\|_{L^\infty(I\times\mathbb{R}^3)} < \min\left\{\frac{1}{2}, \frac{q_*-1}{2}\right\}, \qquad Q_{\rm loc} = \frac{\bar{Q}}{1+\alpha} > 1. \tag{361}$$

The reconstructed fields solve the linearized dynamical equations, with nonlinear residuals beginning at second order. □

The conserved homogeneous label C_T is not a pointwise positivity theorem for the full inhomogeneous Noether density. Nor does a finite-interval Gronwall bound exclude all physical growth or establish nonlinear stability about the perturbed solution. The annulus excludes the uncontrolled zero-mode and arbitrarily high-momentum limits. These qualifications are part of the result.

C. Full nonlinear local Cauchy theorem on the strongly regular domain

The all-momentum result Theorem XIII.1 remains a quadratic theorem on source-free homogeneous backgrounds, while the exact canonical operators in Sections VI A and VI L hold for nonlinear fields. The nonlinear Cauchy problem can now be closed on an open regular component of the vacuum gravity–clock phase space. The result below concerns the exact completed action Equation (59): the nonlinear acceleration function, elliptic trace operator, curvature–lapse coupling, curvature-square term, sixth-order Ricci-gradient term, braid, and smooth coefficient profiles are retained. "Local well posedness" is local in time; it does not mean global existence, long-time nonlinear stability, or a bounded-domain initial-boundary-value theorem.

Let $\Sigma = \mathbb{T}^3 = (\mathbb{R}/2\pi L\mathbb{Z})^3$, let $\widehat{h}$ be a fixed smooth flat reference metric, and put $\Lambda = (1-\Delta_{\widehat{h}})^{1/2}$. For an integer $s \ge 18$, define

$$\|(k,\varpi)\|^2_{\mathbb{X}^s} = \|k\|^2_{H^{s+3}} + \|\varpi\|^2_{H^s}. \tag{362}$$

The index 18 is a conservative sufficient threshold, not an asserted optimal one. It leaves the derivative margin required by the order-three pseudodifferential calculus after the two-derivative lapse reconstruction and Sobolev embedding in three spatial dimensions.

Definition XIV.2 (Strongly regular SCFT-A datum)**.** A smooth vacuum datum (h_0, π_0, N_0, K_0) is *strongly regular* when:

(R1) it satisfies the exact trace relation Equation (80), the local lapse constraint Equation (85), and the momentum constraint; h_0 is positive, $N_0 > 0$, and the range of $Q_0 = N_0^{-1}$ is compactly contained in one smooth coefficient chart of the completed action;

(R2) $\mathscr{A}_N : H^{r+2} \to H^r$ is uniformly positive and the full negative lapse Hessian in Equation (89) is coercive on the entire $H^1(\Sigma)$ lapse space, including constants;

(R3) for every nonzero covector ξ,

$$g_\xi \equiv \frac{\mathsf{G}^{ij}_{\rm full}\xi_i\xi_j}{|\xi|^2_h} \ge g_0 > 0, \qquad \tau_6 \ge \tau_0 > 0, \qquad \ell \ge \ell_0 > 0; \tag{363}$$

(R4) the spatial-harmonic Faddeev–Popov operator in Equation (371) is invertible on mean-zero vector fields. Constant translations are fixed by a base-point convention.

All four properties persist in a sufficiently small $\mathbb{X}^s$ neighborhood. Constants below depend on the radius of a bounded regular set and on positive lower bounds for these margins, but not on a Fourier regularization cutoff.

Theorem XIV.3 (Full nonlinear local Hadamard well-posedness)**.** *Let $s \geq 18$ and let (h_0, π_0, N_0, K_0) be a strongly regular SCFT-A vacuum datum on $\mathbb{T}^3$. Impose the momentum constraint and fix the spatial-harmonic representative described below. There exist $T_* > 0$ and a neighborhood $\mathcal{O}$ of the reduced datum in $\mathbb{X}^s$ such that every compatible datum in $\mathcal{O}$ determines a unique SCFT-A development, modulo the already fixed spatial translations, with*

$$\begin{aligned} h &\in C([-T_*, T_*]; H^{s+3}) \cap C^1([-T_*, T_*]; H^s), \\ \pi &\in C([-T_*, T_*]; H^s) \cap C^1([-T_*, T_*]; H^{s-3}), \\ N, K, \beta &\in C([-T_*, T_*]; H^{s+1}), \qquad \partial_t N, \partial_t K \in C([-T_*, T_*]; H^{s-2}). \end{aligned} \tag{364}$$

The solution map is continuous from $\mathcal{O} \subset \mathbb{X}^s$ to $C([-T_*, T_*]; \mathbb{X}^s)$, and higher Sobolev regularity persists on the same interval. The primary lapse constraint, local lapse constraint, momentum constraints, spatial-harmonic gauge, and covariant clock equation all propagate. The solution continues while its $\mathbb{X}^s$ norm remains finite and the four strong-regularity margins remain strictly positive.

1. *Tame elimination of the trace and lapse*

Write $\varphi = \log(N/N_0)$ and define

$$\mathcal{F}(h, \pi, K, \varphi) = \left(\mathscr{A}_N K + P - \frac{3}{2}\mathcal{B}_{\mathrm{A}},\ \frac{\mathcal{C}_N}{M_{\mathrm{Pl}}^2 \sqrt{h}} \right). \tag{365}$$

For $r \geq 3$, the exact derivative count gives the smooth map

$$H^{r+4} \times H^r \times H^{r+2} \times H^{r+2} \longrightarrow H^r \times H^r. \tag{366}$$

In particular, ${}^{(3)}R \in H^{r+2}$, $D^{(3)}R_{ij} \in H^{r+1}$, and the fourth-order metric source $\Delta_h(N\ell^{(3)}R)$ in Equation (85) lies in H^r; no derivative is silently omitted.

Lemma XIV.4 (Auxiliary graph and tame estimates)**.** *At a strongly regular datum, Equation* (365) *has a unique local solution $(K, N) = \mathcal{G}(h, \pi)$, including the constant lapse mode. The map is C^∞ and tame. On every bounded regular set and for $3 \leq r \leq s - 1$,*

$$\|K\|_{H^{r+2}} + \|\log N\|_{H^{r+2}} \leq C_R\big(1 + \|h\|_{H^{r+4}} + \|\pi\|_{H^r}\big), \tag{367}$$

$$\|\delta K\|_{H^{r+2}} + \|\delta \log N\|_{H^{r+2}} \leq C_R\big(\|\delta h\|_{H^{r+4}} + \|\delta\pi\|_{H^r}\big). \tag{368}$$

The same bounds hold for differences.

Proof. The derivative of the first component of $\mathcal{F}$ in K is the positive second-order operator $\mathscr{A}_N$. Eliminate that variation. The Schur complement of the remaining relative-lapse block is precisely minus the operator whose quadratic form is Equation (89). Coercivity and elliptic regularity therefore make that block an isomorphism $H^{r+2} \to H^r$, including constants. Block Gaussian factorization makes $D_{(K,\varphi)}\mathcal{F}$ an isomorphism, and the Banach implicit-function theorem gives the graph.

For the estimates, commute Λ^r through the two uniformly elliptic operators, apply the elliptic estimate, and use Moser product and composition bounds. Each commutator has one fewer derivative on the unknown than the principal term. Induction in r gives Equation (367); applying the same argument to the linearized system gives Equation (368), and integration along a line segment gives the difference form. No constant-mode projection is made because the lapse Hessian is coercive on the full lapse space. □

With $h \in H^{s+3}$ and $\pi \in H^s$, take $r = s - 1$ to obtain $N, K \in H^{s+1}$. The two-derivative offset is sharp: at a flat unbraided rolling datum a conformal metric variation obeys

$$\frac{\delta \log N(\xi)}{\zeta(\xi)} = -\frac{2|\xi|^2(1 + \ell|\xi|^2)}{m^2 + 2|\xi|^2} \sim -\ell|\xi|^2, \qquad m^2 = Q^2 U'' > 0. \tag{369}$$

Thus the proof never assigns the lapse the same spatial regularity as the metric.

2. Spatial-harmonic reduction and the exact reduced Hamiltonian

Define the spatial-harmonic vector relative to $\widehat{h}$ by

$$V^i(h) = h^{jk}\big(\Gamma^i_{jk}(h) - \widehat{\Gamma}^i_{jk}\big). \tag{370}$$

For an infinitesimal diffeomorphism generated by X,

$$DV_h[\mathcal{L}_X h]^i = \Delta_h X^i + {}^{(3)}R^i{}_j X^j + \mathcal{B}_h(V, DX), \tag{371}$$

where the last term vanishes on the harmonic slice. At the flat reference this is $\Delta_{\widehat{h}} X$, invertible on mean-zero vector fields. The implicit-function theorem therefore gives a unique nearby harmonic representative after fixing residual translations; this is the local Ebin slice in the present coordinates [42, 43].

The momentum constraint is the momentum map for the cotangent action,

$$\int_\Sigma \pi^{ij}\mathcal{L}_X h_{ij} = \int_\Sigma X^i \mathcal{H}_i. \tag{372}$$

Hence $\mathcal{H}_i = 0$ makes π annihilate the vertical diffeomorphism directions. Cotangent reduction identifies the local quotient of the zero momentum level by spatial diffeomorphisms with the cotangent bundle of the harmonic slice [44]. Its canonical symplectic matrix is

$$\mathbb{J} = \begin{pmatrix} 0 & I \\ -I & 0 \end{pmatrix}, \qquad \mathbb{J}^* = -\mathbb{J}. \tag{373}$$

The lapse second-class pair does not alter this bracket. If $\chi = (p_N, \mathcal{C}_N)$, then

$$\begin{pmatrix} 0 & -\Delta_N \\ \Delta_N & \Omega \end{pmatrix}^{-1} = \begin{pmatrix} \Delta_N^{-1}\Omega\Delta_N^{-1} & \Delta_N^{-1} \\ -\Delta_N^{-1} & 0 \end{pmatrix}. \tag{374}$$

Functionals of (h, π) have vanishing brackets with p_N, so the Dirac correction between two such functionals vanishes. Defining the shift-independent reduced Hamiltonian by stationary substitution,

$$H_{\mathrm{red}}(h, \pi) = \widetilde{H}_C\big(h, \pi, K(h, \pi), N(h, \pi)\big), \tag{375}$$

the exact reduced equations are

$$\partial_t U = \mathbb{J}\nabla H_{\mathrm{red}}(U), \qquad U = (h, \pi). \tag{376}$$

The shift reconstructed by differentiating $V(h) = 0$ solves Equation (371); the tame bounds and $\dot{h} \in H^s$ give $\beta \in H^{s+1}$.

3. Exact reduced Hessian and sixth-order coercivity

Let

$$L(U) = D^2 H_{\mathrm{red}}(U) = L(U)^*. \tag{377}$$

The stationary trace and lapse eliminations are Schur complements and preserve formal self-adjointness. Elliptic parameter dependence from Theorem XIV.4 makes $L(U)$ a smooth tame Douglis–Nirenberg pseudodifferential matrix with block orders

$$\operatorname{ord} L_{hh} = 6, \qquad \operatorname{ord} L_{h\pi}, \operatorname{ord} L_{\pi h} \le 2, \qquad \operatorname{ord} L_{\pi\pi} = 0. \tag{378}$$

Freeze the coefficients at a point, put $\rho = |\xi|_h > 0$, and impose the principal harmonic and momentum tangencies

$$\xi^j k_{ij} - \frac{1}{2}\xi_i \operatorname{tr}_h k = 0, \qquad \xi_j \varpi^{ij} = 0. \tag{379}$$

Then

$$\sigma_2(D\,\mathrm{Ric})[k]_{ij} = \frac{\rho^2}{2}k_{ij}, \qquad r_\xi(k) = \sigma_2(D^{(3)}R)[k] = \frac{\rho^2}{2}\operatorname{tr}_h k. \tag{380}$$

The sixth-order Ricci-gradient term contributes $N\tau_6\rho^6|k|^2/4$. The leading metric–lapse and lapse blocks are

$$B_4[k] = -\frac{N\ell}{2}\rho^2 r_\xi(k), \qquad C_2 = -2Ng_\xi\rho^2, \tag{381}$$

so lapse elimination contributes the favorable Schur term

$$-B_4^* C_2^{-1} B_4[k] = \frac{N\ell^2}{8g_\xi}\rho^2|r_\xi(k)|^2 \geq 0. \tag{382}$$

On Equation (379), the leading constrained Hessian is

$$\mathcal{E}_{\mathrm{pr}} = 4N\left(|\varpi|^2 - \frac{(\mathrm{tr}_h\,\varpi)^2}{3}\right) + \frac{N\tau_6}{4}\rho^6|k|^2 + \frac{N\ell^2}{8g_\xi}\rho^2|r_\xi(k)|^2. \tag{383}$$

Since $(\mathrm{tr}\,\varpi)^2 \leq 2|\varpi|^2$,

$$\mathcal{E}_{\mathrm{pr}} \geq \frac{4N}{3}|\varpi|^2 + \frac{N\tau_6}{4}\rho^6|k|^2. \tag{384}$$

In canonical physical coordinates the eigenvalues of the product of the leading momentum and restoring matrices are exactly

$$N^2\tau_6, \qquad N^2\tau_6, \qquad N^2\left(\tau_6 + \frac{\ell^2}{3g_\xi}\right), \tag{385}$$

corresponding to two tensor polarizations and one scalar direction. They are real, nonzero, and uniform on a bounded strongly regular set.

4. Exact loss-free nonlinear energy

Principal positivity by itself is insufficient. Set

$$R = \begin{pmatrix} \Lambda^3 & 0 \\ 0 & I \end{pmatrix}, \qquad A(U) = R\mathbb{J}L(U)R^{-1}, \qquad S(U) = R^{-*}L(U)R^{-1}. \tag{386}$$

Here A has order three and S order zero. The self-adjointness of L and skew-adjointness of $\mathbb{J}$ give the exact identity

$$\boxed{SA + A^*S = 0.} \tag{387}$$

Both terms are the same operator $R^{-*}L\mathbb{J}LR^{-1}$ with opposite signs. The cancellation is therefore for the complete variable-coefficient generator, not only its principal homogeneous symbol.

By Equation (384), sharp Gårding gives

$$\langle W, SW\rangle \geq c\|W\|_{L^2}^2 - C\|W\|_{H^{-1/2}}^2. \tag{388}$$

Only finitely many low spectral directions can violate positivity. Choose a fixed smooth real function f below the uniform positive principal threshold so that $\lambda + f(\lambda) \geq c_0 > 0$ on $\operatorname{spec} S$, and set $F(U) = f(S(U))$. Functional calculus makes F finite-rank, smoothing, and self-adjoint, and

$$\widetilde{S} = S + F \geq c_0 I, \qquad \widetilde{S}A + A^*\widetilde{S} = FA + A^*F \in \Psi^0. \tag{389}$$

Thus the homogeneous modes are included rather than projected away.

Put $Z = \widetilde{S}^{1/2}R\delta U$. Parameter-dependent elliptic functional calculus gives $\widetilde{S}^{\pm 1/2} \in \Psi^0$, and the forced variational equation becomes

$$\partial_t Z = \mathscr{K}(U)Z + C(U, \partial_t U)Z + \widetilde{f}, \tag{390}$$

where $\mathscr{K}^* = -\mathscr{K}$, $\mathscr{K} \in \Psi^3$ is elliptic, and $C \in \Psi^0$. Define

$$\mathsf{P}(U) = I + \mathscr{K}(U)^*\mathscr{K}(U) = I - \mathscr{K}(U)^2 \in \Psi^6. \tag{391}$$

For $0 \le r \le s$, complex powers satisfy

$$[\mathsf{P}^{r/6}, \mathscr{K}] = 0, \qquad (\partial_t \mathsf{P}^{r/6})\mathsf{P}^{-r/6} \in \Psi^0, \qquad \mathsf{P}^{r/6} C \mathsf{P}^{-r/6} \in \Psi^0. \tag{392}$$

The first identity is exact because P is a polynomial in the skew-adjoint $\mathscr{K}$; the other two follow from the parameter-dependent resolvent formula and symbol composition [45, 46]. The finite regularity in Theorem XIV.3 is sufficient: after mollifying coefficient curves, the finitely many symbol seminorms required by Calderón–Vaillancourt and order-three composition are bounded by Moser estimates in terms of the same $\mathbb{X}^s$ norm and Theorem XIV.4; passage to the limit introduces no hidden C^∞ solution hypothesis.

Theorem XIV.5 (Loss-free variational energy)**.** *For a solution curve in a bounded strongly regular set, define*

$$E_r[U; \delta U] = \|\mathsf{P}(U)^{r/6} \widetilde{S}(U)^{1/2} R \delta U\|_{L^2}^2. \tag{393}$$

Uniformly for $0 \le r \le s$,

$$c_R \|\delta U\|_{\mathbb{X}^r}^2 \le E_r \le C_R \|\delta U\|_{\mathbb{X}^r}^2, \tag{394}$$

and every forced variational solution satisfies

$$\frac{\mathrm{d}}{\mathrm{d}t} E_r \le C_R \big(1 + \|U\|_{\mathbb{X}^s}\big) E_r + C_R \|f\|_{\mathbb{X}^r}^2. \tag{395}$$

No norm of δU above $\mathbb{X}^r$ occurs, and the constants are independent of any regularization cutoff.

Proof. Ellipticity of $\mathsf{P}^{r/6}$, positivity of $\widetilde{S}$, and the grading by R give Equation (394). Differentiating Equation (393) along Equation (390), the skew term cancels exactly:

$$2\,\mathrm{Re}\langle \mathsf{P}^{r/6} Z, \mathsf{P}^{r/6} \mathscr{K} Z\rangle = 2\,\mathrm{Re}\langle \mathsf{P}^{r/6} Z, \mathscr{K} \mathsf{P}^{r/6} Z\rangle = 0. \tag{396}$$

The remaining terms are order zero by Equation (392); Cauchy–Schwarz controls the forcing. This proves Equation (395). In particular, the order-two and order-one pieces that defeat the uncorrected commutator energy are already inside the exact Hessian, square-root conjugation, and $\mathsf{P}^{r/6}$. □

Proposition XIV.6 (Difference estimate)**.** *If U_1, U_2 are two strongly regular solutions, then on their common interval*

$$\|U_1(t) - U_2(t)\|_{\mathbb{X}^{s-1}} \le C_R e^{C_R |t|} \|U_1(0) - U_2(0)\|_{\mathbb{X}^{s-1}}. \tag{397}$$

Proof. Use the fundamental theorem of calculus,

$$\mathbb{J}\nabla H_{\mathrm{red}}(U_1) - \mathbb{J}\nabla H_{\mathrm{red}}(U_2) = \mathbb{J} \int_0^1 L(U_2 + \theta(U_1 - U_2))\, \mathrm{d}\theta\, (U_1 - U_2). \tag{398}$$

The averaged Hessian remains self-adjoint, has the same block orders and uniform principal coercivity, and satisfies the same tame bounds. Apply Theorem XIV.5 at level $s-1$ and Gronwall's inequality. □

5. *Existence, uniqueness, continuous dependence, and continuation*

Choose self-adjoint Friedrichs cutoffs J_ϵ on the reduced bundle and solve

$$\partial_t U_\epsilon = J_\epsilon \mathbb{J} \nabla H_{\mathrm{red}}(J_\epsilon U_\epsilon), \qquad U_\epsilon(0) = J_\epsilon U_0. \tag{399}$$

These are finite-dimensional smooth ODEs. Because the cutoffs are spectral functions of Λ, they are self-adjoint and commute with R and $\mathbb{J}$. The exact symmetrizer identity survives on the cutoff range, and every leftover cutoff commutator from the order-zero conjugations has a bound independent of ϵ.

Fix a smooth center U_c in the coordinate neighborhood and write $V_\epsilon = U_\epsilon - U_c$. The fundamental theorem of calculus gives

$$\mathbb{J}\nabla H_{\mathrm{red}}(U_\epsilon) = \mathbb{J}\nabla H_{\mathrm{red}}(U_c) + \mathbb{J} \int_0^1 L(U_c + \theta V_\epsilon)\, \mathrm{d}\theta\, V_\epsilon. \tag{400}$$

The averaged Hessian has the same coercive principal symbol. Treating the first term as smooth forcing in Theorem XIV.5 gives

$$\frac{\mathrm{d}}{\mathrm{d}t}\big(1+\|V_\epsilon\|^2_{\mathbb{X}^s}\big) \le \Phi_R\big(1+\|V_\epsilon\|^2_{\mathbb{X}^s}\big), \tag{401}$$

until the curve leaves the radius-R regular set. Hence for a time $T_* > 0$ independent of ϵ,

$$\sup_{|t|\le T_*} \|U_\epsilon(t)\|_{\mathbb{X}^s} \le 2R. \tag{402}$$

The difference estimate at level $s-1$ makes the regularized family Cauchy in $C([-T_*, T_*]; \mathbb{X}^{s-1})$. Weak-* compactness at level s, tame continuity of the auxiliary maps, and lower semicontinuity pass the reduced equation to the limit. The energy estimate applied to time translates gives strong continuity in $\mathbb{X}^s$ and the time regularity in Equation (364). This proves existence.

Uniqueness follows from Theorem XIV.6. Top-norm continuous dependence follows by smoothing the initial data, using the uniform high-regularity estimate for the smoothed solutions, the level-$s-1$ difference estimate, and then sending first the data difference and then the smoothing scale to zero. This is the Bona–Smith argument [48, 49]. The same estimates give persistence of higher regularity. Reapplying the theorem at a later time yields the continuation criterion in Theorem XIV.3.

6. *Propagation of all constraints*

Let

$$\Delta_N = \frac{\delta \mathcal{C}_N}{\delta N}\bigg|_{h,\pi}, \qquad D_h[\xi] = \int_\Sigma \pi^{ij}\mathcal{L}_\xi h_{ij}. \tag{403}$$

Spatial covariance gives the exact identities

$$\{D_h[\xi], H_C\} = \int_\Sigma \mathcal{C}_N \mathcal{L}_\xi N, \qquad \{\mathcal{C}_N, D_h[\beta]\}_{h,\pi} = \mathcal{L}_\beta \mathcal{C}_N - \Delta_N(\mathcal{L}_\beta N). \tag{404}$$

Theorem XIV.7 (Constraint propagation)**.** *Choose the lapse velocity*

$$\lambda = \dot N = \mathcal{L}_\beta N - \Delta_N^{-1}\{\mathcal{C}_N, H_C\}_{h,\pi}. \tag{405}$$

Then data with $p_N = \mathcal{C}_N = \mathcal{H}_i = 0$ retain these constraints throughout the lifespan in Theorem XIV.3. The homogeneous lapse mode is included.

Proof. Equation Equation (404) gives

$$(\partial_t - \mathcal{L}_\beta)\mathcal{C}_N = \{\mathcal{C}_N, H_C\}_{h,\pi} + \Delta_N(\lambda - \mathcal{L}_\beta N) = 0. \tag{406}$$

Also $\dot p_N = -\mathcal{C}_N$, while

$$\frac{\mathrm{d}}{\mathrm{d}t} D_h[\xi] = \int_\Sigma \mathcal{C}_N \mathcal{L}_\xi N + D_h[[\xi, \beta]], \tag{407}$$

which is homogeneous in the constraints. Strong regularity gives the bounded full-space inverse of Δ_N, including constants. Diffeomorphism invariance gives $\nabla_\mu E^{\mu\nu} = E_T \nabla^\nu T$; since the clock gradient remains timelike, the reconstructed metric equations imply the clock equation. Differentiating the elliptic graph $\mathcal{C}_N(h, \pi, N(h,\pi)) = 0$ shows that its time derivative is exactly Equation (405), so the reduced and Dirac evolutions agree. □

7. *Explicit nonempty rolling domain and the retained Cauchy calculations*

Take a flat torus and an unbraided rolling value $Q_* \in (Q_a, Q_L)$ with $U''(Q_*) > 0$, where $U = \widetilde{\mathcal{K}}$, and set

$$N_* = Q_*^{-1}, \qquad H_*^2 = \frac{Q_* U'(Q_*) - U(Q_*)}{3} > 0, \qquad \pi_*^{ij} = -M_{\mathrm{Pl}}^2 \sqrt{h_*}\, H_* h_*^{ij}. \tag{408}$$

Then $K_* = 3H_*$, $q_i = 0$, ${}^{(3)}R_{ij} = 0$, and the two auxiliary Jacobians are

$$A_* = 1 - \frac{3\nu_*}{2}\Delta_*, \qquad L_* = -2\Delta_* + m_*^2, \qquad m_*^2 = Q_*^2 U''(Q_*) > 0. \tag{409}$$

Their Fourier eigenvalues are strictly positive even at zero momentum. Furthermore $g_\xi = 1$, $\tau_6, \ell > 0$, and the flat Faddeev–Popov operator is Δ_* on mean-zero vector fields. Therefore Theorem XIV.2 holds, and by openness Theorem XIV.3 applies to a genuine infinite-dimensional neighborhood, not merely the homogeneous solution.

For the representative point $Q_* = 101/100$, the exact values are

$$\begin{aligned} &N_* = \frac{100}{101}, && \nu_* H_d^2 = \frac{1}{2\,10^{170}}, && \ell_* H_d^2 = \frac{1}{2\,10^{30}}, && \tau_6 H_d^4 = 10^{-340}, \\ &\frac{U''_*}{H_d^2} = \frac{10^{36}}{9999\sqrt{9999}}, && \frac{m_*^2}{H_d^2} = \frac{1020100\,10^{30}}{9999\sqrt{9999}} > 0. \end{aligned} \tag{410}$$

No positive floor has been rounded to zero. The tiny fixed value of τ_6 can make lifespan constants poor, but it does not invalidate local well posedness at this fixed action point; no estimate is uniform as $\tau_6 \downarrow 0$.

The fully expanded local lapse constraint retained from the earlier Cauchy analysis is the unbraided $\mathcal{B}_\mathrm{A} = 0$, $\Sigma_\mathrm{A} = 1$ specialization of Equation (85). Writing $d = \Delta_h \log N$, $r_\nu = \nu - Q\nu'$, and $r_\ell = \ell - Q\ell'$, it is

$$\begin{aligned} 0 = {}& 2P^{ij}_{\mathrm{TF}} P^{\mathrm{TF}}_{ij} + \frac{2}{3}PK + \frac{1}{3}K^2 + \frac{r_\nu}{2}|DK|^2 + QU' - U - \frac{{}^{(3)}R}{2} \\ &+ a_0^2\big(\mathcal{J}_{\mathrm{A},\sigma} - 2Y\mathcal{J}_{\mathrm{A},\sigma,Y}\big) - 2D_i(\mathcal{J}_{\mathrm{A},\sigma,Y} q^i) + \frac{\tau_6}{2}|D^{(3)}R_{ij}|^2 + \frac{\eta_R}{2}{}^{(3)}R^2 \\ &+ \frac{1}{2}\left[r_\ell{}^{(3)}Rd + \frac{1}{N}\Delta_h(N\ell^{(3)}R)\right]. \end{aligned} \tag{411}$$

Thus the fourth-order metric source and every switch derivative relevant to this chart are explicit; Equation (411) is the same equation as Equation (148), reproduced here because it is used directly in the Cauchy construction.

Now take $h_* = \delta$ on the torus of side $2\pi L$ and set

$$E^{ij} = \mathrm{diag}(0,1,-1), \qquad \pi^{ij}_\epsilon = M_{\mathrm{Pl}}^2\sqrt{h_*}\left[-H_* h_*^{ij} + \epsilon E^{ij}\cos(x^1/L)\right]. \tag{412}$$

The perturbation is transverse and trace free; the momentum constraint holds exactly for every ϵ. Since $P = -3H_*$, the exact trace solution is $K = 3H_*$ even for spatially varying lapse. With $\varphi = \log(N/N_*)$, the remaining nonlinear lapse equation is exactly

$$\begin{aligned} 0 = {}& 4\epsilon^2\cos^2(x^1/L) - 3H_*^2 + QU'(Q) - U(Q) \\ &+ a_0^2\big(\mathcal{J}_{\mathrm{A},\sigma}(Y) - 2Y\mathcal{J}_{\mathrm{A},\sigma,Y}(Y)\big) - 2\partial_i\big(\mathcal{J}_{\mathrm{A},\sigma,Y}(Y)\partial^i\varphi\big), \qquad Q = Q_* e^{-\varphi}, \quad Y = \frac{|\nabla\varphi|^2}{a_0^2}. \end{aligned} \tag{413}$$

The curvature and trace-gradient terms vanish because of these chosen initial fields; they have not been removed from the theory.

Proposition XIV.8 (Inhomogeneous datum and positive mean lapse response)**.** *For sufficiently small $|\epsilon|$, Equation* (413) *has the unique nearby solution supplied by Theorem XIV.4. It is even and smooth in ϵ, and*

$$\varphi_\epsilon = \epsilon^2\left[\frac{2}{m_*^2} + \frac{2}{m_*^2 + 8/L^2}\cos(2x^1/L)\right] + O(\epsilon^4) \tag{414}$$

in the auxiliary Sobolev space. Consequently

$$\frac{1}{\mathrm{Vol}\,\Sigma}\int_\Sigma \varphi_\epsilon\,\mathrm{d}^3x = \frac{2\epsilon^2}{m_*^2} + O(\epsilon^4) > 0 \tag{415}$$

for sufficiently small nonzero ϵ.

Proof. The free amplitude enters through ϵ^2, so uniqueness gives $\varphi_{-\epsilon} = \varphi_\epsilon$ and the linear response vanishes. Because $\varphi = O(\epsilon^2)$, nonlinear acceleration-gradient terms begin at order ϵ^4. At order ϵ^2,

$$(-2\Delta_* + m_*^2)\varphi_2 = 4\cos^2(x^1/L) = 2 + 2\cos(2x^1/L). \tag{416}$$

The two eigenvalues are m_*^2 and $m_*^2 + 8/L^2$, whose exact inversion gives Equation (414). Smoothness gives the displayed remainder, and integration gives Equation (415). □

This calculation demonstrates explicitly that nonzero spatial modes source a nonzero homogeneous lapse response. The $O(\epsilon^4)$ remainder is not set to zero, and no finite-amplitude closed form is claimed.

At the exact Minkowski zero-stiffness plateau $H_* = 0$ and $m_*^2 = 0$. For the same first-order transverse-traceless momentum perturbation, with no first-order homogeneous expansion and with the first-order lapse mean fixed, the quadratic equation would be

$$-2\Delta_*\varphi_2 = 4\cos^2(x^1/L). \tag{417}$$

Its right-hand side has nonzero integral, so there is no periodic solution. This is an obstruction to that proposed torus family, not a proof that SCFT-A is ill posed. Allowing compatible homogeneous gravitational data changes the quadratic constraint. The rolling construction removes this particular obstruction through $m_*^2 > 0$. This statement also does not conflict with the bounded-domain Dirichlet initial-constraint result below, where the constant lapse mode is fixed by boundary data rather than inverted on a closed periodic leaf.

8. *Exact commutator audit and why the corrected energy succeeds*

The earlier Cauchy analysis identified a genuine failure of a *naive* energy argument. On the one-dimensional circle take $a(x) = 2 + \cos x$ and

$$u_n = n^{-7}e^{inx}, \qquad v_n = (n+1)^{-4}e^{i(n+1)x}, \qquad n \geq 1. \tag{418}$$

The H^7 and H^4 norms remain uniformly bounded, while the magnitude of the $n+1$ Fourier coefficient of $[\partial_x^4, a\partial_x^6]u_n$, paired with $\partial_x^4 v_n$, is exactly

$$\frac{(n+1)^4 - n^4}{2n} = 2n^2 + 3n + 2 + \frac{1}{2n} \longrightarrow \infty. \tag{419}$$

Thus the uncorrected commutator is not controlled by the proposed $H^7 \times H^4$ energy. This is a counterexample to that proof shortcut, not to SCFT-A evolution. The exact construction above removes the obstruction in the required way: the full Hessian is first conjugated to the skew-adjoint $\mathscr{K}$ plus an order-zero operator, and differentiation is by $\mathsf{P}^{r/6}$, a function of $\mathscr{K}^*\mathscr{K}$. Therefore $[\mathsf{P}^{r/6}, \mathscr{K}] = 0$ exactly, which is the missing variable-coefficient cancellation.

9. *Boundary scope and specified-matter extension*

The theorem is a Cauchy theorem on a compact manifold without boundary. Every integration by parts in the trace, lapse, momentum-map, and energy identities has zero boundary flux, and the elliptic and pseudodifferential operators have their standard closed-manifold domains. No boundary data are required or permitted for this torus Cauchy problem.

A bounded spatial region is a distinct initial-boundary-value problem. For the scalar model $A = -\Delta$, the sixth-order Green form is

$$\int_\Omega (uA^3v - vA^3u) = \sum_{j=0}^{2}\int_{\partial\Omega}\left[(A^{2-j}v)\partial_n(A^ju) - (A^ju)\partial_n(A^{2-j}v)\right]. \tag{420}$$

Conditions $u = Au = A^2u = 0$ annul this scalar form but do not, by themselves, verify the coupled metric complementing condition, momentum-constraint preservation, or lapse reconstruction. The lapse–trace subsystem also requires the surface functional and trace condition stated below. No full nonlinear bounded-domain theorem is claimed.

Corollary XIV.9 (Specified regular matter)**.** *Theorem XIV.3 extends to a specified minimally coupled matter model whose gauge-reduced equations are locally symmetrizable hyperbolic in H^s, whose constraint algebra closes, and whose stress tensor contributes at most lower spatial order to the metric equation. The combined energy is the sum of Equation* (393) *and the matter symmetrizer energy.*

Proof. Minimal coupling is linear in ADM lapse and shift, so it does not alter the gravitational lapse Hessian. The sixth-order gravitational block dominates at high frequency. The direct-sum principal symmetrizer has only lower-order off-diagonal couplings, bounded by the product Sobolev energy. Kato iteration and matter constraint propagation then apply [47]. □

This is a theorem schema, not a substitute for choosing matter variables. Because the manuscript leaves S_{vis} as a general visible-matter functional, the unconditional theorem proved here is the vacuum gravity–clock theorem.

D. Complementary bounded-domain and exact-vacuum results

These previously established results remain useful and are not superseded by the boundaryless Cauchy theorem.

1. Boundary conditions for the lapse–trace subsystem

For fixed spatial metric the spatial-repair Hamiltonian has the surface term

$$\int_\Omega \sqrt{h}\, N\ell^{(3)}R\Delta_h \ln N = -\int_\Omega \sqrt{h}\, D_i(N\ell^{(3)}R)D^i \ln N + \int_{\partial\Omega} \sqrt{\sigma}\, N\ell^{(3)}R\, n^i D_i \ln N. \tag{421}$$

For a Dirichlet lapse problem subtract $M_{\rm Pl}^2/2$ times the last integral from the Hamiltonian. Otherwise fixing $\delta N = 0$ alone would not remove the normal derivative of δN. In the trace inversion take $n^i \nu D_i K = 0$, the natural no-flux condition for Equation (145).

2. Small inhomogeneous initial-constraint solutions on the plateau

Proposition XIV.10 (Local nonlinear initial-constraint result)**.** *Let Ω be a fixed smooth bounded domain and $0 < \alpha < 1$. For a positive metric sufficiently close to δ_{ij} in $C^{4,\alpha}$ and sufficiently small momentum data in $C^{0,\alpha}$ satisfying $D_j\pi^{ij} = 0$, there is a unique small lapse $N = e^\phi$, with $\phi \in C^{1,\alpha}$ and $\phi|_{\partial\Omega} = 0$, solving the nonlinear lapse constraint on the plateau. The auxiliary trace belongs to $C^{2,\alpha}$ with the no-flux condition. Smallness constants may depend on δ/κ_m, κ_m^{-1}, a_0, Ω, and α. This is an initial-constraint theorem, not a bounded-domain evolution theorem.*

Proof. On the plateau $U = 0$, $\nu = \nu_0 = \delta/\kappa_m > 0$, and $\ell = \ell_0 = 1/\kappa_m$. For a trial ϕ,

$$K - \frac{3\nu_0}{2}\left(\Delta_h K + D_i\phi D^i K\right) = -P, \qquad n^i D_i K = 0. \tag{422}$$

The positive mass and ellipticity give a uniform $C^{2,\alpha}$ Neumann solution for small $\|\phi\|_{C^{1,\alpha}}$, with

$$\|K(\phi_1) - K(\phi_2)\|_{C^{2,\alpha}} \le C\|P\|_{C^{0,\alpha}}\|\phi_1 - \phi_2\|_{C^{1,\alpha}}. \tag{423}$$

Let $q_i = D_i\phi$, $\mathcal{M}(q) = \mu_\sigma(|q|^2/a_0^2)/\gamma_{\rm N}$, and $\mathcal{J}_+(Y) = \mathcal{J}_{{\rm A},\sigma}(Y) + Y$. Put

$$\mathcal{T} = 2P^{ij}_{\rm TF}P^{\rm TF}_{ij} + \frac{2}{3}PK + \frac{1}{3}K^2 + \frac{\nu_0}{2}|DK|^2 + \frac{\tau_6}{2}|D^{(3)}R_{ij}|^2 + \frac{\eta_R}{2}{}^{(3)}R^2. \tag{424}$$

Then the lapse constraint is exactly

$$\begin{aligned} 0 = {} & D_i[(2 + \ell_0{}^{(3)}R)D^i\phi] - 2D_i[\mathcal{M}(q)q^i] + (1 + \ell_0{}^{(3)}R/2)|q|^2 \\ & + a_0^2[\mathcal{J}_+(Y) - 2Y\mathcal{M}(q)] + \mathcal{T} - {}^{(3)}R/2 + (\ell_0/2)\Delta_h{}^{(3)}R. \end{aligned} \tag{425}$$

The first operator is uniformly elliptic for small curvature. Its Dirichlet inverse maps $f + D_iF^i$, with $f, F^i \in C^{0,\alpha}$, into $C^{1,\alpha}$. The vector nonlinearity $\mathcal{M}(q)q$ is smooth, cubic at the origin, and Lipschitz with arbitrarily small constant on a small ball; the remaining lapse nonlinearities are at least quadratic. The trace-dependent terms are quadratic in the momentum data and Lipschitz in ϕ with a small coefficient. Therefore the equation is a contraction on a sufficiently small $C^{1,\alpha}$ ball, with

$$\|\phi\|_{C^{1,\alpha}} \le C\left(\|h_{ij} - \delta_{ij}\|_{C^{4,\alpha}} + \|\pi^{ij}/M_{\rm Pl}^2\|^2_{C^{0,\alpha}}\right). \tag{426}$$

Choosing the data so that $\|\phi\|_\infty < \ln(1001/1000)$ keeps $Q = e^{-\phi}$ inside the plateau. The spatial momentum constraint was imposed on the input data. □

3. An exact nonlinear homogeneous vacuum evolution

Take

$$p_1 = -\frac{1}{3}, \qquad p_2 = p_3 = \frac{2}{3}, \qquad \sum_i p_i = \sum_i p_i^2 = 1. \tag{427}$$

For any real inverse-time parameter ε and $1 + \varepsilon t > 0$,

$$\boxed{\mathrm{d}s^2 = -\mathrm{d}t^2 + \sum_i (1+\varepsilon t)^{2p_i} (\mathrm{d}x^i)^2, \qquad T = t} \tag{428}$$

solves the complete local vacuum equations. Here $Q = 1$, $q_i = 0$, ${}^{(3)}R = 0$, $D_i K = 0$, and $U = U' = 0$, so every added spatial operator and its first variation vanishes and the equations reduce to vacuum Einstein Kasner evolution. For $\varepsilon \neq 0$,

$$R_{\alpha\beta\gamma\delta} R^{\alpha\beta\gamma\delta} = \frac{64\varepsilon^4}{27(1+\varepsilon t)^4}. \tag{429}$$

On any interval $|t| \leq T_0$ with $|\varepsilon| T_0 \leq 1/2$, this is a controlled nontrivial nonlinear homogeneous family.

E. Uniform linear evolution through the local transition

Take a flat torus $\Sigma = \mathbb{T}^3$ and a finite source-free upper-branch interval $J \subset [Q_a + \eta, Q_b]$, $0 < \eta < L/3$, containing both varying switch regions. In the dimensionless variables of Equation (317), define

$$c_\eta = \inf_{Q \in [Q_a+\eta, Q_b],\, x \in [0,\infty]} \min \left\{ 1, \delta^2, K_p, \frac{\widehat{V}_{\mathrm{full}}}{x(1+x^2)} \right\} > 0. \tag{430}$$

Positivity follows from Theorem XIII.1 after compactifying momentum by $y = x/(1+x)$. Uniform continuity extends a positive fraction of the margin to a small unbraided exterior collar.

Proposition XIV.11 (Linear inhomogeneous evolution)**.** *For every nonnegative integer s, the completed linear physical equations about the stated background have unique mean-zero solutions in $C(J; H^{s+3}) \cap C^1(J; H^s)$ for initial data in $H^{s+3} \times H^s$. The same holds on the exact Minkowski plateau. The energy obeys $E_s(t) \leq E_s(t_0) e^{C_J |t - t_0|}$, with C_J independent of Fourier cutoff.*

Proof. For each scalar mode,

$$\frac{\mathrm{d}}{\mathrm{d}t}(a^3 K_p \dot{\zeta}_p) + a^3 V_p^{\mathrm{full}} \zeta_p = 0. \tag{431}$$

With $E_p = a^3(K_p |\dot{\zeta}_p|^2 + V_p^{\mathrm{full}} |\zeta_p|^2)$,

$$\dot{E}_p = -\partial_t(a^3 K_p) |\dot{\zeta}_p|^2 + \partial_t(a^3 V_p^{\mathrm{full}}) |\zeta_p|^2. \tag{432}$$

Uniform bounds on logarithmic derivatives of the positive coefficients give $|\dot{E}_s| \leq C_J E_s$ after applying the fixed comoving Sobolev weights and summing. The spectral gap and Equation (430) make this energy equivalent to the graded norm. Fourier truncation and convergence then give existence, uniqueness, and continuous dependence. On the plateau the coefficients are constant and the energy is conserved. $\square$

F. Linear symmetrizer and the separate spectral boundary problem

For a homogeneous scalar mode set $Y_k = (\sqrt{V_k}\zeta_k, \sqrt{K_k}\dot{\zeta}_k)^T$. Its exact evolution is

$$\dot{Y}_k = \begin{pmatrix} \dot{V}_k/(2V_k) & \sqrt{V_k/K_k} \\ -\sqrt{V_k/K_k} & -3H - \dot{K}_k/(2K_k) \end{pmatrix} Y_k. \tag{433}$$

The identity matrix symmetrizes its oscillatory part; the remaining symmetric part contains the logarithmic time derivatives controlled above. This linear construction is consistent with, but is not used in place of, the exact nonlinear operator symmetrizer Equation (387).

On a smooth bounded domain let $A = -\Delta_D > 0$ be the positive Dirichlet Laplacian. The reduced Minkowski scalar operators

$$K(A) = 3 + 2(\nu_0 A)^{-1}, \qquad V(A) = (2\ell_0 + 8\eta_R)A^2 + (\ell_0^2 + 3\tau_6)A^3 \tag{434}$$

commute and define a positive conserved spectral energy on $D(A^{3/2}) \times L^2$. For sufficiently smooth fields $D(A^3)$ implements $\zeta = \Delta\zeta = \Delta^2\zeta = 0$ at the boundary. The same construction applies to each tensor amplitude with $K = 1$ and $V = A + \tau_6 A^3$. These conditions close the reduced *linear* boundary problem; they have not been shown to reconstruct constraint-preserving data for the full nonlinear metric, lapse, and shift. That bounded-domain problem remains distinct from Theorem XIV.3.

XV. MATTER-MIXED SCALAR PERTURBATIONS OF THE COMPLETED ACTION

A. Fluid variables and the full quadratic action

The matter calculation in this section uses the same action as Equation (59), including all four spatial operators. For each independently conserved, isentropic species define

$$h_A = \rho_A + p_A > 0, \qquad c_A^2 = \frac{\dot{p}_A}{\dot{\rho}_A}, \qquad \dot{\rho}_A = -3Hh_A. \tag{435}$$

A Schutz–Sorkin representation gives a first-order scalar fluid action [27–29]. With $\mathcal{V} = \sum_A h_A v_A$ and $\Delta_\rho = \sum_A \delta\rho_A$, the full quadratic action is

$$\begin{aligned} S^{(2)}_{\text{mix}} = S^{(2)}_{\text{grav,full}} + \int \mathrm{d}t\mathrm{d}^3x\, a^3 \sum_A \Bigg[&\left(h_A\chi - \dot{\delta\rho}_A - 3H(1+c_A^2)\delta\rho_A\right) v_A \\ &- \frac{xh_A}{2} v_A^2 - \frac{c_A^2}{2h_A}(\delta\rho_A)^2 - \alpha\delta\rho_A - 3h_A v_A\dot{\zeta}\Bigg], \qquad x = p^2 = \frac{k^2}{a^2}. \end{aligned} \tag{436}$$

Here $S^{(2)}_{\text{grav,full}}$ is precisely Equation (241), not its two-derivative truncation. Baryons, photons, and neutrinos in this calculation denote the barotropic sectors $c_b^2 = 0$ and $c_\gamma^2 = c_\nu^2 = 1/3$. This finite-dimensional matter model does not include recombination, Thomson collisions, polarization, or collisionless multipoles. Those require a Boltzmann treatment rather than a relabeling of perfect-fluid solutions [51].

B. Exact lapse and shift elimination

Use $A, b, C, J, \mathcal{D}$ from Equation (240) and set

$$E = A_k - 9bH^2, \qquad \mathscr{T} = AA_k + 3W_s^2 + 18bH(W_s - H) = \mathcal{D}K. \tag{437}$$

The exact auxiliary equations and their solutions are

$$\begin{aligned} b\chi &= A\dot{\zeta} - J\alpha + \mathcal{V}/M_{\text{Pl}}^2, \\ 0 &= E\alpha - J\chi + 3J\dot{\zeta} + 2C\zeta - \Delta_\rho/M_{\text{Pl}}^2, \end{aligned} \tag{438}$$

$$\alpha = \frac{2J\dot{\zeta} - 2bC\zeta + (J\mathcal{V} + b\Delta_\rho)/M_{\text{Pl}}^2}{\mathcal{D}}, \tag{439}$$

$$\chi = K\dot{\zeta} + \frac{2JC}{\mathcal{D}}\zeta + \frac{E\mathcal{V} - J\Delta_\rho}{M_{\text{Pl}}^2\mathcal{D}}. \tag{440}$$

Their determinant is $-\mathcal{D}$. Neither an effective replacement of a two-derivative sound speed nor a change of initial conditions in a base-action integrator reproduces these constraints.

After substitution, the reduced first-order density is

$$\frac{L^{(2)}_{\rm mix,red}}{a^3} = M_{\rm Pl}^2\left[K\dot\zeta^2 - V_{\rm full}\zeta^2\right] - \sum_A\left[v_A\delta\dot\rho_A + 3H(1+c_A^2)v_A\delta\rho_A + \frac{xh_A}{2}v_A^2 + \frac{c_A^2}{2h_A}(\delta\rho_A)^2\right]$$
$$+\frac{2E}{\mathcal{D}}\dot\zeta\mathcal{V} - \frac{2J}{\mathcal{D}}\dot\zeta\Delta_\rho + \frac{E\mathcal{V}^2 - 2J\mathcal{V}\Delta_\rho - b\Delta_\rho^2}{2M_{\rm Pl}^2\mathcal{D}} + \frac{2JC}{\mathcal{D}}\zeta\mathcal{V} + \frac{2bC}{\mathcal{D}}\zeta\Delta_\rho. \tag{441}$$

The term $2M_{\rm Pl}^2 B\zeta\dot\zeta$ has been integrated by parts, with the derivative at fixed comoving k. Thus the same $V_{\rm full}$ as in Equation (243) occurs. All terms proportional to b, ℓ, τ_6, and η_R are retained.

C. Density kinetic matrix and the correct high-momentum limit

Write $\mathbf{H} = \mathrm{diag}(h_A)$ and $\boldsymbol{h} = (h_A)$. The exact matrix multiplying the quadratic velocity term is

$$\mathbf{R}_{\rm full} = x\mathbf{H} - \frac{E}{M_{\rm Pl}^2\mathcal{D}}\boldsymbol{h}\boldsymbol{h}^T, \qquad \mathscr{P}_{\rm full} = x - \frac{Eh_{\rm vis}}{M_{\rm Pl}^2\mathcal{D}}, \quad h_{\rm vis} = \sum_A h_A, \tag{442}$$

$$\det\mathbf{R}_{\rm full} = x^{N_f-1}\left(\prod_A h_A\right)\mathscr{P}_{\rm full}. \tag{443}$$

Where this matrix is invertible, the density-only kinetic form is

$$\frac{L^{(2)}_{\rm kin}}{a^3} = M_{\rm Pl}^2K\dot\zeta^2 + \frac{1}{2}\left(\dot{\boldsymbol{\delta}}\rho - \frac{2E}{\mathcal{D}}\boldsymbol{h}\dot\zeta\right)^T\mathbf{R}_{\rm full}^{-1}\left(\dot{\boldsymbol{\delta}}\rho - \frac{2E}{\mathcal{D}}\boldsymbol{h}\dot\zeta\right), \tag{444}$$

up to terms containing at most one time derivative. Since $x, h_A > 0$, $\mathbf{R}_{\rm full} > 0$ is equivalent to $\mathscr{P}_{\rm full} > 0$. A zero of $\mathscr{P}_{\rm full}$ is a singularity of this additional velocity elimination; it is not a denominator in the canonical system below.

At a fixed finite homogeneous background, put $A_0 = Q^2D_s - 6H^2 + 6HQ\mathcal{B}_{\rm A,Q}$ and $\sigma = \Sigma_{\rm A} > 0$. For $\nu > 0$,

$$E = A_0 + (2\sigma - 9\nu H^2)x,$$
$$\mathcal{D} = W_s^2 + \nu x(A_0 + 6HW_s + 2\sigma x),$$
$$\boxed{\Upsilon^{\rm full}_{\rm vis} \equiv \lim_{x\to\infty}\frac{\mathscr{P}_{\rm full}}{x} = 1.} \tag{445}$$

The approach is of order x^{-2} for fixed background coefficients. Together with $K \to 3$, this gives positive ultraviolet kinetic blocks for the gravity–clock scalar and the isentropic fluids. It applies also to a fixed radiation-dominated background. It is not the factor 7/8: that number is obtained only when the trace-gradient operator is removed before the high-momentum limit. In fact

$$\lim_{x\to\infty}\lim_{\nu\to 0^+}\frac{\mathscr{P}_{\rm full}}{x} = 1 - \frac{2\sigma h_{\rm vis}}{M_{\rm Pl}^2W_s^2}, \qquad \lim_{\nu\to 0^+}\lim_{x\to\infty}\frac{\mathscr{P}_{\rm full}}{x} = 1. \tag{446}$$

The ultraviolet limit therefore cannot be used to substitute a base-action radiation calculation for the completed theory. Nor can a formal $x \to \infty$ result establish a physical effective-theory window: no physical cutoff is established by this calculation.

D. Canonical evolution without a density-reduction pole

Before the integration by parts in Equation (441), the shift equation gives an especially simple exact identity,

$$\Pi_\zeta = \frac{\partial L^{(2)}_{\rm mix}}{\partial\dot\zeta} = 2M_{\rm Pl}^2a^3\chi. \tag{447}$$

This follows because $-3A\dot{\zeta} + 3J\alpha + A\chi - 3\mathcal{V}/M_{\rm Pl}^2 = 2\chi$ on the shift constraint. The closed equations are

$$\alpha = \frac{2J\chi + (3J\mathcal{V} + A\Delta_\rho)/M_{\rm Pl}^2 - 2AC\zeta}{\mathscr{T}}, \tag{448}$$

$$\dot{\zeta} = \frac{b\chi + J\alpha - \mathcal{V}/M_{\rm Pl}^2}{A},$$

$$\dot{\chi} + 3H\chi = C\alpha + (x - 8\eta_R x^2 - 3\tau_6 x^3)\zeta, \tag{449}$$

$$\dot{\delta\rho}_A + 3H(1 + c_A^2)\delta\rho_A + h_A(3\dot{\zeta} + xv_A - \chi) = 0, \tag{450}$$

$$\dot{v}_A - 3Hc_A^2 v_A - \alpha - \frac{c_A^2}{h_A}\delta\rho_A = 0. \tag{451}$$

The only additional canonical inversion is $\mathscr{T} \neq 0$; $A > 0$ by construction. In particular, there is no division by $\mathscr{P}_{\rm full}$. The explicit finite-interval response in Section XVIII uses these equations.

XVI. FIXED SCFT-A PRIMORDIAL COMPLETION

The low/intermediate and late-time profiles defined in Section V C are part of one fixed SCFT-A action. This section completes that same action at high clock charge, before the finite DBI boundary is reached, and specifies the positive clock-norm profile that controls the primordial lapse-gradient operator. There is no second benchmark or alternate theory in the construction.

A. Clock-norm profile in the unified SCFT-A action

The final action is Equation (59). Its positive clock-norm profile is built from the flat switch (33),

$$U_\Sigma(Q) \equiv S\left(\frac{Q - Q_{\Sigma-}}{Q_{\Sigma+} - Q_{\Sigma-}}\right),$$

$$\Sigma_{\rm A}(Q) \equiv 1 - (1 - \sigma_{\rm E})U_\Sigma(Q), \tag{452}$$

with the fixed exact values

$$\boxed{\sigma_{\rm E} = \frac{1}{16}, \qquad Q_{\Sigma-} = \frac{7}{4}, \qquad Q_{\Sigma+} = \frac{19}{10}.} \tag{453}$$

Hence $\Sigma_{\rm A} = 1$ for $Q \leq 7/4$, $\Sigma_{\rm A} = 1/16$ for $Q \geq 19/10$, and $1/16 \leq \Sigma_{\rm A} \leq 1$. The suppression persists through part of the matter era, not just radiation domination. The locations of this transition are determined anew by the revised background and are not observational redshifts. Because $\mathcal{J}_{\rm A}(0) = 0$, the regulator contributes neither homogeneous energy nor a homogeneous clock current on FLRW. Because the matter point $Q_m = 1$, the late point $Q_d = 103/100$, and the stationary weak-field branch all lie in the $\Sigma_{\rm A} = 1$ plateau, the homogeneous endpoint and local Newton calibration are unchanged. The completed stationary and lensing equations still contain the spatial operators; their controlled AQUAL limit is derived in Section XX A.

B. Smooth high-charge kinetic completion

The matching DBI profile is real only for $Q < 2$. The final SCFT-A kinetic function leaves that finite boundary outside the physical high-charge branch by switching to a smooth continuation after the complete braiding region. The upper braiding switch is

$$Q_R = 1 + (1 + \nu_{\rm A})\Delta Q = \frac{193}{100}, \qquad Q_E \equiv Q_R + 2\Delta Q = \frac{199}{100}. \tag{454}$$

For $Q \le Q_R$, retain the low/intermediate profile already defined in Equation (41), with the local replacement Equation (51). For $Q \ge Q_R$, define

$$V_K(Q) \equiv S\left(\frac{Q - Q_R}{Q_E - Q_R}\right), \tag{455}$$

$$\varrho_{\rm DBI}(Q) \equiv \frac{\mathcal{K}_{{\rm DBI},QQ}}{\mathcal{K}_{{\rm DBI},Q}} = \frac{1}{(Q-1)[1-\lambda_D(Q-1)^2]}, \tag{456}$$

$$\varrho_{\rm A}(Q) \equiv \begin{cases} [1 - V_K(Q)]\varrho_{\rm DBI}(Q) + 8V_K(Q), & Q_R \le Q < Q_E, \\ 8, & Q \ge Q_E, \end{cases} \tag{457}$$

$$\mathcal{F}_K(Q) \equiv \mathcal{K}_{{\rm A},Q}(Q_R) \exp\left[\int_{Q_R}^{Q} \varrho_{\rm A}(s)\,{\rm d}s\right], \tag{458}$$

$$\mathcal{K}_{\rm A}(Q) \equiv \mathcal{K}_{\rm A}(Q_R) + \int_{Q_R}^{Q} \mathcal{F}_K(s)\,{\rm d}s. \tag{459}$$

Here $\lambda_\infty = 8$. The DBI expression is evaluated only below $Q_E < 2$; the second branch is defined independently, avoiding an undefined product at or beyond the former wall. The braid is extended by $\mathcal{B} = 0$ for $Q \ge Q_R$. The resulting SCFT-A positive-clock domain is $(0, \infty)$ for the fixed $\lambda_D = 1$. The flatness of V_K at both endpoints makes $\mathcal{K}_{\rm A}$ C^∞ at Q_R and Q_E. Moreover,

$$\mathcal{K}_{{\rm A},Q} = \mathcal{F}_K > 0, \qquad \mathcal{K}_{{\rm A},QQ} = \varrho_{\rm A}\mathcal{F}_K > 0. \tag{460}$$

For $Q \ge Q_E$ the continuation is elementary,

$$\begin{aligned} \mathcal{K}_{{\rm A},Q}(Q) &= F_E e^{\lambda_\infty (Q - Q_E)}, \\ \mathcal{K}_{\rm A}(Q) &= K_E + \frac{F_E}{\lambda_\infty}\left[e^{\lambda_\infty(Q-Q_E)} - 1\right], \end{aligned} \tag{461}$$

where the matching values obtained from Equations (458) and (459) are

$$F_E/\kappa_m \simeq 4.429866605156511, \qquad K_E/\kappa_m \simeq 0.8370916680467161. \tag{462}$$

On the unbraided tail the conserved current gives $\mathcal{K}_{{\rm A},Q} = C_T a^{-3}$, and therefore

$$Q(a) = Q_E + \frac{1}{\lambda_\infty}\ln\left(\frac{C_T a^{-3}}{F_E}\right), \qquad c_{\rm ad}^2 = \frac{\mathcal{K}_{,Q}}{Q\mathcal{K}_{,QQ}} = \frac{1}{\lambda_\infty Q} > 0. \tag{463}$$

The high-charge function is regular at every finite Q. Its pressure fraction tends to zero only logarithmically as $a \to 0$. More explicitly, with $F = C_T a^{-3}$,

$$\rho_T/M_{\rm Pl}^2 = (Q - 1/8)C_T a^{-3} - K_E + F_E/8, \qquad p_T/M_{\rm Pl}^2 = K_E + (C_T a^{-3} - F_E)/8.$$

Hence $a^3\rho_T$ is not constant on this tail. The limit $c_{\rm ad}^2 \to 0$ does not establish observationally acceptable clustering at finite redshift. The value $\lambda_\infty = 8$ is close to the matching DBI logarithmic slope $\mathcal{K}_{{\rm DBI},QQ}/\mathcal{K}_{{\rm DBI},Q} = 1000000/125643 \simeq 7.959058602548485$ at Q_R, so the continuation avoids an artificial sharp change in stiffness.

C. Completed constraint structure across the clock-norm transition

The clock-norm profile multiplies the adopted smooth acceleration function: $\widehat{\mathcal{J}}(Q, Y) = \Sigma_{\rm A}(Q)\mathcal{J}_{{\rm A},\sigma}(Y)$. It introduces no lapse or shift time derivative. Its exact contribution to the canonical lapse constraint is

$$\mathcal{C}_N^{(\widehat{\mathcal{J}})} = M_{\rm Pl}^2\sqrt{h}\left\{a_0^2\left[\widehat{\mathcal{J}} - Q\widehat{\mathcal{J}}_{,Q} - 2Y\widehat{\mathcal{J}}_{,Y}\right] - 2D_i\left(\widehat{\mathcal{J}}_{,Y} q^i\right)\right\}. \tag{464}$$

All Q derivatives, the curvature–lapse terms, and the inverse trace Legendre operator are retained in Equation (89). In particular, if G_σ is the smooth acceleration Hessian, the profile contributes $\Sigma_{\rm A}\mathsf{G}_\sigma$ to the gradient coefficient and

$$\Delta M_\Sigma = -a_0^2 Q\Sigma_{{\rm A},QQ}\mathcal{J}_{{\rm A},\sigma} - 2D_i\left(\Sigma_{{\rm A},Q}\mathcal{J}_{{\rm A},\sigma,Y} q^i\right) \tag{465}$$

to the local coefficient in the full negative lapse Hessian. Positivity of Σ_A alone does not control this local term or the curvature contribution. A sufficient regular-domain condition is a strict coercive lower bound on the *full* Schur form,

$$-\delta^2 H_C[N\varphi, N\varphi] \geq c\|\varphi\|^2_{H^1}, \qquad c > 0, \tag{466}$$

with the boundary and coefficient hypotheses needed for its bounded weak inverse. This is a condition on the configuration. On a strongly regular vacuum Cauchy datum, Theorem XIV.3 guarantees a nonzero local interval on which the corresponding margins remain positive and gives continuation for as long as they do. It does not prove that the margins remain positive globally along an arbitrary primordial trajectory. The explicit local sufficient conditions are given in Section VI L.

On a homogeneous flat background the canonical lapse symbol is

$$\mathscr{L}^{\mathrm{full}}_{N,p} = Q\left[\widetilde{\mathcal{K}}_{,QQ} + 3H\mathcal{B}_{\mathrm{A},QQ} + \frac{3\mathcal{B}^2_{\mathrm{A},Q}}{2(1+3\nu p^2/2)}\right] + \frac{2\Sigma_\mathrm{A} p^2}{Q}. \tag{467}$$

This is not the momentum-independent braided rank coefficient of a two-derivative truncation. It must be used together with the full quadratic scalar and matter reductions. None of these constraint conditions supplies a cubic interaction bound or an effective-theory cutoff.

D. Primordial coefficient and completed matter criterion

The acceleration coefficient on a homogeneous background is

$$\sigma_s(Q) = -\left.\frac{\partial}{\partial Y}[\Sigma_\mathrm{A}(Q)\mathcal{J}_{\mathrm{A},\sigma}(Y)]\right|_{Y=0} = \Sigma_\mathrm{A}(Q). \tag{468}$$

Its primordial value 1/16 is a fixed action choice. It does not restore the radiation normalization of a different perturbation theory. The completed density-matrix criterion is Equation (442), and its fixed-background high-momentum limit is one by Equation (445). The two limits in Equation (446) explain why setting the trace-gradient coefficient to zero first gives a different answer. Neither limit establishes a primordial adiabatic spectrum for the completed action. The finite-time response below keeps all spatial terms and avoids singular density-only eliminations.

E. Fixed SCFT-A parameter point

The numerical calculation measures rates in units of H_d and densities in units of $M^2_{\mathrm{Pl}}H^2_d$. It does not set the physical ratio H_d/M_{Pl} to one. The exact dimensionless benchmark parameters are

$$\Delta Q = \frac{3}{100}, \quad \nu_\mathrm{A} = 30, \quad \lambda_D = 1, \quad \frac{\kappa_m}{H_d^2} = 10^{30}, \quad Q_d b_d = \frac{4}{5}H_d, \quad -\frac{\kappa_d}{b_d^2} = \frac{1}{10}, \quad C_T = H_d^2. \tag{469}$$

The remaining exact choices are $\delta = 10^{-140}$, $\sigma = 10^{-6}$, $s_\mathrm{N} = 10$ and $a_0/H_d = 1$. The fixed primordial-completion constants are those in Equations (453), (454) and (457). For the representative visible loading used only as an existence test,

$$\frac{\rho_{b0}}{M^2_{\mathrm{Pl}}H^2_d} = \frac{3}{20}, \qquad \frac{\rho_{\gamma 0}}{M^2_{\mathrm{Pl}}H^2_d} = \frac{387}{10^6}, \qquad \frac{\rho_{\nu 0}}{M^2_{\mathrm{Pl}}H^2_d} = \frac{258}{10^6}. \tag{470}$$

These values are not an observational fit. They define one fixed baryon–radiation–clock background on which the SCFT-A signs can be audited.

XVII. GLOBAL SCFT-A COSMOLOGICAL TRAJECTORIES

The unified SCFT-A action contains both the regular primordial completion and the late braided branch. We reconstruct a source-free trajectory and one representative visible-loaded trajectory directly from the homogeneous constraints.

A. Constraint-preserving reconstruction

Set $N \equiv \ln a$ and

$$F(Q,H) \equiv \mathcal{K}_{,Q} + 3H\mathcal{B}_{,Q} = C_T e^{-3N}. \tag{471}$$

For the source-free branch, elimination of F gives

$$H(Q) = \frac{1}{2}\left[Q\mathcal{B}_{,Q} + \sqrt{Q^2\mathcal{B}_{,Q}^2 + \frac{4}{3}\left(Q\mathcal{K}_{,Q} - \mathcal{K}\right)}\right], \qquad a(Q) = \left[\frac{C_T}{F(Q)}\right]^{1/3}. \tag{472}$$

The derivative identities are

$$H_{,Q} = \frac{3H\mathcal{B}_{,Q} + Q\mathcal{D}_s}{3\mathcal{W}_s}, \qquad F_{,Q} = \frac{2H\Xi_s}{\mathcal{W}_s}, \tag{473}$$

$$Q' = -\frac{3F\mathcal{W}_s}{2H\Xi_s}, \qquad H' = -\frac{F(Q\mathcal{D}_s + 3H\mathcal{B}_{,Q})}{2H\Xi_s}. \tag{474}$$

The source-free diagnostics are

$$\frac{\rho_T}{M_{\rm Pl}^2} = QF - \mathcal{K}, \qquad \frac{p_T}{M_{\rm Pl}^2} = \mathcal{K} - H\mathcal{B}_{,Q}Q', \qquad w_T = \frac{p_T}{\rho_T}, \tag{475}$$

$$q_{\rm dec} = -1 - \frac{H'}{H}, \qquad c_s^2(t,0) = \frac{\mathcal{C}_s}{Q^2\Xi_s}, \qquad \frac{Q_s(t,0)}{M_{\rm Pl}^2} = \frac{4Q^2\Xi_s}{\mathcal{W}_s^2}, \tag{476}$$

$$\frac{\mathrm{d}\mathcal{N}_T}{\mathrm{d}H} = -\frac{1}{Q^2 H_{,Q}}. \tag{477}$$

For visible matter, write $\rho_b = \rho_{b0}a^{-3}$ and $\rho_r = (\rho_{\gamma 0} + \rho_{\nu 0})a^{-4}$. The Friedmann constraint is

$$3M_{\rm Pl}^2 H^2 = \rho_b + \rho_r + M_{\rm Pl}^2(QF - \mathcal{K}). \tag{478}$$

With $h_{\rm vis} = \rho_b + 4\rho_r/3$, differentiation of the current and Friedmann constraints gives

$$\begin{aligned} Q' &= \frac{-6HF + 3\mathcal{B}_{,Q}(h_{\rm vis}/M_{\rm Pl}^2 + QF)}{2H\Xi_s}, \\ H' &= -\frac{\mathcal{D}_s(h_{\rm vis}/M_{\rm Pl}^2 + QF) + 3H\mathcal{B}_{,Q}F}{2H\Xi_s}. \end{aligned} \tag{479}$$

These equations determine the SCFT-A homogeneous branch without introducing a dark-matter density independent of the clock charge.

B. Source-free and visible-loaded backgrounds

Both homogeneous branches are reconstructed on $10^{-15} \le a \le 900$ from the specified action and loading. The output contains the clock norm, expansion rate, derivatives, and scaled current and Friedmann residuals. The source-free clock norm approaches Q_d from above. The high-charge continuation, upper braiding switch, and late plateau are included. These are homogeneous background solutions, not finite-momentum stability diagnostics or an observational fit.

The loaded background is used without retuning in Section XVIII C. The positivity of background quantities such as Ξ_s does not imply positive finite-momentum restoring coefficients; that separate question is answered by the completed perturbation equations and the endpoint audit.

C. Scope and charge scaling

For the source-free system, changing $C_T \mapsto \eta C_T$ with $\eta > 0$ leaves the intrinsic curve $H(Q)$ and all diagnostics expressed as functions of Q unchanged while

$$N_\eta(Q) = N_1(Q) + \frac{1}{3}\ln\eta, \qquad a_\eta(Q) = \eta^{1/3}a_1(Q). \tag{480}$$

SCFT-A therefore supplies a positive-charge family translated in $\ln a$. The visible-loaded example is one fixed background, not a fit. The next section computes a full-action finite-time response. It does not assume a primordial adiabatic initial condition or establish a CMB spectrum, matter-power spectrum, nonlinear basin, or quantum cutoff.

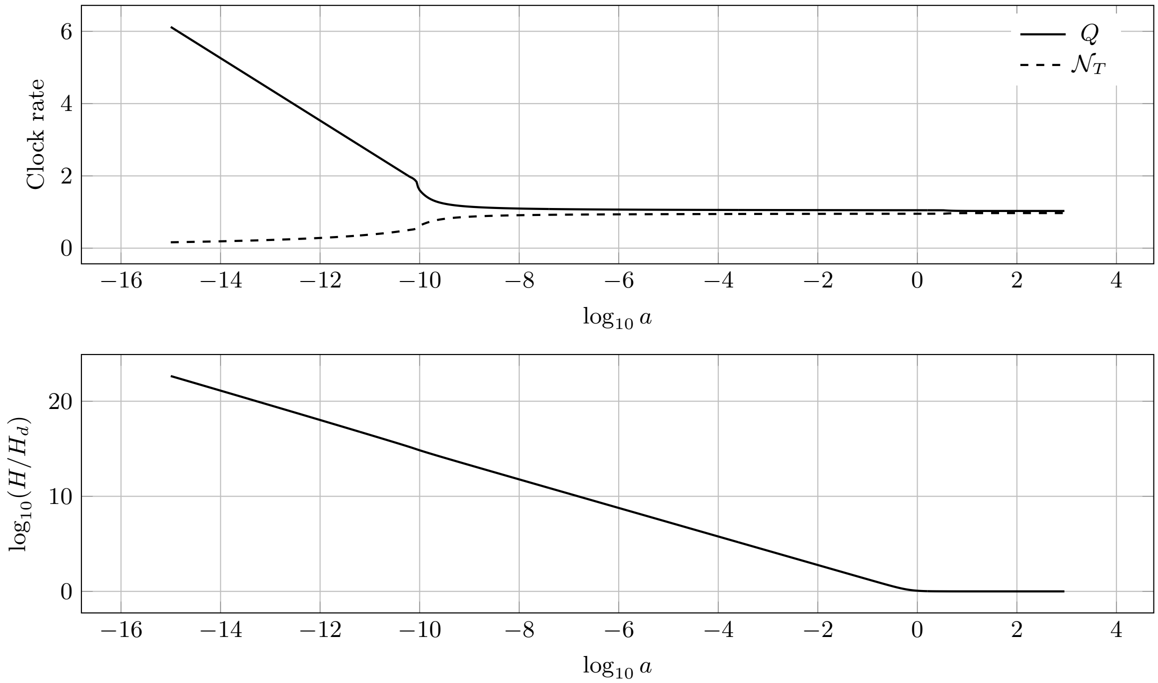

FIG. 2. Reconstructed source-free homogeneous solution of the completed action. Upper panel: Q and $\mathcal{N}_T = Q^{-1}$; lower panel: $\log_{10}(H/H_d)$. The scale-factor normalization is internal. The plotted coordinates are recomputed for the revised coefficient point and exported with the verification files.

XVIII. COMPLETED-ACTION FINITE-WAVELENGTH RESPONSE

The purpose of this calculation is to test the perturbations of Equation (59) itself. It is a finite-time response audit, not a primordial adiabatic transfer calculation. In particular, regular superhorizon initial data derived for a two-derivative action are not assumed to solve the completed constraints when ℓp^2 is large.

A. A numerically regular first-order system

Let $N = \ln a$, $r^2 = x/H^2$, $\epsilon_H = H'/H$, $\delta_A = \delta\rho_A/\rho_A$, and $\vartheta_A = Hv_A$. Introduce

$$u = \frac{H\chi}{x} = -H\psi, \qquad \overline{J} = J/H, \qquad \overline{\mathscr{T}} = \mathscr{T}/H^2,$$
$$\overline{h}_A = \frac{h_A}{M_{\rm Pl}^2 H^2}, \quad \overline{\rho}_A = \frac{\rho_A}{M_{\rm Pl}^2 H^2}, \quad \overline{\mathcal{V}} = \sum_A \overline{h}_A \vartheta_A, \quad \overline{\Delta} = \sum_A \overline{\rho}_A \delta_A. \tag{481}$$

The symbol u in this section is a perturbation variable, not the kinetic interpolation $u(Q)$ used in the local construction. Then Equations (448) to (451) become

$$\begin{aligned}
\alpha &= \frac{2\overline{J}r^2 u + 3\overline{J}\overline{\mathcal{V}} + A\overline{\Delta} - 2Ar^2(1+\ell x)\zeta}{\overline{\mathscr{T}}},\\
\zeta' &= \frac{br^2 u + \overline{J}\alpha - \overline{\mathcal{V}}}{A},\\
u' &= (\epsilon_H - 1)u + (1+\ell x)\alpha + (1 - 8\eta_R x - 3\tau_6 x^2)\zeta,\\
\delta_A' &= -(1+w_A)\left[3\zeta' + r^2(\vartheta_A - u)\right],\\
\vartheta_A' &= (\epsilon_H + 3w_A)\vartheta_A + \alpha + \frac{w_A}{1+w_A}\delta_A.
\end{aligned} \tag{482}$$

Here $w_A = c_A^2$ is constant for the stated barotropic model. To avoid subtracting large background terms, the canonical denominator is computed as

$$\overline{\mathscr{T}} = \frac{2Q^2\Xi_s}{H^2} + 4\Sigma_{\rm A} r^2 + 3b\left(\frac{Q^2 D_s}{H^2} + 2\Sigma_{\rm A} r^2\right). \tag{483}$$

All four spatial completion terms occur in this system. No density-only reduction is used.

Proposition XVIII.1 (Finite-interval linear regularity)**.** *On a compact N interval and a compact nonzero wavenumber band, suppose the background coefficients are continuous and bounded, $H > 0$, and $|\mathscr{T}|$ has a positive lower bound. Then Equation* (482) *has a unique finite solution for each finite initial datum, uniformly on that band.*

Proof. The displayed equations form $\boldsymbol{y}' = \mathbf{M}(N,k)\boldsymbol{y}$ with continuous, bounded coefficients. The fundamental matrix exists and

$$\|\boldsymbol{y}(N)\| \le \|\boldsymbol{y}(N_i)\| \exp\left[\int_{N_i}^{N} \|\mathbf{M}(s,k)\|\,\mathrm{d}s\right]. \tag{484}$$

The stated coefficient and denominator bounds are uniform on the band. □

This bound allows large amplification; it is not a stability theorem.

B. Metric observables and the completed gravitational slip

The Newtonian-gauge fields are

$$\begin{aligned} \Psi_{\rm N} &= u - \zeta, \qquad \Phi_{\rm N} = \alpha - u' + \epsilon_H u, \\ \delta_A^{\rm N} &= \delta_A + 3(1+w_A)u. \end{aligned} \tag{485}$$

Using the u' equation gives the exact perfect-fluid identity

$$\boxed{\Phi_{\rm N} - \Psi_{\rm N} = -\ell p^2\alpha + (8\eta_R p^2 + 3\tau_6 p^4)\zeta.} \tag{486}$$

Thus universal matter coupling does not imply equal scalar metric potentials for this completed gravitational action. The no-slip identity of its two-derivative truncation cannot be imported into the response calculation. Collisionless anisotropic stress would require an additional matter treatment and is not included in Equation (486).

C. A corrected three-fluid response on the loaded background

The background is fixed by Equations (469) and (470). On $1 \le a \le 10$ the spatial coefficients are $\nu = \delta/(2\kappa_m)$, $\ell = \eta_R = 1/(2\kappa_m)$ and $\tau_6 = \delta^2/\kappa_m^2$, with $\kappa_m/H_d^2 = 10^{30}$ and $\delta = 10^{-140}$. The response initial datum is

$$(\zeta, u, \delta_b, \delta_\gamma, \delta_\nu, \vartheta_b, \vartheta_\gamma, \vartheta_\nu)_{a=1} = (0,0,1,0,0,0,0,0). \tag{487}$$

The lapse follows from the corrected action's constraint. This unit baryon-density input normalizes a linear response; multiplication by a physical small initial amplitude rescales every output. The sampled wavenumbers are

$$\frac{k_j}{H_d} = \frac{3}{100}\left(\frac{100000}{3}\right)^{j/41}, \qquad j = 0,\ldots,41. \tag{488}$$

All outputs are evaluated at 1001 common points in $N \in [0, \ln 10]$. The action's current and Friedmann constraints are solved on 4001 background nodes and interpolated with cubic splines. DOP853 uses relative and absolute tolerances 2×10^{-10} and 2×10^{-15}, and maximum step 0.01. Refinement uses 8001 background nodes, tolerances 2×10^{-11} and 2×10^{-16}, and maximum step 0.005. RK45 independently checks $k/H_d = 0.03, 10, 1000$. The exact rational coefficient is used consistently; no coefficient is retuned between modes. The flat-switch complement is evaluated directly before multiplication by κ_m, avoiding catastrophic cancellation in $1 - W$. The exact value $\tau_6 H_d^4 = 10^{-340}$ is stored with an extended exponent range; its finite-band contribution $3\tau_6 p^4 \le 3\,10^{-328}$ lies below binary64 update resolution. The all-momentum conclusions rely on the symbolic expressions, not resolution of this term in the finite-band scan.

TABLE II. Recomputed curvature-completed unit responses. The exact wavenumber is fixed by the index in Equation (488). Printed decimals are stored floating-point results, not exact real numbers; all 42 rows are provided in the verification archive.

j	Maximum sampled unit response	Channel-normalized refinement discrepancy
0	1.0011357323900973	$3.078104394635406 \times 10^{-12}$
24	1.0000053656122538	$9.666787227462226 \times 10^{-14}$
30	1.0000004240527078	$7.602012281390097 \times 10^{-15}$
35	1.000000013729301	$4.591882429849647 \times 10^{-13}$
38	1.0000000014248187	$1.3540961597973225 \times 10^{-12}$
41	1.0000000001399332	$2.914335439641036 \times 10^{-13}$

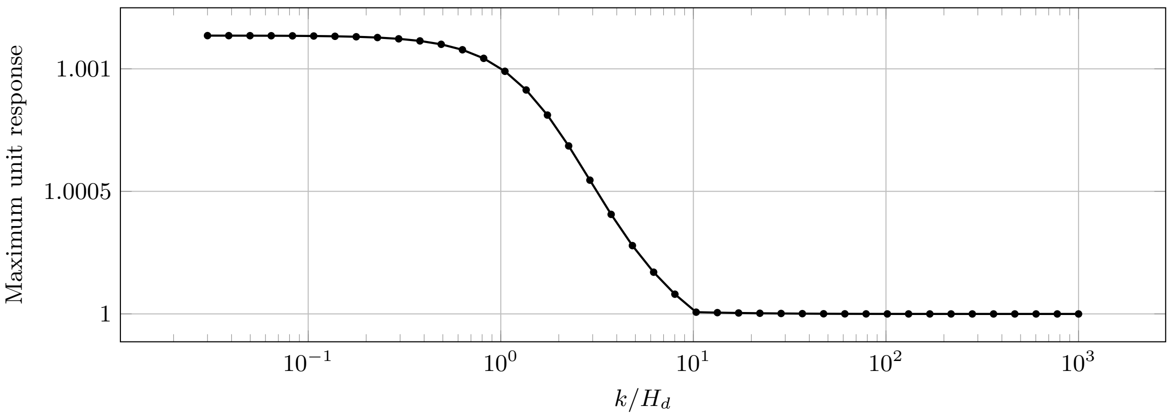

FIG. 3. Maximum absolute response among the curvature, both Newtonian metric potentials, and three Newtonian density contrasts for Equation (487), using the curvature-completed action. Each point is the maximum over 1001 sampled times on $1 \leq a \leq 10$.

Over the specified six observable channels, the fine calculation gives

$$\max_{j,N,\, X\in\{\zeta,\Phi_{\rm N},\Psi_{\rm N},\delta_A^{\rm N}\}} |X| \simeq 1.0011357323900973. \tag{489}$$

All sampled responses remain finite and close to their unit normalization on this interval. This is a positive finite-grid response result for the stated input and interval. It does not certify a continuum maximum, all initial states, or a primordial transfer spectrum. The endpoint restoring sign is established independently and exactly by Theorem XII.1.

The archive contains all eight evolved variables, the reconstructed lapse, both metric potentials, all Newtonian density contrasts, and constraint and refinement diagnostics. Recombination, polarization, collisionless neutrino multipoles, calibrated primordial statistics, and observational likelihoods are not included [51].

XIX. INTERACTIONS OF THE COMPLETED ACTION AND EFFECTIVE-THEORY LIMITS

Quadratic positivity, finite-time evolution, and quantum perturbative control are different questions. The following expansion retains the four spatial operators and the smooth acceleration tip of Equation (59). Its vertices are therefore those of the same action as the linear response. No two-derivative interaction scale is assigned to the completed theory.

A. An exact scalar action before expansion

Use the scalar variables of Equation (256), with the covariant shift $N_i = \partial_i\psi$, and put $q(t) = \dot{T}(t)$. Define

$$A = H + \dot{\zeta}, \qquad V^i{}_j = h^{ik} D_k D_j \psi, \qquad v = V^i{}_i, \qquad Q_{\rm loc} = \frac{q}{1+\alpha}. \tag{490}$$

The pure-scalar restriction of the completed action, to all perturbative orders, is

$$\frac{\mathcal{L}_{\rm sc}}{M_{\rm Pl}^2 a^3} = e^{3\zeta}\Bigg\{\frac{1+\alpha}{2}\,{}^{(3)}R + \frac{-3A^2+2Av+\frac{1}{2}[\mathrm{Tr}(V^2)-v^2]}{1+\alpha} + (1+\alpha)\widetilde{\mathcal{K}}(Q_{\rm loc})$$
$$+\mathcal{B}_{\rm A}(Q_{\rm loc})(3A-v) - (1+\alpha)a_0^2\Sigma_{\rm A}(Q_{\rm loc})\mathcal{J}_{{\rm A},\sigma}(Y)$$
$$-\frac{1+\alpha}{2}\left[\nu(Q_{\rm loc})D_iKD^iK + \ell(Q_{\rm loc}){}^{(3)}RD_i\mathcal{A}^i + \tau_6 D_i{}^{(3)}R_{jk}D^{i(3)}R^{jk} + \eta_R{}^{(3)}R^2\right]\Bigg\}, \tag{491}$$

where

$$^{(3)}R = -\frac{e^{-2\zeta}}{a^2}[4\partial^2\zeta + 2(\partial\zeta)^2], \qquad Y = \frac{e^{-2\zeta}(\partial\alpha)^2}{a^2a_0^2(1+\alpha)^2}. \tag{492}$$

Equations (491) and (492) fix the scalar vertices without an imported Horndeski cubic formula. They follow from $NK^i{}_j = A\delta^i{}_j - V^i{}_j$. Tensor and vector responses generated at second order do not enter the pure-scalar cubic action: they multiply their vanishing first-order constraint or field equations. Their contributions to quartic interactions must nevertheless be retained in a complete higher-order calculation.

B. Classical mixed vertices and the limits of effective-theory control

The companion fixes the nonlinear ideal-fluid completion by $\rho_A(n) \propto n^{1+w_A}$ and derives its full cubic density in independent current variables. Combined with the displayed gravitational cubic functional and first-order auxiliary solutions, this determines the classical cubic mixed interactions for that matter model. It is not a microscopic photon or neutrino action.

One necessary interaction diagnostic can be made explicit. On the exact Minkowski plateau, $\alpha_1 = -(1+\ell_0p^2)\zeta$ and $v = \sqrt{2}M_{\rm Pl}\sqrt{K_{p,{\rm M}}}\zeta$. The smooth-tip quartic vertex therefore contains the equal-momentum coefficient

$$\chi_4(p) = \frac{\mu_{\rm A}(\sigma)}{8\gamma_{\rm N}\sigma^2a_0^2M_{\rm Pl}^2}\frac{p^4(1+\ell_0p^2)^4}{K_{p,{\rm M}}^2}. \tag{493}$$

This dimensionless quantity describes the coefficient of one canonically normalized derivative vertex before angular and combinatorial factors. It is not the full scattering amplitude. The conditions $\chi_4 \ll 1$, $|\nabla\alpha|/a_0 \ll \sigma$, and small metric and lapse amplitudes are necessary checks in a strict tip expansion. Cubic exchange, other quartics, generated tensors, and matter interactions must be included before a complete strong-coupling scale can be assigned. For the sixth-order dispersions, a frequency bound and a momentum bound are distinct; the identity $\omega^2 = V/K$ alone does not establish either cutoff [30, 31].

Shift symmetry forbids an explicit T-dependent potential but permits a constant vacuum term, arbitrary functions of Q, and independent foliation invariants. It therefore does not protect the exact kinetic plateau, the small chosen coefficients, or the restriction to the displayed operator subset. Renormalization results for other foliation theories require their own actions and constraint measures [52]; they cannot be imported from a positive quadratic spectrum. The present work supplies a classical existence construction, with no demonstrated radiative protection or complete quantum validity window. These remaining tasks are not claimed solved by the coefficient hierarchy.

XX. COSMOLOGICAL EMBEDDING OF THE STATIONARY FORCE LAW

A. Completed coupled stationary equations

Within the exact vacuum plateau, let $\nu_0 = \delta/\kappa_m$, $\ell_0 = 1/\kappa_m$, and $\tau_6 = \delta^2/\kappa_m^2$. For a stationary conformally scalar weak field $h_{ij} = (1-2\Psi)\delta_{ij}$, $N = 1+\Phi$, and $T = t$, the leading stationary density, keeping the full acceleration function but the quadratic metric-gradient terms, is

$$\frac{\mathcal{L}_{\rm stat}}{M_{\rm Pl}^2} = (\nabla\Psi)^2 - 2\nabla\Phi\cdot\nabla\Psi - 2\ell_0\Delta\Phi\Delta\Psi - 8\eta_R(\Delta\Psi)^2 - 3\tau_6|\nabla\Delta\Psi|^2 - a_0^2\mathcal{J}_{{\rm A},\sigma}(|\nabla\Phi|^2/a_0^2) - \frac{\rho_b}{M_{\rm Pl}^2}\Phi. \tag{494}$$

The trace-gradient term vanishes because $K = 0$. Write $\mu_{\rm reg}(s) = \mu_\sigma(s^2)$, which equals $\mu_{\rm A}(s)$ for $s \geq 2\sigma$. Varying both potentials gives

$$\nabla \cdot [\mu_{\rm reg}(s)\nabla\Phi] + \gamma_{\rm N}\Delta(\Psi - \Phi) - \gamma_{\rm N}\ell_0\Delta^2\Psi = 4\pi G_{\rm N}\rho_b, \qquad s = |\nabla\Phi|/a_0, \tag{495}$$

$$\Delta\left[(1 + 8\eta_R\Delta - 3\tau_6\Delta^2)\Psi - (1 - \ell_0\Delta)\Phi\right] = 0, \qquad \Phi_{\rm lens} = \frac{\Phi + \Psi}{2}. \tag{496}$$

The harmonic term in the second equation is fixed by boundary or matching data. The coupled equations avoid dividing by $1 - 8\eta_R p^2 - 3\tau_6 p^4$, which can vanish in an isolated spatial-potential elimination even though the coupled Minkowski scalar restoring coefficient is positive. Such a zero is not, by itself, a physical mode instability.

Outside the regularized tip and for smooth fields varying on a common scale L, sufficient asymptotic conditions for recovery of the seed AQUAL equation are

$$\frac{\ell_0 + 8\eta_R}{L^2} \ll 1, \qquad \frac{\tau_6}{L^4} \ll 1, \qquad \gamma_{\rm N}\left[\frac{2\ell_0 + 8\eta_R}{L^2} + \frac{(\ell_0 + 8\eta_R)^2 + 3\tau_6}{L^4}\right] \ll \min\{\mu_{\rm A}(s), \mu_{\rm A}(s) + s\mu'_{\rm A}(s)\}, \quad s \geq 2\sigma. \tag{497}$$

These are derivative-expansion conditions, not identities at every wavelength. The exact coupled form is Equations (495) and (496). Inside the tip the function is changed deliberately, and its strict deep-acceleration asymptotic is not the seed $\mu_{\rm A}(s) \sim s$ law. No observational acceptability claim is made here for sourced solutions matched to cosmological boundary data.

B. Embedding and force-law hierarchy

The following kinematic and scale estimates must be used together with the completed coupled equations, not in place of them.

The formal stationary calculation in Section X establishes an operator limit. It does not construct a galaxy in the evolving positive-charge solution. In a local patch of that solution, write

$$T = \bar{T}(t) + \bar{Q}(t)\pi(t, \boldsymbol{x}). \tag{498}$$

To first weak-field order in Newtonian coordinates,

$$\frac{\delta Q}{\bar{Q}} = \dot{\pi} + \frac{\dot{\bar{Q}}}{\bar{Q}}\pi - \Phi_{\rm N}, \qquad \mathcal{A}_i = -\partial_i\left(\frac{\delta Q}{\bar{Q}}\right) + \frac{\dot{\bar{Q}}}{\bar{Q}}\partial_i\pi = \partial_i(\Phi_{\rm N} - \dot{\pi}). \tag{499}$$

The acceleration expression follows by projecting the gradient of $\ln Q$, including the first-order spatial component of u_μ. Its clock-dependent terms cannot be dropped merely because $HL \ll 1$; the behavior of π must be solved. Equivalently, in unitary gauge the exact linear momentum constraint is

$$J\alpha - A\dot{\zeta} + b\chi = \frac{\mathcal{V}}{M_{\rm Pl}^2}. \tag{500}$$

Setting the clock-comoving fluid momentum, $\dot{\zeta}$, and χ to zero while keeping $J \neq 0$ would force $\alpha = 0$. With a nonzero shift, its $b\chi$ term must also be retained. A static lapse potential on the zero-braid Minkowski reference state therefore cannot be transplanted unchanged into the cosmological unitary slicing. Time dependence of that slicing, clock flow, or matter momentum supplies terms that must be retained at the order at which the momentum equation is used. The nonstationary khronon response is known to matter even in related theories without the present braid [32].

On a constant-regulator patch, the acceleration part of the quasi-static lapse operator is

$$\bar{\mu}_Q(s) = 1 - \sigma(Q) + \frac{\sigma(Q)}{\gamma_{\rm N}}\mu_{\rm A}(s). \tag{501}$$

Only the $\sigma = 1$ plateau has the stated deep-MOND normalization. In a clock-norm transition, extra $\sigma_Q\mathcal{J}$ terms in Equation (464) must also be included. The benchmark reaches $\sigma = 1$ before its late branch, so clock-norm suppression alone does not obstruct late galaxies; the clock and braiding matching problem remains.

There is also a stronger scale requirement than $|m^2_{\rm loc}|L^2 \ll 1$ in a region where $\mu \ll 1$. Comparing the Helmholtz term with the local elliptic operator requires

$$|m^2_{\rm loc}|L^2 \ll \min\{\mu_{\rm A}(s), \mu_{\rm A}(s) + s\mu'_{\rm A}(s)\}, \tag{502}$$

when the potential and gradients vary over a common scale L. For a general profile the direct condition is $|m^2_{\rm loc}\Phi| \ll |\boldsymbol{\nabla}\cdot(\mu_{\rm A}\boldsymbol{\nabla}\Phi)|$ wherever that comparison is nonzero. Boundary data must fix the potential entering the mass term; in a vacuum region the smallness test is instead made against the separate differential terms or their linearized eigenvalues, not their vanishing on-shell sum. Exact asymptotically flat, zero-charge boundary conditions now use the repaired vacuum sector in Section XIII. Its quadratic health does not prove that a sourced nonlinear galaxy can be matched to the positive-charge cosmological branch.

Finally, the finite Newton calibration is not complete recovery of general relativity. The adopted high-acceleration function obeys

$$\mathcal{J}_{\rm A}(Y) = -\frac{Y}{s_{\rm N}+1} + O(1) \quad (Y\to\infty), \qquad -M^2_{\rm Pl}a_0^2\mathcal{J}_{\rm A} \supset \frac{M^2_{\rm Pl}}{s_{\rm N}+1}\mathcal{A}_\mu\mathcal{A}^\mu. \tag{503}$$

The surviving preferred-foliation operator is not removed by defining $G_{\rm N}$. Preferred-frame, post-Newtonian, binary, and inhomogeneous tensor tests require their own solutions. The completed tensor dispersion is Equation (238); only its low-momentum limit equals the photon speed. This does not supply preferred-frame tests or protect coefficients against radiative corrections.

An embedded galaxy calculation must solve the metric and clock equations with cosmological boundary data, demonstrate a controlled quasi-static ordering, apply Equations (497) and (502), and check the local fluctuation spectrum within Supplemental Material, Eq. (21). Proposition XIV.1 supplies localized positive-charge linear vacuum data and Theorem XIII.3 supplies an exact flat-vacuum quadratic repair, but neither result solves the sourced nonlinear matching problem. The stationary AQUAL equation is retained only in the controlled hierarchy where the higher-spatial-derivative repair terms are negligible; successful galactic phenomenology of the revised benchmark has not been demonstrated.

C. A scale-separated coefficient point

The former choice $\kappa_m/H_d^2 = 120$ made $(\ell_0+8\eta_R)/L^2 = 1/[24(H_dL)^2]$, which could not be small on subhorizon scales. This is repaired by the revised exact coefficient point, not by omitting any term from the action. With $\mathfrak{k} = 10^{30}$,

$$\frac{\ell_0+8\eta_R}{L^2} = \frac{5}{\mathfrak{k}(H_dL)^2}, \qquad \frac{\tau_6}{L^4} = \frac{\delta^2}{\mathfrak{k}^2(H_dL)^4}. \tag{504}$$

Choose the declared theoretical test scale $H_dL = 10^{-6}$ and acceleration $s = 1/100$, with $a_0/H_d = 1$, $s_{\rm N} = 10$ and $\gamma_{\rm N} = 11/10$. Then

$$\frac{\ell_0+8\eta_R}{L^2} = 5\,10^{-18}, \qquad \frac{\tau_6}{L^4} = 10^{-316}, \qquad \mu_{\rm A}(1/100) = \frac{1000101}{101000101}. \tag{505}$$

Since $\mu'_{\rm A}(s) > 0$, the smaller acceleration-Hessian coefficient is $\mu_{\rm A}(s)$. The dimensionless correction ratio in Equation (497) is exactly

$$\mathcal{R}_{\rm stat} = \frac{11\cdot 101000101}{10\cdot 1000101}\left(6\,10^{-18} + 25\,10^{-36} + 3\,10^{-316}\right) < 10^{-14}. \tag{506}$$

Moreover $s > 2\sigma$, and a potential variation of order $sa_0L = 10^{-8}$ fits inside the exact kinetic plateau, where $U' = U'' = \mathcal{B} = 0$. Thus the local mass term vanishes and the scale and acceleration conditions have a nonempty simultaneous domain. By continuity the strict margins persist on a neighborhood of the declared scale and acceleration; this is not an isolated equality.

The change of κ_m alters the exterior kinetic function. The broad homogeneous curves and all 42 matter responses have therefore been recomputed. The local all-momentum proof is dimensionless and still applies; the generalized endpoint polynomial explicitly retains $\mathfrak{k}$ and proves positivity at the revised point. These checks repair the coefficient hierarchy within the same operator family. They do not construct a nonlinear sourced solution joining the $Q \simeq 1$ stationary plateau to the $Q \simeq Q_d$ cosmological clock, or prove a uniform singular-perturbation limit for arbitrary boundary data. The AQUAL reduction is asserted only under the stated smooth common-scale ordering, with boundary layers excluded from that local approximation.

XXI. STRUCTURAL PREDICTIONS AND CONSISTENCY CONDITIONS

The derived quantities are the homogeneous current and reciprocal response, the specified vacuum scalar and tensor spectra, the constrained perfect-fluid response, and the coupled stationary equations. They are predictions of one fixed action. The explicitly stated homogeneous, linear, and strongly regular vacuum Cauchy domains have been established. The revised local stationary hierarchy is certified in Equation (506); a nonlinear sourced solution matched to the cosmological clock remains a separate problem.

XXII. RELATION TO EXISTING THEORIES

The relevant precedents are action-level, not merely interpretive. Kinetic gravity braiding already supplies scalar–metric kinetic mixing and self-accelerating branches [6, 7]. Relativistic khronon models combine one metric, a foliation scalar, generalized-dark-matter behavior, and a stationary MOND operator [8, 9, 32]. Higher spatial derivatives and lapse-gradient terms are part of the established spatially covariant and nonprojectable operator basis [18, 35, 36, 39]. A preferred direction derived from a scalar differs from the independent vector sectors of TeVeS and AeST [10, 11].

The contribution here is the explicit combination of a convex local kinetic replacement, positive spatial floors, and a curvature-square term with a continuum endpoint positivity certificate. The reciprocal sign is an additional branch diagnostic. Neither the field-first interpretation nor a change of clock variable alone constitutes the mathematical advance. The coefficients are constructed to meet classical sign conditions; a microscopic derivation or radiative stability argument is absent.

The nonanalytic unregulated MOND term and its smooth replacement have different interaction expansions. General results about mixed-derivative gravity or well-posed Einstein evolution cannot simply be transferred to this action: the action-specific lapse operator, reduced sixth-order Hessian, gauge slice, and loss-free energy must be checked [40–42, 45, 46, 49, 50]. Those checks are supplied in Section XIV C. The comparison above identifies the narrow contribution rather than claiming the underlying operator families as new.

XXIII. DISCUSSION

The concrete advances are the explicit rational coupling certificate, a coefficient hierarchy admitting a controlled local stationary ordering, a contracting unbraided solution, and an all-mode decreasing scalar energy at the expanding de Sitter endpoint. The full scalar reduction and the local transition positivity proof apply to the same revised coefficients. The constraint-domain mode count and the homogeneous self-accelerating endpoint are retained. All numerical curves and finite-time matter responses have been recalculated after changing the exterior stiffness.

These results have defined domains. The contracting solution is unbraided; the decreasing endpoint energy is a linear theorem; the local stationary hierarchy assumes smooth common-scale fields and does not solve cosmological matching. In addition, the exact vacuum gravity–clock equations are locally Hadamard well posed on the strongly regular boundaryless torus domain of Theorem XIV.3. The theorem includes the homogeneous lapse mode, tame auxiliary reconstruction, a loss-free variable-coefficient energy, existence, uniqueness, continuous dependence, and constraint propagation. It is not a global stability theorem, a nonlinear bounded-domain theorem, or an unconditional theorem for the unspecified visible-matter functional.

The coefficient functions are deliberately engineered to demonstrate compatible classical inequalities. This is a mathematical rationale for an existence construction, not a derivation from microscopic physics. The supplied ideal-fluid cubic functional improves the interaction specification, but a complete quantum cutoff and radiative-stability argument remain absent. No nonlinear or quantum conclusion follows merely from choosing smaller spatial coefficients. These limitations concern this theoretical paper itself, independently of any later observational program.

XXIV. CONCLUSION

A single specified operator family admits the displayed reciprocal expanding and unbraided contracting branches, positive local scalar and tensor quadratic forms, and a de Sitter scalar energy that decreases for every linear initial state. The revised exact coefficient point restores a nonempty controlled stationary hierarchy while preserving the proved endpoint and local-transition inequalities. The supporting calculations use a rigorous interval moment bound, exact rational inequalities, independent symbolic elimination, and recomputed finite-time ideal-fluid responses.

The manuscript establishes these classical results together with full nonlinear local Hadamard well-posedness of the vacuum gravity–clock Cauchy problem on the stated strongly regular boundaryless torus domain. It does not establish global nonlinear stability, a nonlinear initial-boundary-value theorem, a complete strong-coupling domain, radiative protection, an unconditional theorem for the unspecified visible-matter functional, or a nonlinear sourced solution joining the local and cosmological clock sectors. A completed dark-sector unification theorem would require those additional results.

COMPUTATIONAL VERIFICATION

The reproducibility package contains `certify_coefficients.py`, `exact_algebra.py`, and `reproduce_numerics.py`. The coefficient certificate passes 33 checks; the symbolic and exact scale audit passes 16 checks, including the independently expanded ideal-fluid cubic density. The numerical calculation uses new arrays for the revised coefficient point. Its maximum sampled response is 1.0011357323900973, its largest channel-scaled refinement discrepancy is $1.6975908959798724 \times 10^{-11}$, and its largest scaled background residual on the fine response grid is $5.028079805054185 \times 10^{-13}$. The independent-integrator checks and complete per-mode diagnostics are supplied. Numerical decimals are approximations; exact claims use rational or symbolic expressions and proved enclosures. No claimed theorem depends on interpreting a floating-point output as exact.

[1] A. G. Riess *et al.*, Observational evidence from supernovae for an accelerating universe and a cosmological constant, Astron. J. **116**, 1009–1038 (1998). `https://doi.org/10.1086/300499`
[2] S. Perlmutter *et al.*, Measurements of Ω and Λ from 42 high-redshift supernovae, Astrophys. J. **517**, 565–586 (1999). `https://doi.org/10.1086/307221`
[3] N. Aghanim *et al.* (Planck Collaboration), Planck 2018 results. VI. Cosmological parameters, Astron. Astrophys. **641**, A6 (2020). `https://doi.org/10.1051/0004-6361/201833910`
[4] S. Weinberg, The cosmological constant problem, Rev. Mod. Phys. **61**, 1–23 (1989). `https://doi.org/10.1103/RevModPhys.61.1`
[5] T. Clifton, P. G. Ferreira, A. Padilla, and C. Skordis, Modified gravity and cosmology, Phys. Rep. **513**, 1–189 (2012). `https://doi.org/10.1016/j.physrep.2012.01.001`
[6] C. Deffayet, O. Pujolàs, I. Sawicki, and A. Vikman, Imperfect dark energy from kinetic gravity braiding, J. Cosmol. Astropart. Phys. **10**, 026 (2010). `https://doi.org/10.1088/1475-7516/2010/10/026`
[7] T. Kobayashi, M. Yamaguchi, and J. Yokoyama, Generalized G-inflation: Inflation with the most general second-order field equations, Prog. Theor. Phys. **126**, 511–529 (2011). `https://doi.org/10.1143/PTP.126.511`
[8] L. Blanchet and C. Skordis, Relativistic khronon theory in agreement with modified Newtonian dynamics and large-scale cosmology, J. Cosmol. Astropart. Phys. **11**, 040 (2024). `https://doi.org/10.1088/1475-7516/2024/11/040`
[9] L. Blanchet and C. Skordis, Khronon-tensor theory reproducing MOND and the cosmological model, arXiv:2507.00912 [gr-qc] (2025). `https://arxiv.org/abs/2507.00912`
[10] J. D. Bekenstein, Relativistic gravitation theory for the modified Newtonian dynamics paradigm, Phys. Rev. D **70**, 083509 (2004); Erratum Phys. Rev. D **71**, 069901 (2005). `https://doi.org/10.1103/PhysRevD.70.083509`
[11] C. Skordis and T. Złośnik, New relativistic theory for modified Newtonian dynamics, Phys. Rev. Lett. **127**, 161302 (2021). `https://doi.org/10.1103/PhysRevLett.127.161302`
[12] A. H. Chamseddine and V. Mukhanov, Mimetic dark matter, J. High Energy Phys. **11**, 135 (2013). `https://doi.org/10.1007/JHEP11(2013)135`
[13] L. Mirzagholi and A. Vikman, Imperfect dark matter, J. Cosmol. Astropart. Phys. **06**, 028 (2015). `https://doi.org/10.1088/1475-7516/2015/06/028`
[14] D. L. Wiltshire, Cosmic clocks, cosmic variance and cosmic averages, New J. Phys. **9**, 377 (2007). `https://doi.org/10.1088/1367-2630/9/10/377`
[15] D. L. Wiltshire, Average observational quantities in the timescape cosmology, Phys. Rev. D **80**, 123512 (2009). `https://doi.org/10.1103/PhysRevD.80.123512`
[16] A. Einstein, *Äther und Relativitätstheorie* (Julius Springer, Berlin, 1920); English translation, Ether and the Theory of Relativity, in *The Collected Papers of Albert Einstein*, Vol. 7 (Princeton University Press, 2002).
[17] J. Bellorín and A. Restuccia, Consistency of the Hamiltonian formulation of the lowest-order effective action of the complete Hořava theory, Phys. Rev. D **84**, 104037 (2011). `https://doi.org/10.1103/PhysRevD.84.104037`
[18] X. Gao, Hamiltonian analysis of spatially covariant gravity, Phys. Rev. D **90**, 104033 (2014). `https://doi.org/10.1103/PhysRevD.90.104033`
[19] R. J. Scherrer, Purely kinetic *k* essence as unified dark matter, Phys. Rev. Lett. **93**, 011301 (2004). `https://doi.org/10.1103/PhysRevLett.93.011301`
[20] M. Milgrom, A modification of the Newtonian dynamics as a possible alternative to the hidden mass hypothesis, Astrophys. J. **270**, 365–370 (1983). `https://doi.org/10.1086/161130`
[21] J. Bekenstein and M. Milgrom, Does the missing mass problem signal the breakdown of Newtonian gravity?, Astrophys. J. **286**, 7–14 (1984). `https://doi.org/10.1086/162570`
[22] B. P. Abbott *et al.*, Gravitational waves and gamma-rays from a binary neutron star merger: GW170817 and GRB 170817A, Astrophys. J. Lett. **848**, L13 (2017). `https://doi.org/10.3847/2041-8213/aa920c`
[23] T. Baker, E. Bellini, P. G. Ferreira, M. Lagos, J. Noller, and I. Sawicki, Strong constraints on cosmological gravity from GW170817 and GRB 170817A, Phys. Rev. Lett. **119**, 251301 (2017). `https://doi.org/10.1103/PhysRevLett.119.251301`
[24] P. Creminelli and F. Vernizzi, Dark energy after GW170817 and GRB 170817A, Phys. Rev. Lett. **119**, 251302 (2017). `https://doi.org/10.1103/PhysRevLett.119.251302`

[25] J. M. Ezquiaga and M. Zumalacárregui, Dark energy after GW170817: Dead ends and the road ahead, Phys. Rev. Lett. **119**, 251304 (2017). https://doi.org/10.1103/PhysRevLett.119.251304
[26] S. Tsujikawa, The effective field theory of inflation/dark energy and the Horndeski theory, Lect. Notes Phys. **892**, 97–136 (2015). https://doi.org/10.1007/978-3-319-10070-8_4
[27] B. F. Schutz and R. Sorkin, Variational aspects of relativistic field theories, with application to perfect fluids, Ann. Phys. (N.Y.) **107**, 1–43 (1977). https://doi.org/10.1016/0003-4916(77)90200-7
[28] J. D. Brown, Action functionals for relativistic perfect fluids, Class. Quantum Grav. **10**, 1579–1606 (1993). https://doi.org/10.1088/0264-9381/10/8/017
[29] R. Kase and S. Tsujikawa, Scalar-field dark energy nonminimally and kinetically coupled to dark matter, Phys. Rev. D **101**, 063511 (2020). https://doi.org/10.1103/PhysRevD.101.063511
[30] C. Cheung, P. Creminelli, A. L. Fitzpatrick, J. Kaplan, and L. Senatore, The effective field theory of inflation, J. High Energy Phys. **03**, 014 (2008). https://doi.org/10.1088/1126-6708/2008/03/014
[31] D. Blas, O. Pujolàs, and S. Sibiryakov, Models of non-relativistic quantum gravity: The good, the bad and the healthy, J. High Energy Phys. **04**, 018 (2011). https://doi.org/10.1007/JHEP04(2011)018
[32] E. E. Flanagan, Khronometric theories of modified Newtonian dynamics, Astrophys. J. **958**, 107 (2023). https://doi.org/10.3847/1538-4357/acf6cb
[33] T. Jacobson and D. Mattingly, Gravity with a dynamical preferred frame, Phys. Rev. D **64**, 024028 (2001). https://doi.org/10.1103/PhysRevD.64.024028
[34] T. Jacobson, Einstein-aether gravity: A status report, PoS QG-PH, 020 (2007). https://doi.org/10.22323/1.043.0020
[35] P. Hořava, Quantum gravity at a Lifshitz point, Phys. Rev. D **79**, 084008 (2009). https://doi.org/10.1103/PhysRevD.79.084008
[36] D. Blas, O. Pujolàs, and S. Sibiryakov, Consistent extension of Hořava gravity, Phys. Rev. Lett. **104**, 181302 (2010). https://doi.org/10.1103/PhysRevLett.104.181302
[37] P. Magain and C. Hauret, On the nature of cosmological time, arXiv:1505.02052 [astro-ph.CO] (2015). https://arxiv.org/abs/1505.02052
[38] P. Magain and C. Hauret, Variable time flow as an alternative to dark energy, arXiv:1606.06169 [astro-ph.CO] (2016). https://arxiv.org/abs/1606.06169
[39] M. Colombo, A. E. Gümrükçüoğlu, and T. P. Sotiriou, Hořava gravity with mixed derivative terms, Phys. Rev. D **91**, 044021 (2015). https://arxiv.org/abs/1410.6360.
[40] A. Coates, M. Colombo, A. E. Gümrükçüoğlu, and T. P. Sotiriou, The uninvited guest in mixed derivative Hořava gravity (2016). https://arxiv.org/pdf/1604.04215.
[41] W. Donnelly and T. Jacobson, Hamiltonian structure of Hořava gravity, Phys. Rev. D **84**, 104019 (2011). https://arxiv.org/abs/1106.2131.
[42] L. Andersson and V. Moncrief, Elliptic–hyperbolic systems and the Einstein equations, Ann. Henri Poincaré **4**, 1–34 (2003). https://arxiv.org/abs/gr-qc/0110111.
[43] D. G. Ebin, The manifold of Riemannian metrics, in Global Analysis, Proc. Sympos. Pure Math. **15**, 11–40 (1970). https://users.math.msu.edu/users/parker/993/Ebin.pdf.
[44] J. Marsden and A. Weinstein, Reduction of symplectic manifolds with symmetry, Rep. Math. Phys. **5**, 121–130 (1974). https://www.cds.caltech.edu/~marsden/bib/1974/01-MaWe1974/MaWe1974.pdf.
[45] R. T. Seeley, Complex powers of an elliptic operator, Proc. Sympos. Pure Math. **10**, 288–307 (1967).
[46] M. E. Taylor, *Pseudodifferential Operators and Nonlinear PDE*, Progress in Mathematics **100**, Birkhäuser (1991). https://www.math.unc.edu/Faculty/met/.
[47] T. Kato, Quasi-linear equations of evolution, with applications to partial differential equations, Lecture Notes in Math. **448**, 25–70 (1975); see also Abstract evolution equations, linear and quasilinear, revisited, Lecture Notes in Math. **1540**, 103–125 (1993). https://doi.org/10.1007/BFb0085477.
[48] J. L. Bona and R. Smith, The initial-value problem for the Korteweg–de Vries equation, Philos. Trans. R. Soc. Lond. A **278**, 555–601 (1975). https://doi.org/10.1098/rsta.1975.0035.
[49] M. Ifrim and D. Tataru, Local well-posedness for quasilinear problems: a primer (2020). https://arxiv.org/abs/2008.05684.
[50] R. Feola, F. Giuliani, F. Iandoli, and J. E. Massetti, Local well posedness for a system of quasilinear PDEs modelling suspension bridges (2023). https://arxiv.org/abs/2306.11037.
[51] C.-P. Ma and E. Bertschinger, Cosmological perturbation theory in the synchronous and conformal Newtonian gauges, Astrophys. J. **455**, 7–25 (1995). https://doi.org/10.1086/176550
[52] J. Bellorín, C. Bórquez, and B. Droguett, Renormalization of the nonprojectable Hořava theory, Phys. Rev. D **110**, 084020 (2024). https://doi.org/10.1103/PhysRevD.110.084020

ETHICS, CONSENT TO PARTICIPATE, AND CONSENT TO PUBLISH

Ethics, Consent to Participate, and Consent to Publish declarations: not applicable.

FUNDING

No funding was received for this work.

DATA AVAILABILITY

All scripts, exact-check reports, numerical data, verification outputs, and LaTeX sources associated with this work are publicly available at https://github.com/mauromontenegro333/Space-Clock-Field-Theory-A.